INTERNATIONAL
HELLENIC
UNIVERSITY

CFD Investigation Inside Solar Flat Plate Collectors

Keivan Haghverdi
SID: 3302180004

SCHOOL OF SCIENCE & TECHNOLOGY
A thesis presented for the degree of
master of science in engineering

October 2020
Thessaloniki - Greece

INTERNATIONAL
HELLENIC
UNIVERSITY

CFD Investigation Inside Solar Flat Plate Collectors

Keivan Haghverdi
SID: 3302180004

Supervisor: Dr. Dimitrios Misirlis

Supervising Committee Members:

SCHOOL OF SCIENCE & TECHNOLOGY
A thesis presented for the degree of
master of science in engineering

October 2020
Thessaloniki - Greece

Abstract

This dissertation was written as a part of the MSc in energy systems at the International Hellenic University. The main focus of this study is to investigate the performance of a polycarbonate flat plat solar collector. The aim of this research project is to investigate the possibility of using polymer material in production of solar flat plate collector design. Using the suggested material will result in more cost effective flat plate collectors production while being more environmental friendly. this project work focuses on the process of energy conversion from the collector to the working fluid. This is accomplished by employing a polymer honeycomb structure placed as the channels of a collector to transfer heat to water as a working fluid and induce a gradient of heat capacitance. The other focus area is the fluid behaviour inside the collector and investigating the temperature, velocity and pressure patterns in different regions of the collector to gain a broader insight regarding the performance of the collector and its design.

This novel poly-carbonate collector is tested theoretically using Computational Fluid Dynamics (CFD) and the results was compared to experimental data available. The obtained CFD data and the experimental findings are coupled and show a good agreement. All the obtained results are validated with the literature. The result of the simulation clearly shows an acceptable performance of this polymer design and its efficiency is comparable to the classic models which costs more both in material and production. An in depth analysis of the results also revealed some weak points of the design such as re-circulation streams and the cause of the problem which help us calibrate and improve our further designs in future works.

Contents

1 Introduction **8**
- 1.1 The need for renewable technologies . . . 8
- 1.2 Solar thermal energy . . . 9
- 1.3 Solar thermal collectors . . . 9
- 1.4 Research aim . . . 9
- 1.5 Research scope . . . 10
  - 1.5.1 The need for flat plate solar collectors . . . 10
  - 1.5.2 Introduction to the flat plate collectors . . . 10
  - 1.5.3 Research methodology . . . 12
  - 1.5.4 Thesis outline . . . 12

2 Literature Review **13**
- 2.1 Flat plate collectors design . . . 13
  - 2.1.1 Glazing materials . . . 15
  - 2.1.2 Collector absorber plates . . . 16
  - 2.1.3 Collector construction . . . 16
- 2.2 Flat plate collectors mathematical modeling . . . 17
  - 2.2.1 Heat Transfer . . . 18
  - 2.2.2 Fluid Mechanics . . . 20
  - 2.2.3 Solar Radiation Absorbtion . . . 22
  - 2.2.4 Total energy balance of FPC . . . 23
  - 2.2.5 Heat loss . . . 23
  - 2.2.6 Efficiency factor of a collector . . . 26
  - 2.2.7 Heat removal factor . . . 30
  - 2.2.8 Flat plate collector efficiency η . . . 31

3 Problem Definition **33**
- 3.1 Collector parameters . . . 33

4 CFD Modeling **37**
- 4.1 Finite element method . . . 37
  - 4.1.1 CFD background . . . 38
- 4.2 CFD modeling of solar flat plate collector . . . 39
  - 4.2.1 ANSYS analysis system modules . . . 39
  - 4.2.2 Geometry . . . 41
  - 4.2.3 Meshing grid . . . 43
  - 4.2.4 Setup and source terms . . . 45

5 Results **62**
5.1 CFD results 62
5.1.1 Efficiency 65
5.1.2 Temperature pattern 66
5.1.3 Flow pattern and velocity 67
5.1.4 Pressure contour 72
5.2 Conclusion 74

List of Tables

1.1 Types of Solar Thermal collectors 9

3.1 Collector technical characteristics [20]. 35

List of Figures

1.1 Renewable energy sources . . . 8
1.2 outer schematic of a FPC [4] . . . 11
1.3 FPC Cutaway of main layers [17] . . . 11

2.1 Pipes Inside FPC [12] . . . 13
2.2 FPC design [12] . . . 14
2.3 FPC side view [12] . . . 14
2.4 Various types of flat-plate solar collector absorber configurations for liquid working fluid [12] . . . 17
2.5 FPC optical and thermal efficiency as a function of temperature difference [3] . . . 18
2.6 Conduction Process [6] . . . 19
2.7 Convection and Radiation Process [6] . . . 20
2.8 Laminar flow [7] . . . 21
2.9 Turbulent flow [7] . . . 21
2.10 The development of the flow starting from laminar to transitional to turbulent flow [7] . . . 21
2.11 Heat loss from the top [28] . . . 24
2.12 FPC heat transfer network [12] . . . 24
2.13 Fin and Tube dimensions [12] . . . 27
2.14 Energy balance on fin element [12] . . . 27
2.15 Energy balance on fin element [12] . . . 28
2.16 Fluid element [12] . . . 30

3.1 FPC measurements [20] . . . 34
3.2 FPC cross-section [20] . . . 35
3.3 FPC Tilt angle [20] . . . 36

4.1 ANSYS modules . . . 40
4.2 CFX fluid flow guide . . . 40
4.3 SPACECLAIM 3D environment . . . 41
4.4 Top Header pipe(green) and outlet pipe(orange) . . . 42
4.5 Main box region(purple) . . . 43
4.6 Overall view of the Mesh grid . . . 44
4.7 Pipe and header Mesh grid . . . 45
4.8 Fluid Domain . . . 46
4.9 Fluid Domain basic setting . . . 47
4.10 Fluid Domain - fluid model . . . 47
4.11 Fluid Domain - Initialization . . . 48

4.12 Inlet boundary settings 49
4.13 Inlet pipe region 49
4.14 Porous medium 50
4.15 Honeycomb region momentum source term 52
4.16 Selected regions for tilt angle correction 53
4.17 Selected region momentum source term 53
4.18 Outlet pipe boundary conditions 54
4.19 Outlet pipe region 54
4.20 Heat flux boundary condition 55
4.21 Heat flux - front face 55
4.22 Water Temperature dependence properties part 1 57
4.23 Water Temperature dependence properties part 2 57
4.24 Solver control basic settings 58
4.25 Energy equation time-step 59
4.26 Monitor point 2 location 60
4.27 Monitor point 1 expression definition 60
4.28 Monitor point 2 Cartesian definition 61

5.1 Momentum and mass convergence 63
5.2 heat transfer curve 64
5.3 Outlet temperature 65
5.4 Middle plane temperature 66
5.5 Experimental model temperature distribution [19] 67
5.6 CFD flow pattern 68
5.7 Experimental model flow pattern [20] 68
5.8 Top right region velocity vectors 69
5.9 Middle region velocity vectors 70
5.10 Upward stream above inlet pipe 70
5.11 Inlet stream lines 71
5.12 Outlet stream lines 71
5.13 Near the inlet pipe velocity vectors 72
5.14 Pressure contour at the middle plane 73

Chapter 1

Introduction

1.1 The need for renewable technologies

In today's world, Renewable energies are considered one of the key factors to achieve a sustainable development.Nowadays awareness about environmental issues such as pollution and global warming highlights the importance of reliable energy sources which can help the economy to grow without over exploiting the natural resources of a country. Usually the renewable energies have low carbon foot print and other emissions throughout their life cycles and it helps them to be more nature friendly compared to fossil fuel sources of energy. the problem with fossil fuels are not only the emissions and adverse impacts on the environment, but also it causes economic and political conflict due to its non uniform distribution. Except coal which can be found in most countries, the rest of the fossil fuels such as oil and gas are owned and controlled by a limited number of countries and it raises some problem regarding the energy security for the rest of the countries.

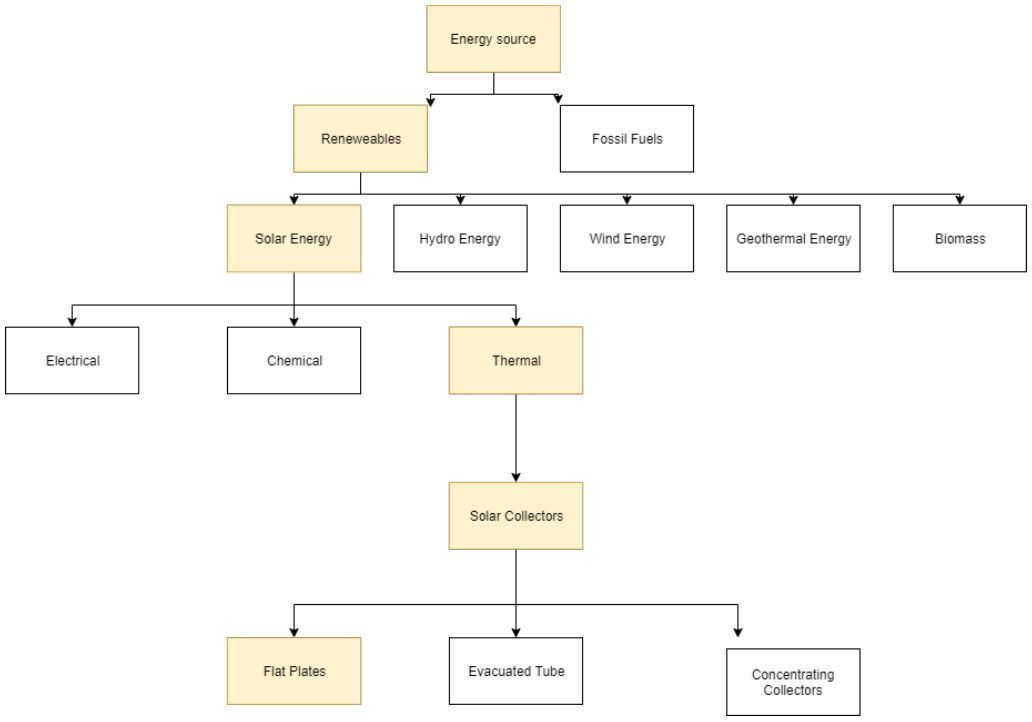

Figure 1.1: Renewable energy sources

However, renewable energies are not monopolized between some few countries and each country can benefit from a certain form of renewable sources which is available to its geography and weather. The Figure 1.1 shows different types of renewable energy sources and indicates the research focuses area of this thesis.

1.2 Solar thermal energy

The energy of the sun radiation can be absorbed and converted to heat as a form of useful energy. Its applications includes heating or cooling the space in a building, providing hot water, distillation, power generation and process heating. reducing the emissions such as green house gases and the independence of grid are some of the advantages for utilizing the solar heat energy.

1.3 Solar thermal collectors

in the recent years, with the rising energy demand and all the concerns about emissions and pollution's of fossil fuels, solar energy has became an attractive energy source. One of the ways to exploit the solar energy is to use solar thermal collectors to absorb the sun radiation and convert it to heat, then transfer it to a fluid flowing through the collector. this heated fluid can be both utilized directly or be stored in a storage tank from which it can be used in a later time.

concentrating and non-concentrating are two different categories of solar thermal collectors. a non-concentrating solar collector approximately has the same area of irradiation interception as the absorbing surface, while in concentrating collectors the absorbing area is much smaller than the intercepting lenses or mirrors which concentrate the light beams on the receiver. Since the radiation flux is higher in the concentrating collectors, they usually achieve higher temperatures compared to non-concentrating solar collectors [30]. Table 1.1 provides you with a list of solar thermal collector types and their characteristics [2].

Table 1.1: Types of Solar Thermal collectors

Motion	Collector type	Absorber type	Concentration ratio	Indicative temperature range (oC)
Stationary	Flat plate collector (FCP)	Flat	1	30-80
	Evacuated tube collector (ETC)	Flat	1	50-200
	Compound parabolic collector (CPC)	Tubular	1-5	60-240
Single axis tracking	Linear Fresnel reflector (LFR)	Tubular	10-40	60-250
	Parabolic trough collector (PTC)	Tubular	15-45	60-300
	Cylindrical trough collector (CTC)	Tubular	10-50	60-300
Two axis tracking	Parabolic dish reflector (PDR)	Point	100-1000	100-500
	Heliostat field collector (HFC)	Point	100-1500	150-2000

1.4 Research aim

The main focus of this study is to investigate the thermal performance of a polymer designed flat plat solar collector. The aim of this research project is to investigate

the possibility of using polymer material in production of solar flat plate collector design. Using the suggested material will result in more cost efficient flat plate collectors production while being more environmental friendly. this project work focuses on the process of energy conversion from the collector to the working fluid. This is accomplished by employing a polymer honeycomb structure placed as the channels of a collector to transfer heat to water as a working fluid. The other focus area is the fluid behaviour inside the collector and investigating the temperature, velocity and pressure patterns in different regions of the collector to gain a broader insight regarding the performance of the collector and its design.

This novel poly-carbonate collector is tested theoretically using Computational Fluid Dynamics (CFD) and the results was compared to experimental data available. The obtained CFD data and the experimental findings are coupled and show a good agreement. All the obtained results are validated with the literature. The result of the simulation clearly shows an acceptable performance of this polymer design and its efficiency is comparable to the classic models which costs more both in material and production. An in depth analysis of the results also revealed some weak points of the design such as re-circulation streams and the cause of the problem which help us calibrate and improve our further designs in future works.

1.5 Research scope

In this part we present a brief introduction about flat plate collectors and the extent to which the research area will be explored in the work and specifies the parameters within the study will be operating. Finally the thesis outline and a briefing about the focus points of this research article.

1.5.1 The need for flat plate solar collectors

The share of renewable energy is increasing in total energy demand and Among all types of renewable sources, solar energy is considerably receiving more attention because of its high potential and availability in most countries. One of the most used methods to exploit the sun radiation energy is by utilizing Solar thermal collectors because of their reasonable costs and simple design and structure. These collectors are easy to set up in building integrated applications and unlike tracking collectors such as parabolic collectors, no extra consideration regarding self shading or wind loading is needed [11].

The FPC(Flat plate collector) usually operates in the low-temperature range (less than 60°C) or in the medium temperature range (less than 100°C). FPC uses both direct beam and diffused radiations and do not need a lot of maintenance or tracking system. They are mostly used for water heating, building heating or air conditioning. it is also used for some applications regarding the process heat [26].

1.5.2 Introduction to the flat plate collectors

FPC is usually fixed in position and there is no need for tracking of the Sun. the orientation of The collectors should be directly toward the equator, facing south in the northern hemisphere and north in the southern hemisphere. The optimum tilt angle of the collector is approximately same as the latitude of the location with

angle variations of 10 to 15 degree. in figure 1.2 you can see the basic schematic of a flat plate collector [22].

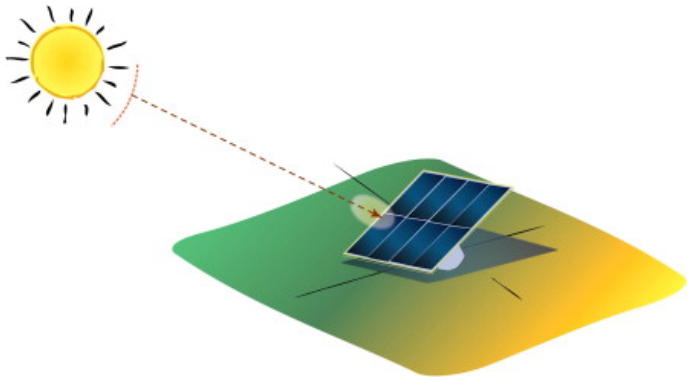

Figure 1.2: outer schematic of a FPC [4]

Flat plate collectors usually have two horizontal pipes in the top and bottom. the inlet pipe is connected to the bottom horizontal pipe from which the heat transfer fluid enters the collector and absorbs the heat from the absorber and moves upward until it reaches the top header and exits the system. If the system is direct, the fluid is connected to storage tank and in the indirect cases, it circulates in a closed cycle which is connected to the heat exchanger [21].

The outer glass of FPC is almost always made of low-iron tempered glass.The reason that flat plate collectors are considered to be the most durable type of collectors in the market is that tempering the glass helps it to be resilient to different weather conditions such as rain and hail. in figure 1.3 you can see the other layers including the absorber plate, pipes, the insulation to minimize the heat loss from back and side of FCP and the collector frame or case to keep the all parts together and protect the whole system from dust and moisture [21].

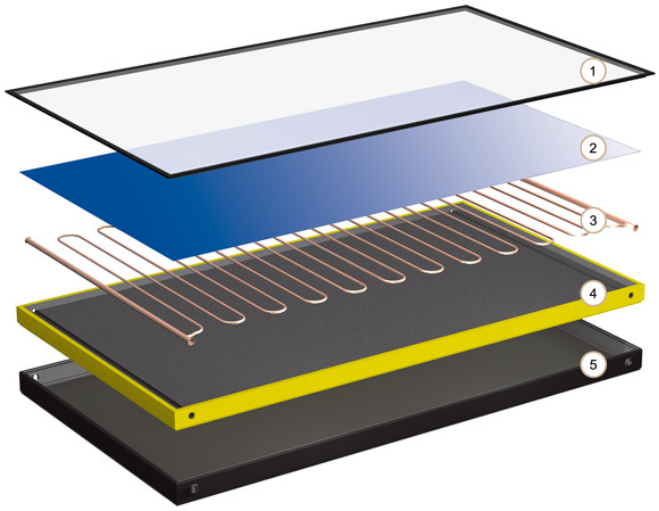

Figure 1.3: FPC Cutaway of main layers [17]

Materials most frequently used for absorber plates are copper, aluminum, and stainless steel. Materials most used for insulation are mineral wool, glass wool, and foam glass [22].

1.5.3 Research methodology

To investigate the efficiency of a flat plate collector, two key factors are considered. The optical performance of the collector and the heat loss. In this article we are focusing on computational fluid dynamics with ANSYS workbench 2020 R2 to determine the heat loss and compare the result with an already existing experimental data of the collector, operating in an indoor test.

1.5.4 Thesis outline

The thesis consists of five Chapters, dedicated to research and to the examination of flat plate solar water collectors and their features. The current Chapter contains information regarding the available renewable energy potentials, utilisation of solar energy over the years, and the need for solar collector technologies to exploit the available solar energy. Finally an analyses of how each chapter is formed and an outline of the research undertaken within that chapter.

Chapter 2 contains a literature review; an overview of solar water heating and different solar water heaters and collectors. An extensive description of absorber coatings and glazing for flat plate solar collectors and Various designs and improvements in Solar Water Systems. The mathematical modeling of a solar flat plate collector and related heat transfer and fluid dynamics theories are also included in this chapter.

Chapter 3 is a problem definition which explains the case study and its characteristics in detail. From the structure and measurements of our solar flat plate collector under investigation to the main issues and problems and the probable strategies to deal with these questions.

Chapter 4 includes a background work on CFD computations and the equations governing the problem. In the following, a step by step walk through of modeling a solar flat plate collector in ANSYS WORKBENCH R20 is presented. The reasoning behind every step, decision and also design ideas are also provided in this chapter.

Chapter 5 includes the results and interpreting the data from the CFD simulation and comparing it with experimental data available and finally the conclusion.

Chapter 2

Literature Review

2.1 Flat plate collectors design

As shown in Figure 2.1 and 2.2, a typical flat plate collector includes two sets of horizontal pipes at the top and bottom of the collector called headers which are connected to inlet and outlet pipes. In the main area of the collector which looks like a big rectangle, is the region where absorber plate is located. Therefore the sun radiation is absorbed in this region. The absorber plate is usually made of a metal sheet with good thermal conductivity. The reason for that is to make sure it absorbs the radiation in an efficient manner and also after absorbing the radiation and increase in its temperature, It should be able to transfer the heat to the working fluid inside the collector. To make this happen, Usually there are some vertical pipes inside this rectangular region which connects the bottom header to the top header. If the absorber plate is a single sheet, then this pipes are directly connected to the absorber plate. This method ensures that the heat conductivity condition is applied in its most optimized form [12]. On top of the flat plate collector, usually there

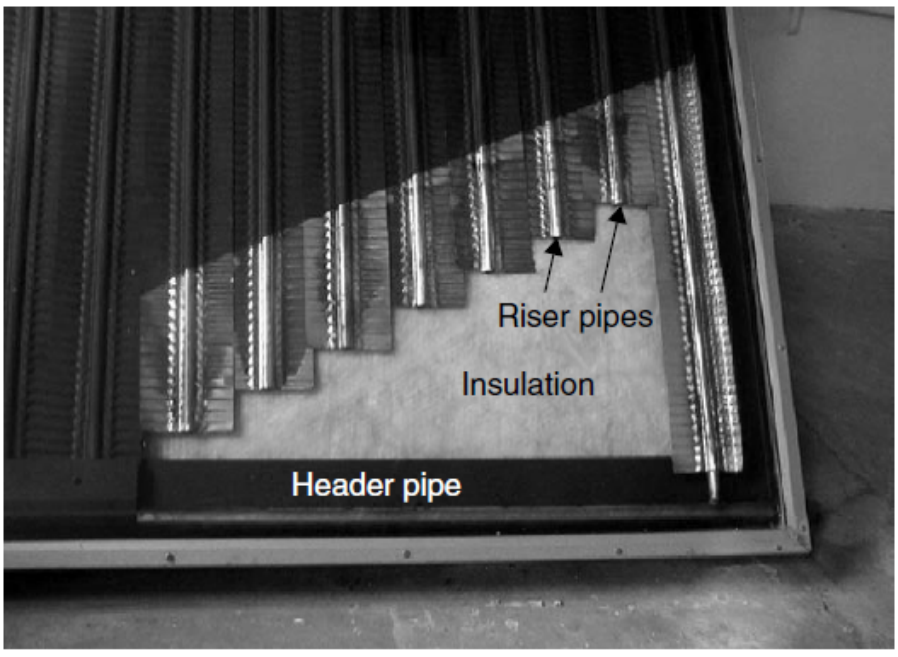

Figure 2.1: Pipes Inside FPC [12]

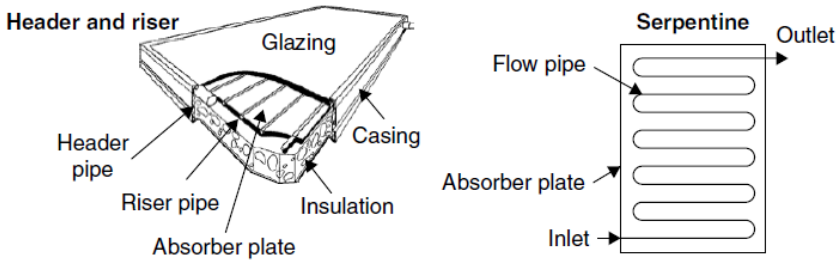

Figure 2.2: FPC design [12]

is a transparent cover made of glass and sometimes plastic. This transparent layer helps us reduce the heat loss from the collector especially in the form of convection. It creates an effect similar to green house effect in the collector which prevents the heat to escape from its environment while it lets the sun radiation to come inside the system. Not only it works for convection heat loss but also it minimizes the radiation heat loss. Because the materials used in this transparent layers are in a way that it is transparent to the short wave length coming from the sun but they will block the infrared radiation which is emitting form the absorber plate.

The main components of a flat-plate collector, as shown in Figure 2.3, are the following [12]:

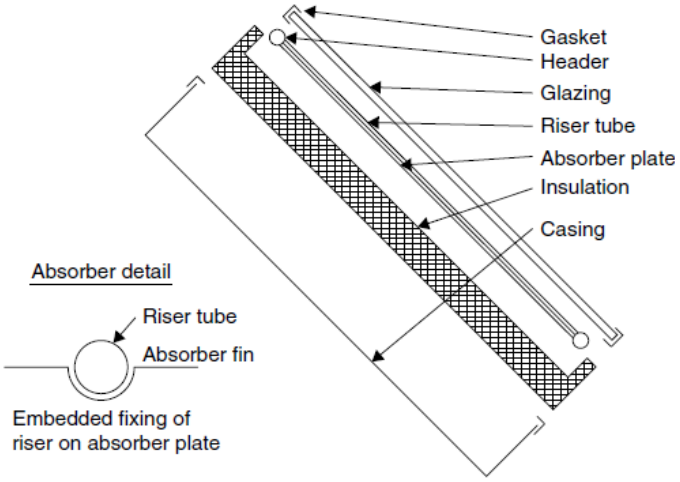

Figure 2.3: FPC side view [12]

- Cover
  One or more sheets of glass or trasnparent plastic.
- Heat removal fluid pipes and passageways
  The layer responsible for moving the working fluid from bottom header to the top header in the rectangular region. It is usually includes Tubes,pipes, fins, or passages which direct the working fluid from bottom header to the top header.
- Absorber plate
  It is a flat sheet made of metal with good conductivity. This sheet is usually

coated with some thin layers of materials which enhance the absorption and reduce the emission from the absorber plate.

- Headers
  Two horizontal pipes on the both top and bottom end of the collector. It is an area that from one side is connected to the main rectangular region of the collector and on the other side it is connected either to inlet or outlet.

- Insulation
  Materials with los heat conductivity to reduce the heat transfer both from conduction and convection in the sides and the back face of the flat plate collector.

- Case
  The casing which surrounds all the different parts of the flat plate collector which protects the components of the system from dust, moisture, and any other material which is going to cause corrosion.

A good flat plate collector design should be in a way that it ensure the maximum amount of energy absorbed from the sun radiation and transfer it to the working fluid in an efficient way. However, apart from this goal, it should also be cost efficient and requires minimum production and maintenance costs. One of the strategies to meet this goal is to increase the life of the system. This means that the flat plate collector should be made durable and be able to withstand many rough weather conditions and sudden changes in temperature and even shocks from impact of hail. Since the flat plate collectors are installed in an open environment exposed to rain and moisture, It should also be taken into consideration and we need to minimize the water penetration into the collector to avoid any corrosion. One of the strategies to make that happen is to use a tempered glass. in the following section, we talk in more detail about glazing and absorber plate.

2.1.1 Glazing materials

Glass is a material which has been widely used for glazing of the solar thermal collectors because it can allow as much as 90% of the incoming short-wave solar irradiation while blocking nearly all of the long-wave radiation emitted outward by the absorber plate. These glazing materials first give a durability to the glass to withstand the temperature change or even shocks from hail impact. Another advantages if glazing the glass is to enhance its optical properties to allow most parts of the light spectrum inside the system and block the long wave length radiation from the absorber plate. In some cases such as this research article, the glass is replaced with a transparent plastic or polymer sheet. This helps reduce the cost and weight of the collector but in some cases it can adversely effect the optical properties compared to glass. previously we have talked about water penetration and how it can reduce the life and performance of a flat plate collector. Another circumstance that comes to mind which may affect the performance of a flat plate collector is dust. It is shown that the effect of dirt and dust only reduces the transmittance by 2-4 % of the maximum value. During summertime when rain is less likely to happen, the collector surface may accumulate more amount of dust but since the magnitude of

sun radiation is high in this period of time, the dust actually protects the collector from overheating [1].

2.1.2 Collector absorber plates

To install a good absorber plate for our flat plate collector, we need to make sure it absorbs the maximum amount of incoming sun radiation and it loses the minimum amount of heat to the atmosphere. After absorbing the radiation and increase of its temperature, it should also be able to transfer this heat to the working fluid so that the temperature of outlet rises to the maximum temperature possible. The absorber plate itself is made of metal but there are some ways of coating that maximizes the absorption while minimizing the emitting radiation. This means that we need a selective surface for the absorber of a collector which should have a coating that has high absorptance for solar radiation (short wavelength) and a low emittance for re-radiation (long wavelength). The nature and the color of the coating and also the incident angle are the three main factors which determines the absorbtance of the collector. the black color is usually the best choice but it is possible to use other colors if necessary [31].
With a decent electrolyte or chemical treatment and suitable coating, it is possible to create a surface with high values of solar radiation absorptance (α) and low values of long-wave emittance (ε). since the collector surface tempreture is higher than the ambient air temperature, the role of the selective surface and coating becomes much more important. The cheapest absorber coating available is matte black paint; However, this is not selective, and the performance of a collector produced in this way is low, especially for operating temperatures more than $40°C$ above ambient [13].

There are variety of design principle to help us design and create a selective solar absorbing surface. Solar absorbers referred to as tandem absorbers, are based on two layers with different optical properties. A semiconducting or dielectric coating with high solar absorptance and high infrared transmittance on top of a nonselective, highly reflecting material such as metal constitutes one type of tandem absorber. Another way to do that is to coat a non-selective, highly absorbing material with a heat mirror that has a high solar transmittance and high infrared reflectance [33].

2.1.3 Collector construction

One of the most important steps for a collector to achieve high performance, is to transfer the absorbed heat to the working fluid with minimum loss. For this to happen, the riser pipes should be firmly bond to absorber plate to ensure the a good thermal bond between the tubes and absorber plate without causing a lot of extra cost for labor or material. One of the principle of our novel polymer collector is that we do not need an absorber plate and the working fluid itself works as the absorber material. This is very important to reduce the production cost and brings simplicity to the design. Most widely use materials for collector plates are copper,aluminum, and stainless steel. For some of the low temperature applications of solar collectors, it is also possible to use UV-resistant plastic extrusions. An important point of notice in the designing of a flat plate collector and its material selection phase is that If the entire collector area is in contact with the heat transfer fluid, the thermal

conductance of the material is not important. Again, since our proposed design fulfill this condition, we are not obliged to use materials with high thermal conductivity which reduce the cost of material even more. In the Figure 2.4 number of different possible design for the collector plate for liquid working fluid is shown.

Figure 2.4a shows a bonded sheet design, in which the fluid passages are integral to

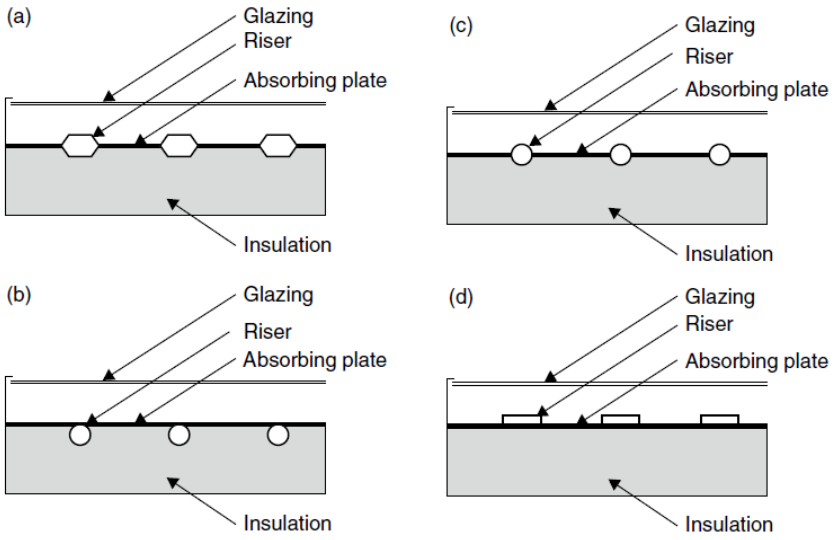

Figure 2.4: Various types of flat-plate solar collector absorber configurations for liquid working fluid [12]

the plate to ensure good thermal conduct between the metal and the fluid. Figures 2.4b and 2.4c show fluid heaters with tubes soldered, brazed, or otherwise fastened to upper or lower surfaces of sheets or strips of copper. Copper tubes are very popular in the applications with hot water or other working liquids fluids because they show a great resistance to corrosion. To reach a low cost bonding method, Thermal cement, clips, clamps, or twisted wires have been tried in many studies and designs. Figure 2.4d shows the use of extruded rectangular tubing to achieve a greater heat transfer area between tube and plate. To assemble this setup, Mechanical pressure, thermal cement, or brazing can be applied. Soft solder is not applicable because the high temperature of the collector plate can melt it down and damage the structure. However, In the polymer flat plate collector, we are avoiding all above mentioned problems of bonding the risers and absorber plate. The risers are replace with a honeycomb transparent polymer structure where working fluid can flow inside and the absorber plate is removed and the heat is directly absorbed by a water mixed with black ink as a working fluid and simultaneously an absorber material. The 1 to 1000 black ink solution in the water is to enhance the water ability to absorbed the radiation in an efficient way and it has been tested in the work of Martinopoulos and Misirlis [19].

2.2 Flat plate collectors mathematical modeling

Flat plate collectors are most widely used solar collectors in the world due to its simple manufacturing and low costs. The advantages of using a solar flat plate collectors are:

- Easy to manufacture.
- Low cost.
- Unlike concentrating collectors, FPC collects both direct beam and diffused radiation.
- Permanently fixed (no sophisticated positioning or tracking equipment is required).
- Little maintenance.

In order to predict the FPC energy performance, several mathematical models have been developed. However, the most embraced one is obtained by following the approach of Hottel-Whillier-Bliss.

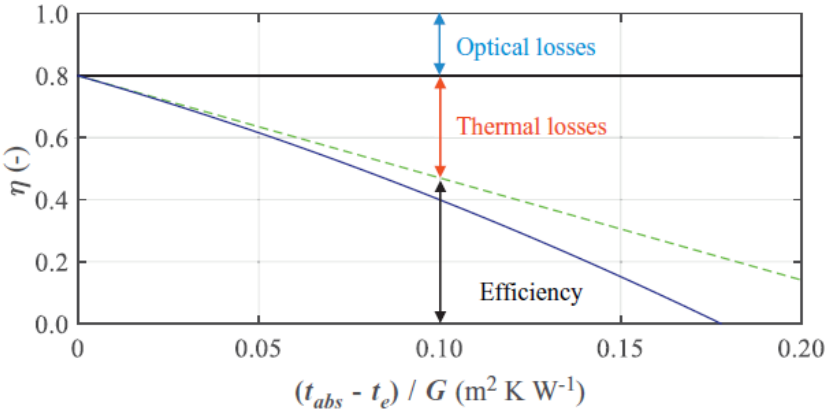

Figure 2.5: FPC optical and thermal efficiency as a function of temperature difference [3]

In Hottel-Whillier-Bliss approach first we estimate the total solar radiation available, then we try to calculate the absorbed thermal energy by the collector. Next, we investigate the heat loss from the back, sides and front of the flat plate collector and substitute it from the original absorbed heat. in the figure 2.5 we can see the efficiency of a flat plate collector, optical and thermal losses based on the temperature difference between the FPC and the ambient. As it is shown, the optical losses are indifferent to any changes in temperature difference since it is only function of geometry and optical parameters. On the other hand, as the temperature difference increases the heat loss increases [3]. The aim of the following sections in this chapter is to review the theoretical background regarding heat transfer and fluid mechanics which are necessary for us in order to have a better understanding of the flat plate collectors.

2.2.1 Heat Transfer

There are three different modes of heat transfer:

- Conduction

- Convection

- Radiation

Conduction happens when there is a temperature difference across a body in which the heat will transfer from the higher temperatures to the lower temperatures. Conduction process is shown in Figure 2.6.

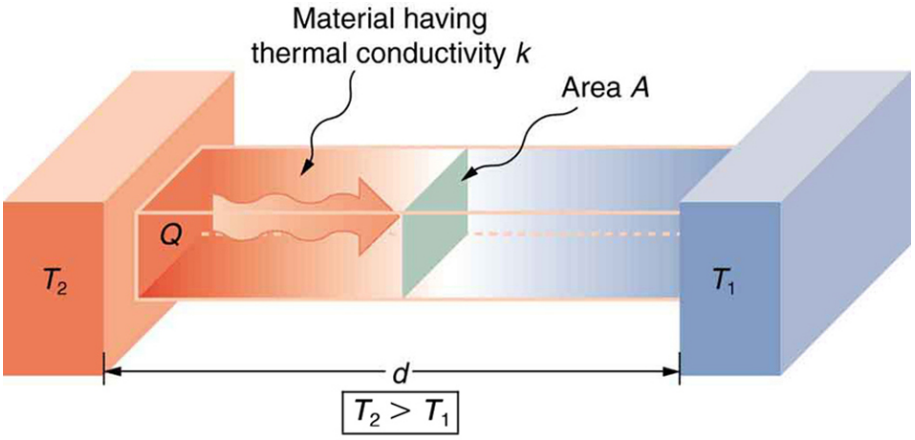

Figure 2.6: Conduction Process [6]

In physics and engineering the conduction rate is explained by Fourier equation:

$$\dot{q} = -kA\nabla T \tag{2.1}$$

Where $\dot{q}$ is the heat flow in watt, A is the area of conduction in heat flow direction and its unit is m^2, k is heat conductivity of the material in $W/m.K$.

∇T is the gradiant of temperature in K/m and it is calculated by:

$$\nabla T = \frac{\partial T}{\partial x}.\hat{i} + \frac{\partial T}{\partial y}.\hat{j} + \frac{\partial T}{\partial z}.\hat{k} \tag{2.2}$$

In pipes or tube shaped bodies the radial form of the Fourier equation is given by:

$$\dot{q_r} = -kA_r\frac{dT}{dr} \tag{2.3}$$

The next mode of heat transfer is convection. This usually happens when there is a motion of a fluid(gas or liquid) over a body. The rate of heat trasnfer by the convection process is given by the Newton law of cooling:

$$\dot{q} = hA_s\Delta T \tag{2.4}$$

where h is the convection heat transfer coefficient in W/m^2K and describes the ability of the fluid to transfer heat via convection. A_s is the respective surface area where convection is happening, ΔT is the temperature difference between the surface temperature T_s and the fluid temperature T_f.

Convection can happen in two forms. First the natural convection where the motion of the fluid is caused by the fluid energy itself and the heated part of the fluid will have a decline in density and will be replaced by a lower temperature fluid

and creates a circulating flow.This phenomenon allows the fluid to continue the heat transfer process in a natural cycle. On the other hand this circulating flow can be created by external sources such as pumps or fans called forced convection and it will increase the heat transfer via convection drastically. The effect of the natural or forced convection is hidden in the convection heat transfer coefficient h in Newton formula.

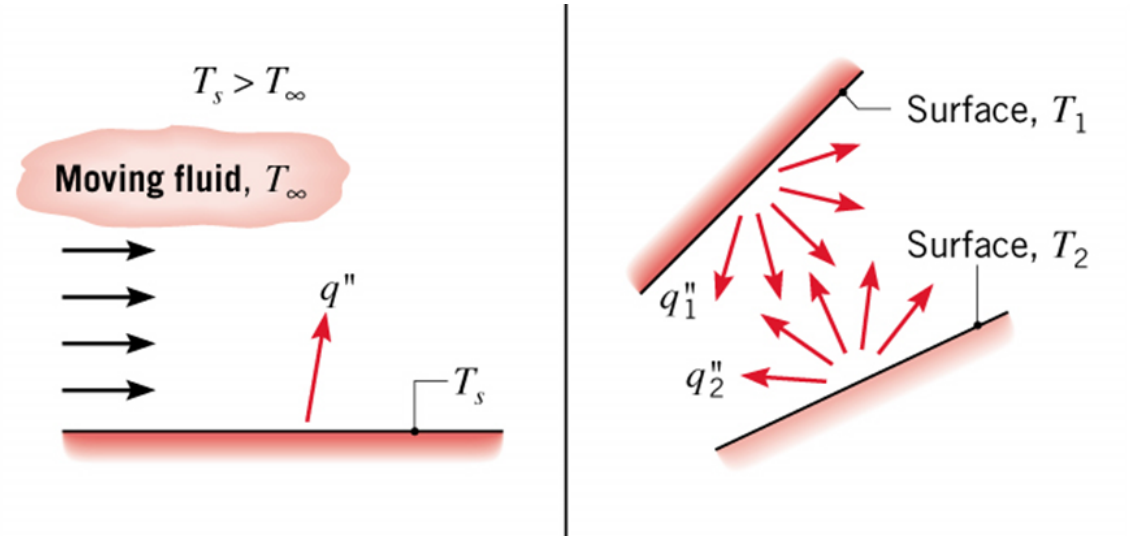

Figure 2.7: Convection and Radiation Process [6]

The third process which allows the heat transfer to happen is called radiation. All objects with higher temperature than 0° kelvin emit radiation. The emitted Energy from an object with temperature T_s is described by:

$$E = \sigma \varepsilon T_s^4 \tag{2.5}$$

Where ε is emissivity ($\varepsilon = 1$ is black body), T_s is the tempreture of the surface of the body and σ is the Stefan Boltzman constant. The rate of the heat exchange via radiation is described by Stefan Boltzmann's law:

$$\dot{q} = \sigma A(T_s^4 - T_a^4) \tag{2.6}$$

Where T_a is the ambient temperature. Figure 2.7 shows how heat transfer happens in the convection and radiation modes.

2.2.2 Fluid Mechanics

Different types of flows can be separated into three groups.

- Laminar
- Turbulent
- Transitional

As it is shown in the Figure 2.8 Laminar Flows are recognized by the smooth movement of the flow particles in layers on top of each other. Usually the particles do not interact with each other and follow their own straight pass.

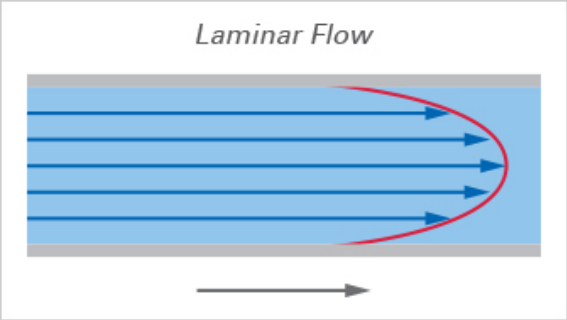

Figure 2.8: Laminar flow [7]

On the other hand, in Figure 2.9 it is obvious that the flow is a flow which its particles move in a chaotic an arbitrary manner and always under constant change of velocity and pressure.

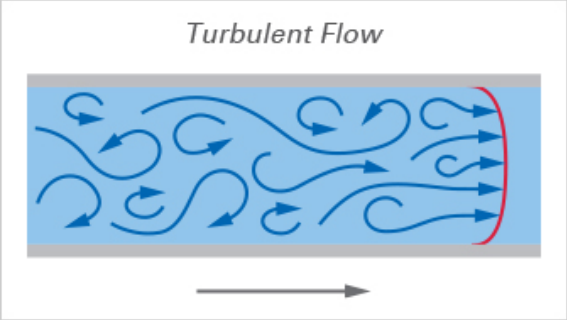

Figure 2.9: Turbulent flow [7]

When the flow shows both of the characteristics from laminar and turbulent, then it is transitional flow. Usually it happens during the development stage of the flow and it can be both in the direction of laminar to turbulent or from turbulent to laminar flow. in Figure 2.10 the different stage of a flow is being shown. All being said, there is always a need to measure these flow types in a quantitative and more accurate way.

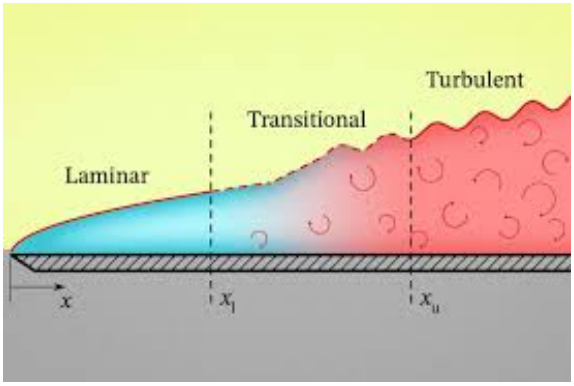

Figure 2.10: The development of the flow starting from laminar to transitional to turbulent flow [7]

Reynolds number

To define the state of flow in a quantitative manner, it is common to look at each flows Reynolds number. The flow in pipes is laminar if it has a Reynolds number smaller than 2300. if the Reynolds number is greater than 4000 it is assumed to be turbulent. Any value between these two is defined as transitional flow. The Reynolds number itself can be calculated using the following formula:

$$Re = \frac{vD\rho}{\mu} \tag{2.7}$$

In which the mean flow velocity is v, the pipe diameter is D, the flow density is shown as ρ and the fluid dynamic viscosity is μ. Another important equation we can use after obtaining the Reynolds number is head loss equation.

$$h_f = \frac{fLV^2}{2Dg} \tag{2.8}$$

In this equation the h_f is head loss, f is friction factor, V is the mean flow velocity and g is the acceleration of gravity. The head loss equation can also be written in terms of pressure drop:

$$\Delta P = f\frac{L\rho V^2}{2D} \tag{2.9}$$

In laminar flows the f is roughly equal to 64/Re. For other situations it is necessary to use the moody chart in order to estimate the friction factor. there are also many formulas to estimate f such as Colebrook-White or Swamee-Jain equations. Here we introduce the Swamee-jain equation but it is possible to use other available equations as pleased.

$$f = \frac{0.25}{\left\{\log\left[\frac{e}{3.7D} + \frac{5.74}{Re^{0.9}}\right]\right\}^2} \tag{2.10}$$

2.2.3 Solar Radiation Absorbtion

To calculate the flat plate collector performance, first we need to know how much of the sun beam radiation is absorbed by the collector. The sun radiation is separated into three categories:

- Direct beam
- Diffused radiation
- ground reflected radiation

Using the isotropic model for sky and sun radiation we calculate S, the absorbed radiation in the absorber-plate of the FPC unit [18]:

$$S = I_b R_b(\tau\alpha)_b + I_d(\tau\alpha)_d\left(\frac{1+\cos\beta}{2}\right) + (I_b + I_d)(\tau\alpha)_g\rho_g\left(\frac{1-\cos\beta}{2}\right) \tag{2.11}$$

Here in this equation, the subscript d, b and g stands for diffused, direct beam and ground beam. I is the intensity of radiation on a horizontal surface, $(\tau\alpha)$ the transmittance absorbance product that represents the effective absorbance of the cover-plate system, the collector slope, ρ_g the diffuse reflections of ground and R_b the ratio of beam radiation on the tilted surface to that on a horizontal surface.

2.2.4 Total energy balance of FPC

The total energy balance of the flat plate collector can be obtained by subtracting the total energy loss from the absorbed energy of sun radiation. In other words, we have already calculated the S in previous section and if there was a way to calculate the total heat loss of the FPC, we could calculate the total Useful energy Q_u.

$$Q_u = A_c[S - U_L(T_{pm} - T_a)] \tag{2.12}$$

This equation is nothing more than total energy absorbed $(A_c \cdot S)$ minus the heat loss derived from Newton cooling law where U_L is the heat transfer coefficient, A_C is the area, T_{pm} is the plate temperature and T_a is the ambient temperature.

https://scialert.net/fulltext/?doi=rjp.2007.35.41

2.2.5 Heat loss

To Determine Q_u from the equation 2.12 we need to calculate the U_L which is the total heat loss from the flat plate collector. Total heat loss can be divided into three parts. The loss from the back of the collector, edge loss and the loss from the top face. Among these three, the loss from the edge and back are easy to calculate since it is only related to the conductivity of those areas and the thickness of the material. For the top face however, the loss due to the radiation should also be taken into consideration. There is also two layer involved in the top heat loss modeling. First the glass cover of the flat plate collector which is the top first layer but also under this layer of glass we have a metal absorber plate. While writing the heat transfer equations for modeling this part, we need to consider that there is heat transfer between these layers and also heat transfer between the ambient(sky) and the glass cover as shown in Figure 2.11. Another factor which should be taken into consideration while modeling the top heat loss is the natural convection between these two parallel plates with a tilt angel from horizon.

$$U_L = U_t + U_b + U_e \tag{2.13}$$

Where in equation 2.13, U_L is the total heatloss, U_t is the loss from the top, U_b is back loss and the U_e is the loss from the sides.

To calculate the back heat loss, ideally we need to consider all three modes of heat transfer which is radiation, convection and conduction. However, since in a well designed flat plat collector the back side is very well insulated and the thermal resistance of the insulation in magnitude is high, the share of the convection and radiation is much more smaller than the share of conduction and therefore negligible.

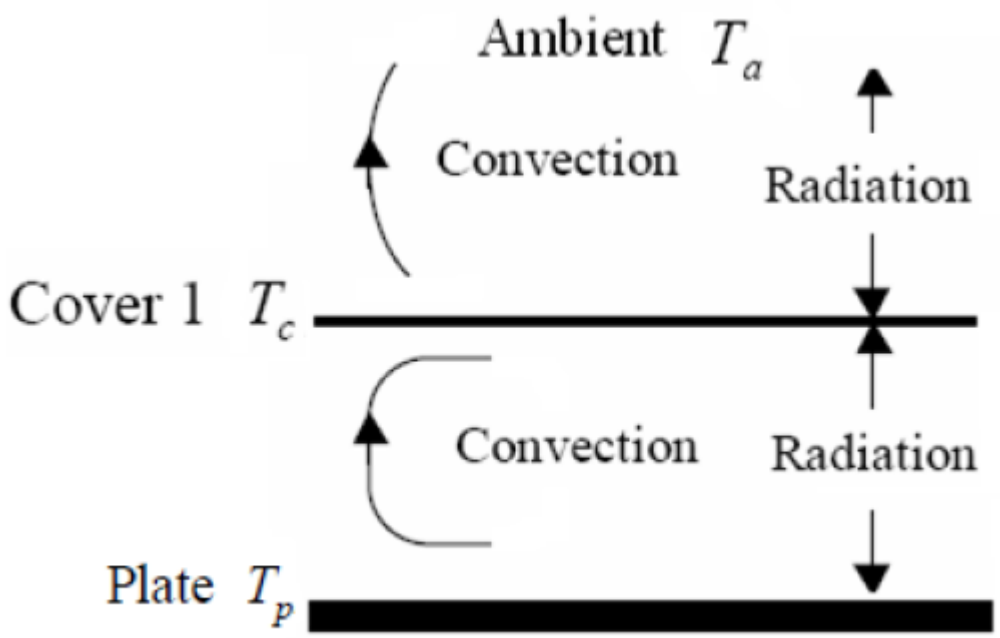

Figure 2.11: Heat loss from the top [28]

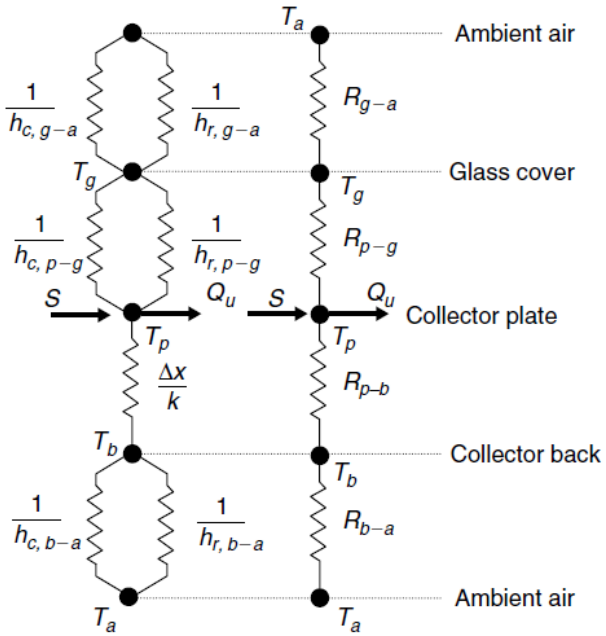

Figure 2.12: FPC heat transfer network [12]

The heat loss from the back with a good approximation can be written as:

$$Q_b = \frac{K_b}{L_b} A_b \left(T_{pm} - T_a\right) \tag{2.14}$$

where A_b is the back side of the collector area, K_b and L_b are the back insulation thermal conductivity and thickness, respectively.

To calculate the edges heat loss, we need to assume that there is one-dimensional sideways heat flow around the perimeter of the collector,and the rest of the procedure is similar to the back loss. The edge heat losses can be estimated by:

$$Q_e = \frac{K_e}{L_e} A_e \left(T_{pm} - T_a\right) \tag{2.15}$$

where K_e and L_e are the edge insulation thermal conductivity and thickness, respectively while A_e is the side area of the flat plate collector.

To calculate the top heat loss, Hottel and Woertz [10] introduced an equation for the estimation of energy transferred to the glass cover and later on Klein [14] had modified this equation to estimate the Top heat loss coefficient U_t:

$$U_t = \left[\frac{N}{\frac{C}{T_{pm}}\left(\frac{T_{pm}-T_a}{N+f}\right)^e} + \frac{1}{h_w}\right]^{-1} + \frac{\sigma(T_{pm}+T_a)(T_{pm}^2+T_a^2)}{\left(\epsilon_p + 0.0059Nh_w\right)^{-1} + \frac{2N+f-1+0.133\epsilon_p}{\epsilon_g} - N} \tag{2.16}$$

where is the Stefan-Boltzmann constant, N is the number of top glass covers which is 1 in our case, is the collector tilt, ϵ_g is the emissivity of the glass, ϵ_p is the emissivity of the absorber plate, T_a is the ambient temperature, T_{pm} is the mean plate temperature and h_w is the wind heat transfer coefficient. The value of f, c and e for tilts $0°< \beta <70°$ are given by the equations below:

$$f = (1 + 0.089h_w - 0.1166h_w\epsilon_p)(1 + 0.07866N) \tag{2.17}$$

$$C = 520(10.000051\beta^2) \tag{2.18}$$

$$e = 0.43(\frac{1-100}{T_{pm}}) \tag{2.19}$$

To finally solve the equation 2.16, the last missing piece of puzzle is The convective heat transfer coefficient h_w. To obtain h_w, first we should introduce Nusselt number Nu. The Nusselt number In fluid dynamics, is the ratio of convective to conductive heat transfer at a boundary in a fluid. Convection uses two mechanism to transfer heat and the first one of them is advection(fluid motion) which is same as fluid mixing and the other mechanism is diffusion(conduction). In case of Nusselt number equal to one, represents heat transfer by only pure conduction [7]. If the value of Nusselt number is something between one and ten($1 < Nu < 10$), then the fluid motion is recognized as slug flow or laminar flow. If the Nusselt number has values greater than ten then it means that the share of convection is much more higher than the conduction and it usually happens in a turbulent flow. In a fully turbulent flow Nusselt number is typically in the range of 100-1000 [25]. To define

define Nusselt number we use:

$$Nu = \frac{hL}{k} \tag{2.20}$$

wehre L is the respective characteristic length or area of convection, k is the thermal conductivity of the fluid. If there was a way to calculate the Nu from a way other than the equation 2.20, then we could use the equation 2.20 to obtain h which is the convection coefficient. Fortunately, there are lots of formulas introduced by different researchers to estimate the Nusselt number in different conditions. Here we introduce the one which is more suitable for this article approach. This equation was introduced by Hollands [9] as:

$$Nu = 1 + 1.44\left[1 - \frac{1708}{\cos\beta.Ra}\right]\left[1 - \frac{\sin(1.8\beta)^{1.6}.1708}{\cos\beta.Ra}\right] + \left[\left(\frac{\cos\beta.Ra}{5830}\right)^{1/3} - 1\right] \tag{2.21}$$

Where Rayleigh number Ra itself is defined as:

$$Ra = \frac{g\beta(\Delta T)d^3}{\upsilon^2} \times Pr \tag{2.22}$$

Where Pr is the Prandtl number.

Now, we gathered every missing piece of the puzzle to calculate the top heat loss U_t from a flat plate collector.

To calculate the collector useful gain, it is important to know the average temperature of the absorber plate which is a complicated function of temperature distribution on the absorber plate, bond conductivity, heat transfer inside of tubes and some other parameters regarding the geometry of the system. To consider these factors along with the energy collected at the absorber plate and the heat loss, the collector efficiency factor and the collector heat removal factor are introduced [32].

2.2.6 Efficiency factor of a collector

In this section we need to introduce the collector efficiency factor F' which is a parameter that shows the temperature distribution in the collector absorber plate in the distance between two riser pipe. The way this parameter is calculated is to think of the temperature gradient only in the direction of the line connecting the two pipes and considering that the temperature is not changing significantly in the direction of the flow so we can disregard it and treat the problem as a 1 dimensional heat transfer case [8].

In Figure 2.13 you can see the absorber plate and the riser pipe connected to it. This is a figure to depict the top heat loss from the absorber plate in a flat plate collector. As shown in the figure, the distance between the tubes is W, the tube diameter is D and the inner diameter of the tube is D_i. The fin, which is the distance between two riser pipe is $(W-D)/2$ long which is shown in the Figure 2.14. The temperature above the pipe which is absorber plate is T_b while the absorber plate thickness is δ and T_b and T_f are the local base temperature and the fluid temperature, respectively.

Similar to a good conductor of electricity where we consider the electric field to be zero, the absorber plate is also a good conductor of heat where we can approximately claim that the temperature gradient through this metal sheet is negligible.

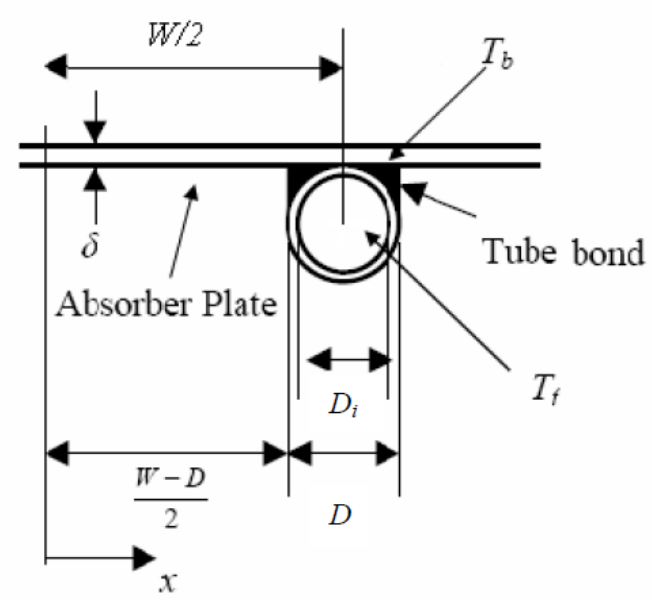

Figure 2.13: Fin and Tube dimensions [12]

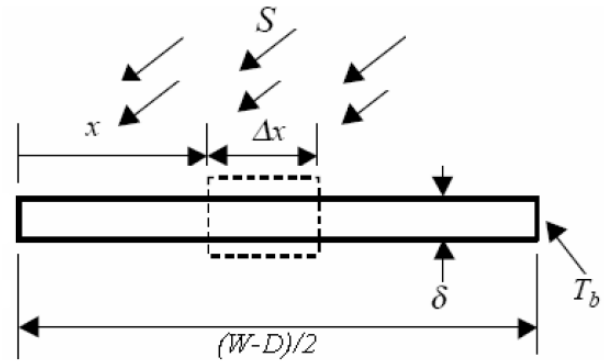

Figure 2.14: Energy balance on fin element [12]

Therefore, the region between the center line separating the tubes and the tube base can be considered as a classical fin problem [27].

Figure 2.14 and 2.15 are showing a tiny element including a distance equal to the fin distance, and it shows the heat flux coming in as sun radiation and also it shows the direction of the flow. By applying the law of energy balance on the fin element based on the Figure 2.14 and 2.15, the following equation is obtained:

$$\frac{d^2T}{dx^2} = \frac{U_L}{k\delta}(T - T_a - \frac{S}{U_L}) \tag{2.23}$$

There are two boundary conditions in this problem which helps us define our case and derive the equation expressing our problem. These boundary conditions are the insulated side of the fin and the base temperature T_b showing in the next two equations.

$$\left.\frac{dT}{dx}\right|_{x=0} = 0 \tag{2.24}$$

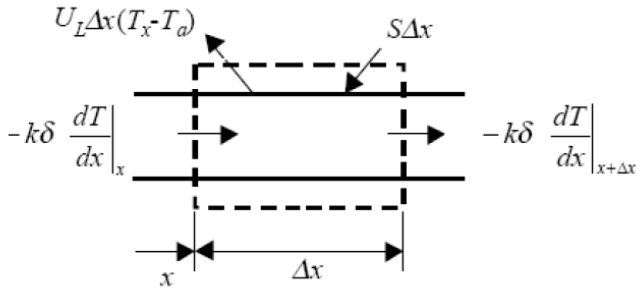

Figure 2.15: Energy balance on fin element [12]

$$T|_{x=\frac{W-D}{2}} = T_b \tag{2.25}$$

The amount of energy in the form of heat which was conducted to the region of the tube per unit length in the flow direction is given by:

$$q'_{fin} = (W - D)F[S - U_L(T_b - T_a)] \tag{2.26}$$

There is a new function F introduced here which stands for the standard fin efficiency of a straight fin with rectangular profiles [27] and it is given by equation 2.27 :

$$F = \frac{\tanh[m(W - D)/2]}{m(W - D)/2} \tag{2.27}$$

where the parameter m equals to:

$$m = \sqrt{\frac{U_L}{k\delta}} \tag{2.28}$$

The energy which was collected above the tube area is also a part of the useful energy gain and we need to consider it in the total gained energy. Thus, it is calculated as below:

$$q'_{tube} = D[S - U_L(T_b - T_a)] \tag{2.29}$$

In addition, the useful gain for the q'_u per unit length in the flow direction for the fin and tube which is the same as the sum of q'_{fin} and q'_{tube} is given by:

$$q'_u = [F(W - D) + D][S - U_L(T_b - T_a)] \tag{2.30}$$

So far, we have calculated the total useful energy gained by the collector q_u. By applying the energy conservation law, we can say that the same amount of energy calculated above needs to be transferred to the working fluid. This happens by the thermal conduction bonds which we discussed in previous sections. The better this bonds are design, the more efficient our collector would work. After this conduction transfers heat to the tubes near the working fluid, then the heat transfer happens via convection to transfer the heat to the working fluid itself. based on above, The useful energy gain per unit of length in the flow direction can be expressed as:

$$q'_u = \frac{T_b - T_f}{\frac{1}{h_{fi}\pi D_i} + \frac{1}{C_b}} \tag{2.31}$$

where, D_i is the inner diameter of a tube, h_{fi} the forced-convection heat transfer coefficient inside of the tubes, T_f the local fluid temperature and C_b the bond conductance.

Finally, our purpose was to introduce the efficiency factor in this section. This is done By eliminating T_b and by introducing the collector efficiency factor F the expression for the useful gain is:

$$q'_u = WF'[S - U_L(T_f - T_a)] \tag{2.32}$$

where the collector efficiency F is given by:

$$F' = \frac{1/U_L}{W[\frac{1}{U_L[D+(W-D)]F} + \frac{1}{C_b} + \frac{1}{\pi D_i h_{fi}}]} \tag{2.33}$$

To connect what we have so far with the characteristic of the working fluid in order to find the temperature change in the fluid, we again point out this fact that all the useful energy gained is going to be absorbed by the working fluid as shown in Figure 2.16. Of course it is just and approximation to simplify our problem in a way that it can be derived via derivative equations governing the physics of a flat plate collector. In reality, there is always heat losses which can not be taken into consideration and hurts the accuracy of our calculation. The numerical analysis methods helps us further overcome this problem but in this section, our goal is only to establish a mathematical model for our collector so it is acceptable to progress with some extent of approximation to simplify the problem, Thus, applying the energy conservation on the system shown in Figure 2.15 and substituting q'_u from equation 2.32, leads us to:

$$\frac{\dot{m}C_p dT_f}{dy} - nWF'[S - U_L(T_f - T_a)] = 0 \tag{2.34}$$

In this equation $\dot{m}$ is the total flow rate of the flat plate collector, which is the same as the inlet mass flow rate which can easily be calculated by the velocity of the flow at the inlet and the are of the inlet pipe. n is the number of tubes and T_f is the temperature of the working fluid at any location in y axis. since we assumed that F' and U_L are independent of position in our coordination system, the fluid temperature at any position y can be calculated from:

$$\frac{T_{fo} - T_a - S/U_L}{T_{fi} - T_a - S/U_L} = exp(-\frac{U_L nWyF'}{\dot{m}C_p}) \tag{2.35}$$

where nWy is equal to the area of the collector A_c ($nWy = A_c$). By replacing it into the equation 2.35 and further simplifying it we have:

$$\frac{T_{fo} - T_a - S/U_L}{T_{fi} - T_a - S/U_L} = exp(-\frac{A_c U_L f'}{\dot{m}C_p}) \tag{2.36}$$

Therefore T_{fo} is equal to:

$$T_{fo} = (T_{fi} - T_a - S/U_L)exp(-\frac{A_c U_L F'}{\dot{m}C_p}) + \left(T_a + \frac{S}{U_L}\right) \tag{2.37}$$

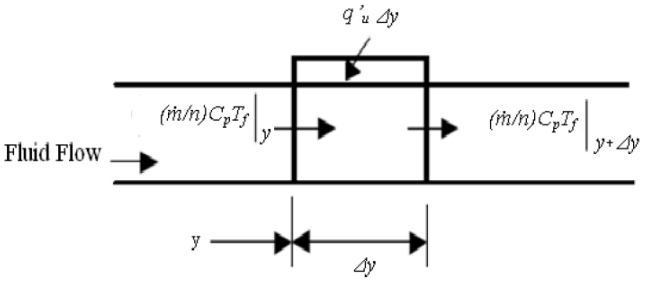

Figure 2.16: Fluid element [12]

2.2.7 Heat removal factor

In this section our goal is to introduce a new factor which helps us in the mathematical modeling of the flat plate collector. The heat removal factor F_R which is a value that relates the maximum possible useful energy gained to the actual useful energy gained. As you can notice, the concept of this factor is very similar to the corrections made while comparing the real efficiency of a system and its nominal value. For the following equations to be logically correct, we need to make this assumption that the temperature in any point of the absorber plate of the collector is a single value as the working fluid enters the system from the inlet pipe. This is an assumttiopn neccesary to make since without it, the problem is too complicated that it would be impossible to try and establish a mathematical understanding of a collector without numerical or computational methods. Therefore we have:

$$F_R = \frac{\dot{m}C_p(T_o - T_i)}{A_c[S - U_L(T_i - T_a)]} \tag{2.38}$$

in The equation 2.38 the term T_o is the fluid output temperature at the end of the outlet pipe which we had already calculated using equation 2.35 in the previos section and replacing the tube length L for y. Then we can express the heat removal factor F_R as:

$$F_R = \frac{\dot{m}C_p}{A_c U_l}[1 - exp(\frac{A_c U_L F'}{\dot{m}C_p})] \tag{2.39}$$

It is worthy to point out that the collector heat removal factor formula that we calculated here is the equivalent to the effectiveness of a conventional heat exchanger [24]. Meaning that the thermal part of a flat plate collector have the same physics as a conventional heat exchanger. The collector heat removal factor times this maximum possible useful energy gain is equal to the actual useful energy gain Q_u when F_R and the overall heat transfer coefficient are used in equation2.12. So the actual useful energy gain Q_u is given by:

$$Q_u = A_c F_R[S - U_L(T_i - T_a)] \tag{2.40}$$

This is a very useful and important equation and applies to all flat plate collectors. Now we found out a way to calculate the energy gained as a function of the temperature of inlet working fluid that is usually known and very convenient to obtain. Before introducing the efficiency factor and heat removal factor of a flat plate solar collector, we had to use the mean plate temperature which as explained is a very

complicated quantity to estimate [24]. By introducing this factor, now we can more easily design a flat plate collector efficiency since a designer has more control over the input parameters than the output. By finding a relation between inlet temperature and the final efficiency of the collector, now it is very easy to have a general estimation of what kind of collector we are designing.

2.2.8 Flat plate collector efficiency η

The efficiency of an energy system is determined by dividing the total energy of desired output leaving the system boundary by the total energy entering the system. Similar to every other system, the performance efficiency is defined as output divided by input. In the case of flat plate collectors, the efficiency η can be calculated as the ratio of useful energy gained, by the total energy the system was received which is equal to the Solar energy radiated to the area of the flat plate collector in a specific period of time. Therefore:

$$\eta_i = \frac{\int Q_u dt}{A_c \int G_t dt} \tag{2.41}$$

G_t is a value to determine the irradiance on a tilted plates and its values can be found in the available charts. To derive the above equation into a more physically understandable equation, we replace the Q_u with what we had calculated in the last section. therefore we can rewrite the instantaneous efficiency η_i as:

$$\eta_i = \frac{Q_u}{A_c G_t} = F_R(\tau\alpha) - F_R U_L \frac{(T_i - T_a)}{G_t} \tag{2.42}$$

As mentioned before, the term G_t provides us with the absorbed radiation energy where $(\tau\alpha)$ is the transmittance absorbptance product. The term $F_R(\tau\alpha)$ indicates how energy is absorbed by the collector and $F_R U_L$ indicates how energy is lost by the collector. For incident angles below about 35°, the product $(\tau \times \alpha)$ is essentially constant and equations 2.40 and 2.42 are linear with respect to the parameter $(T_i - T_a)/G_t$, as long as U_L remains constant [29].

In the experimental models, we do not need to follow this complicated procedure to find out the efficiency of the flat plate collector. In those cases it is just needed to monitor the inlet and outlet temperature of the working fluid. While it is done, the following equation will provide us with the collector efficiency:

$$\eta = \frac{Energy\ exits\ the\ system}{Energy\ enters\ the\ system} \tag{2.43}$$

so it leads us to:

$$\eta = \frac{\dot{m} C_p (T_{outlet} - T_{Inlet})}{A_C I_T} \tag{2.44}$$

The variables in the above equation are defined as:

- $\dot{m}$: Mass flow rate
- C_p: Specific thermal capacity
- A_C: Heat flux boundary layer area
- I_T: solar radiation in the collector plane

- T_{outlet} Flow temperature at the outlet
- T_{Inlet} Flow temperature at the inlet

Now that we obtained an expression to calculate the collector efficiency, the mathematical modeling of the flat plate collectors is finished and we are moving to the next chapter titled as problem definition. In the next chapter we are going to define our polymer collector case in detail and address the potential ideas and the potential ways and strategies to solve these problems.

Chapter 3

Problem Definition

In this section, we are going to explain our case study in more details and the flat plate collectors characteristic that is going to be modeled by using ANSYS WORKBENCH R20 software.

3.1 Collector parameters

The solar flat plate collector that is going to be computationally investigated in this article was originally proposed as a polymer solar collector with hopes to further reduce the production and maintenance costs while keeping the efficiency of the system as high as the classic types of flat plate collectors [20]. Flat plate collectors performance depends on various parameters which can be divided into two main group. The design and operation parameters. Design parameters are those which contain the shape or materials used in the collector such as number of covers, the type and thickness of glazing, the anti-reflecting coating on cover glass, the type of coating on the collector plate, the spacing between the collector and the inner glass, the type and thickness of insulation used, etc. Operation parameters affecting the performance of a solar collector include the mass flow rate of fluid, the amount of incident solar radiation, the inlet and ambient temperatures and sky conditions.

In the design of the collector, the box which includes the collector plate is 1055mm height and 1495mm width. in the top and bottom of this box there is two horizontal pipes, top and bottom header, each with 35mm diameters. for the heat transfer flow to enter the collector, it enters from the inlet pipe and connects to bottom header in 345mm from the corner of collector and from the bottom header the water which works as our heat transfer fluid will be distributed throughout the collector. the whole setup of the collector and its measurements with the location of inlet and outlet is shown in Fig 3.1.

after the transfer fluid is heated by the energy of collector plate, it will start to expand and move upward until it reaches the top header. The top header is connected to the outlet pipe located in the 265mm far from of the opposite top corner. The heated water will be gathered by the outlet pipe and moves to the storage tank. For the glazing, a 3mm thick solid, transparent UV stabilized LEXAN sheet was used to increase the optical and thermal performance. For insulating the back side of the collector, a nanogel filled honeycombed LEXAN sheet of a 10 mm thickness. for the side of the box insulation a 30mm thick extruded polyurethane was used.Inside the main box of the collector which is the absorber plate and the

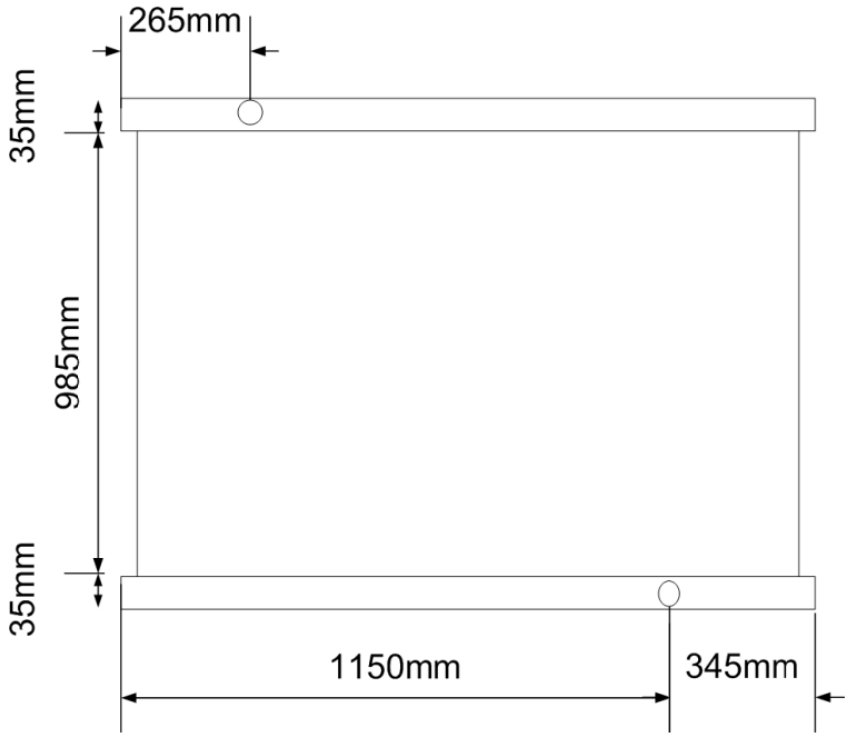

Figure 3.1: FPC measurements [20]

region where fluid is flowing between the op and bottom header is filled with a honeycomb structure which the working fluid moves inside this structure. All of the parts that mentioned above are packed and held in an aluminium casing. In Fig 3.2 a cross-section of the collector and how different parts of the collector is assembled inside the aluminium casing is shown.

The solar flat plate collectors usually operate between 267K–383K temperature so the materials used in the production of the system should be able to withstand this temperature range for a long time which is equal to FPC lifetime because it will assure one of the solar flat plate collectors advantages which is the low maintenance cost during its operation life. in the following Table 3.1 some of the main characteristics of our FPC system is summarized.

One of the most important operation parameters is the heat carrier fluid mass flow rate. The mass flow of our case study FPC is set to 0.028 kg/s . for the experimental unit, The inlet temperature of the heat carrier solution was appropriately set before every measurement, starting from $303K$ (ambient temperature). In order to ensure steady state operation, the system was in operation at least for 10 min before each measurement. During the measurement, the solar radiation was higher than $800W/m^2$, the optical field of the collector was not shaded by more than 5% and the wind velocity was in the 2–4 m/s range [20]. To solve our problem computationally, we are also going to use the same boundary conditions as mentioned above for each individual boundary. Another factor that should be considered is the tilt angle of the collector because as previously mentioned in chapter 2 it can affect the efficiency of the whole unit because of two reasons. First, the collector optical performance and the amount of sun radiation it can potentially absorb, but

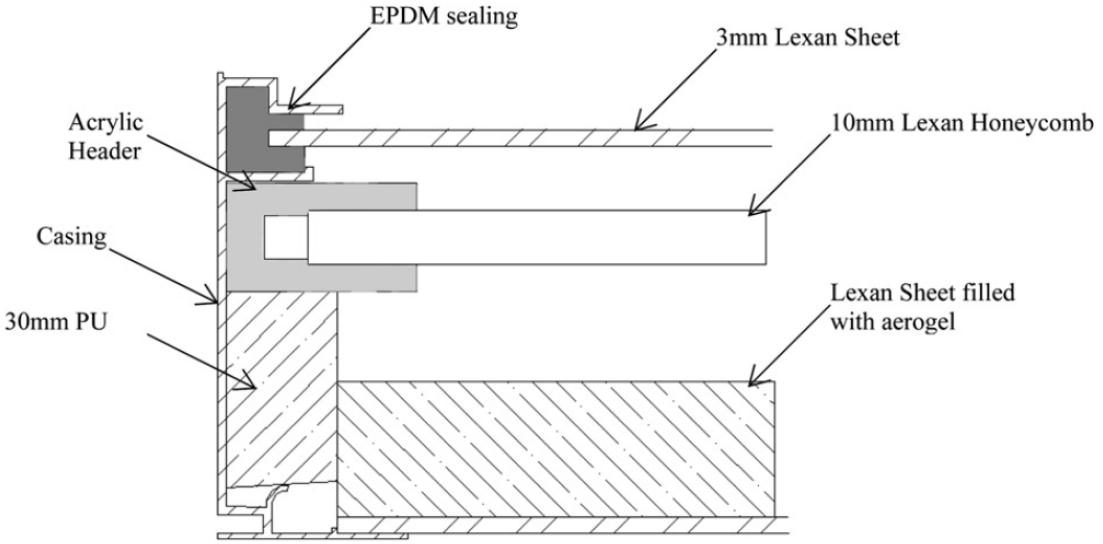

Figure 3.2: FPC cross-section [20]

Table 3.1: Collector technical characteristics [20].

Total area	1448 m^2
Glazing area	1252 m^2
Absorber area	1252 m^2
Number of glazings	1
Glazing material	3 mm solid transparent UV stabilized LEXAN
Heat carrier fluid	Water and Indian ink solution (1000:1)
Absorber	Transparent UV stabilized honeycombed LEXAN sheet (10 mm)
Headers	Acrylic 8 mm rectangular
Fluid weight	~14 kg
Back insulation	Honeycombed LEXAN sheet with a 10 mm thickness filled with nanogel ($k = 0.018$ W mK^{-1})
Side insulation	Extruded PU 30 mm ($\lambda = 0.03$ W/m^2 K)

also it affects the movement of heat carrier fluid inside the collector and can lead to form different kind of streams inside the collector. This happens because of the inlet pipe location is actually in the bottom of the collector and as the carrier fluid absorbs energy and gets heated, it starts to move upward and exit from the outlet pipe. the tilt angle of the collector can affect the way this procedure is done and result in different outlet temperatures. based on the above facts the tilt angle of the collector should be addressed and modeled in the computational simulation of the flat plate collector; see Figure 3.3.

The aim of solving this problem is to grasp a good understanding of the behaviour inside the solar flat plate collector. The most important parameter we are looking for is the total efficiency of the flat plate collector. To calculate the total efficiency of the collector we need to model this problem computationally and obtain the outlet temperature. With a known outlet temperature, the total final useful energy gained will be calculated and then by comparing the final energy and the total solar radiation which hits the solar flat plate collector in a certain period of time, we can

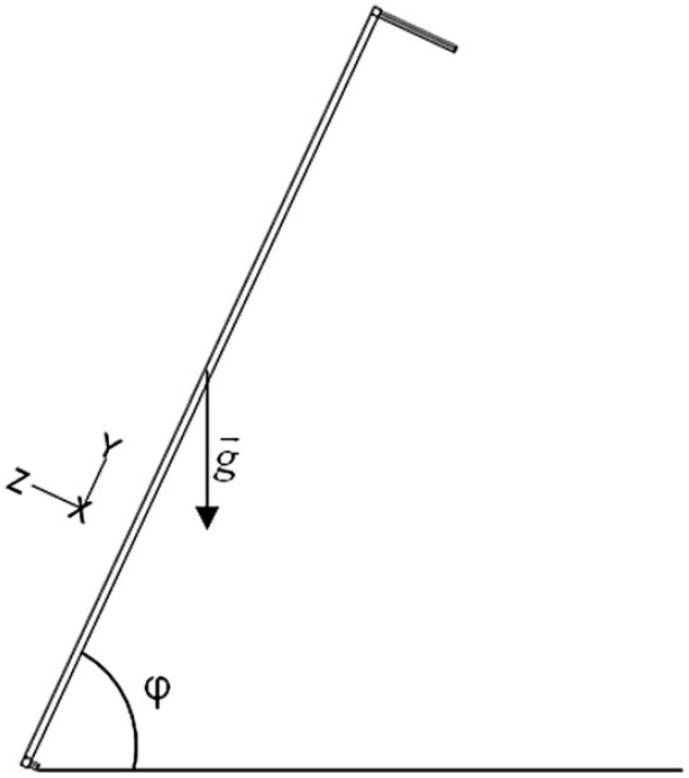

Figure 3.3: FPC Tilt angle [20]

calculate the total efficiency of the system. However, there are also other important factors that helps us to gain an insight about the collectors design and facilitate designing of a more efficient flat plate collector. To achieve this goal, first we have to take a look at the efficiency of each individual part of the solar collector. For instance, to improve the optical efficiency and also to decrease The heat loss from the insulation from the back and sides of the collector, we need the numbers for each of these parameters to be calculated.

Another issue that is need to be studied is the behavior of the heat transfer fluid inside the pipes and the body of our flat plate collector. The moving heat transfer fluid can possibly form some streams and cycles inside the collector and the probability to form unwanted back-streams or a situation when a part of the fluid is trapped and not circulating well is not zero and need to be avoid. If this situation happens when a part of the heat transfer fluid is trapped and not circulating good enough, it can disturb the performance of the collector and reduce the heat transfer and therefore, reducing the total efficiency of the collector. This problems should be carefully monitored and in case of existing, usually can be solved by changing something in the design of the collector such as changing the inlet and outlet locations or the diameters of the pipes or changing the tilt angle of the collector.

The Last part is to provide a temperature gradient in different planes and locations inside the collector, a vector contour for the velocity and the direction of the movement of heat transfer fluid, and a pressure gradient map inside the collector.

Chapter 4

CFD Modeling

In this section we are going to first review the logic behind the Software's which work based on the use of finite element methodology for the computational modeling and simulations and then proceed to the steps need to be done to model a solar flat plate collector specifically in *ANSYS WORKBENCH 2020 R2* software.

4.1 Finite element method

Finite Element Analysis or FEA is a method for numerical simulation using mathematical techniques called Finite Elemenet Method or FEM. It was developed for simulating engineering problems in various fields of engineering such as mechanical engineering. The reason to develop such a method for engineers is that not always an experimental model is possible to create because it is too dangerous, the possibility of creating or testing it is so low such as technologies that could never be tested in space crafts or it would be too much expensive or time consuming to create one. Moreover, the numerical analysis via finite element gives a more detail results compared to pure mathematical approaches without a computer processor, which usually works with numerous approximations to simplify the problem and therefore the results lose a portion of its detail in that procedure. That is why engineers develop such a technique to gain a better insight about their plan and the design of their system to be able to further optimize it [23].

Complex mathematics is required in order to understand the physical phenomena that occur all around us. These include things like fluid dynamics, wave propagation, and thermal analysis. Analyzing most of these phenomena can be done using partial differential equations, but in many complex situations where we have too many variables which are dependant to each other, it makes the old classic techniques to be not so efficient or succesful at all. The mathematical principles of FEA are also useful in other areas, such as computational fluid dynamics or CFD. The key difference here is that FEA focuses on structural analysis and CFD on fluid dynamics [23].

A software which works based on finite element, first needs a defined geometry for the shape and different parts of the system which is intended to numerically modeled. That is why all of the software based on finite element provide an environment that allows the user to either design and create the geometry of the system inside the software environment or integrated These programs into a computer-aided design (CAD) software. The finite element methodology suggests to divide the provided

geometry into a big number of computational nods or elements and then numerically simulate the system by taking the data of the nods on boundary conditions of the problem and then modify this data a little bit based on the physics of the problem and the partial differential equations which describes the problem and for the last step, spreads these data to nearby cells. After doing this over and over in multiple loops of iterations and extrapolation of data, if the physics of the problem was defined well it will lead to reaching a convergence point in the numerical solution. All of these nods have a data assigned to them meaning that the user can monitor the desired parameters such as pressure or temperature in every single point of the system. The core of CFD is based on the Navier-Stokes equations, which examine single-phase fluid flows. For many years, solving CFD problems entailed simplifying equations to the point that they could be done by hand but after the revolution in computing technology, solving these equations numerically became much more easier until we reach today which many commercial software's are available and ready to do this task in a very accurate manner.

4.1.1 CFD background

The development of CFD or computational fluid dynamics software was based on applied numerical analysis techniques which includes partial equations and the solution of linear algebraic equations, ordinary and partial differential equations. In CFD, the modeling of a problem focuses on the momentum and mass behaviour of the fluid which are the parameters defining the main characteristics of the flow. Besides that, it has the ability to simultaneously solve the heat transfer equations and include the information about the heat transfer in a system and the calculation of pressure,temperature and other thermodynamics parameters.

Computational fluid dynamics (CFD) is concerned with the efficient numerical solution of the partial differential equations that describe fluid dynamics. All CFD codes contain three main elements:

- A pre-processor which is a platform for user of the software to define the physics of the problem, including the geometry of the system and the materials used in the system, generating a mesh grid to be able to assign each point in a system a computational cell where Navier-Stokes equations can be applied and calculated and finally defining the boundary conditions and the initial flow parameters.
- A flow solver which is used to solve the partial equations mentioned above and solve those equations based on the defined flow parameters subject to defined boundary condition and the geometry or shape of the system. There are four different methods used as a flow solver:
  - finite difference method
  - finite element method
  - finite volume method
  - the spectral method
- A post-processor which allows the user to interpret the generated data and it assists the user to display the results in an easy format to read such as color contours, plots, vectors and diffrent variables distribution maps.

With using models based on numerical analysis such as FEM or CFD, we can predict the physical performance of a proposed design in a project and the details of the system behaviour inside the system without having to create expensive and large series of experimental models. This will help us to gain a better understanding of our proposed designs and try to further optimize their performance. All of the advantages above sounds fascinating but every method has its strong and weak points. Keep in mind that this numerical analysis are using computational resources such as computer memory and CPU. Therefore, creating a decent model always faces a trade off between results detail and the computational resources and computational time we want to allocate. Thus, a good CFD model consists of necessary details such as boundary conditions and geometry that helps the solver understand the nature of the problem it is facing. Once we are sure the problem is well defined for the solver, the more detail in defining only ads to accuracy of our results but also increase the computational time and resources needed. A good engineer is responsible to find a satisfying balance in this trade off. As time passes on and newer technologies are introduced every year, both computers and computational algorithms have been improved vastly in the last two decades and therefore it is now feasible to analyse more complex geometries and designs within a reasonable computational time. In the 80's there was a boost in progress as a result of the increase of computing power. Initially, only low Rayleigh numbers and small aspect ratios were investigated. More complicated studies, involving higher Ra numbers and aspect ratios, were investigated as more robust computing machines were developed. Later, even the 3D or three dimensional analysis of CFD problems were made possible.

In the field of solar flat plate collectors, The majority of the initial investigations using CFD techniques were based on a model developed by Duffie and Beckman [15] for flat plate solar collectors and this has been frequently used for design, calculations and the prediction of various systems. In this model the heat transfer is assumed to be one-dimensional from the thermal fluid to the ambient and the temperatures at the absorber plate and covers calculated at steady state conditions.

4.2 CFD modeling of solar flat plate collector

This section is a walk through the steps of modeling our problem using the *ANSYS WORKBENCH 2020 R2* software. In the following we explain in details how the CFD model is created and then we provide a detailed analysis of the results generated by the software.

4.2.1 ANSYS analysis system modules

ANSYS software provides the users with many different modules for different fields of engineering and each specific problem should be solved in its own module which suits the nature and the physics of the problem the most. A complete list of available modules in ANSYS is shown in Figure 4.1.

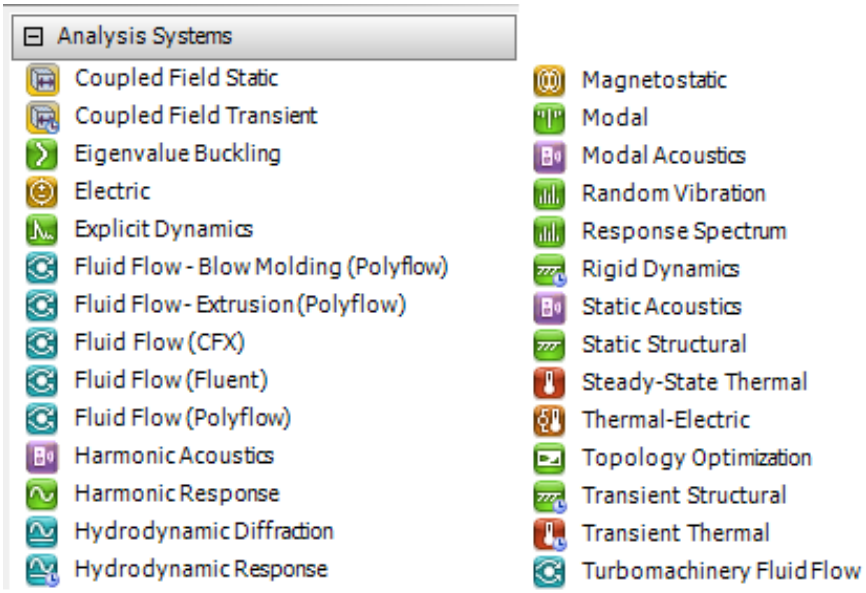

Figure 4.1: ANSYS modules

To begin working with ANSYS the user have to select the most suitable working module from the list in Figure 4.1 which is directly taken form the working environment of the ANSYS software. For this article, *Fluid FLow(CFX)* module was selected. As the name of the module suggests, it is suitable for modeling the problems in fluid mechanics and heat transfer which our problems falls perfectly in this category. After selecting the *Fluid FLow(CFX)* from the analysis system toolbar, a new box as shown in Figure with five different wing appears which guides the user through the next steps.

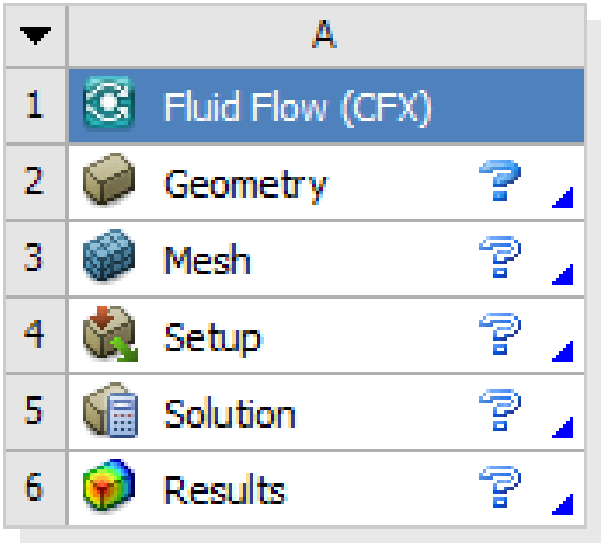

Figure 4.2: CFX fluid flow guide

To proceed the modeling it is needed to respect the orders appeared in the box beginning with Geometry to mesh, setup, solution and finally the results because each of these five wings appeared in the box works correctly only if the previous

up-stream data from all of the above parts is already provided and updated. This leads us to the next step of our

4.2.2 Geometry

In this step, it is needed to create a geometry which represents the shape of the solar flat plate collector we are intending to investigate. *ANSYS WORKBENCH 2020 R2* itself provides a three-dimensional environment to create our desired geometry as shown in Figure 4.3 but it is also possible to import a geometry file from other CAD software's into ANSYS. For this research the geometry was created using the *SPACECLAIM* which is a 3D environment integrated into the *ANSYS WORKBENCH 2020 R2*.

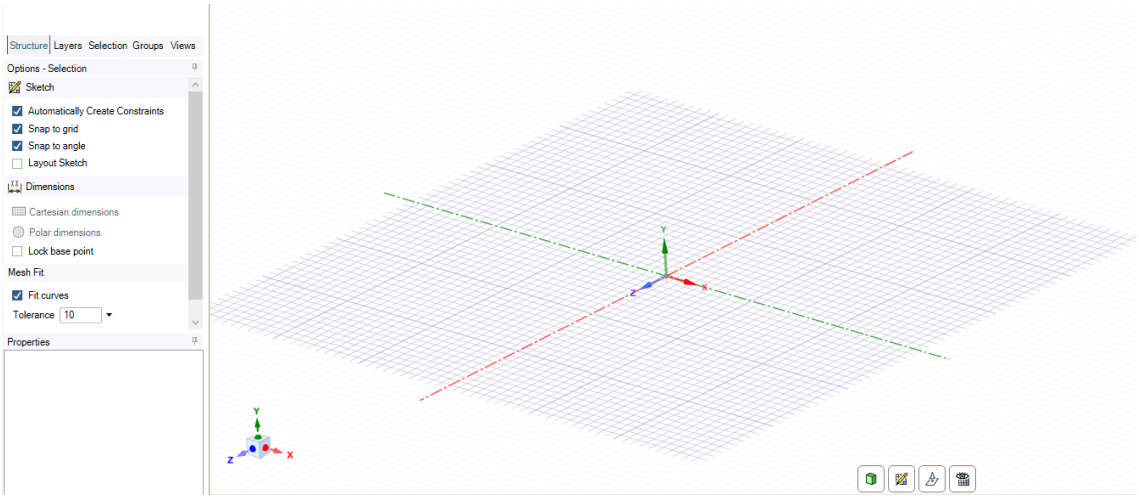

Figure 4.3: SPACECLAIM 3D environment

To create the geometry of our solar flat plate collector, we proceeded as our collectors measurements and different parts was described in the problem definition chapter. The final geometry includes five major parts which is created as individual components in SPACECLAIM. These five regions are:

- Top header pipe
- Outlet pipe
- Absorber box
- Bottom header pipe
- Inlet pipe

The top and bottom header pipes are in shape of two rectangular pipes which is horizontally located on top and bottom of the system. The headers have a $10 \times 10\,mm$ square face in the sides with the length of $1495\,mm$. The inlet and outlet pipes are two cylinder shape pipes which are connected to the headers. The radius of the inlet and outlet pipes are $3.5\,mm$ with the length of $50\,mm$. In figure 4.4 the created geometry of these 2 regions are shown.

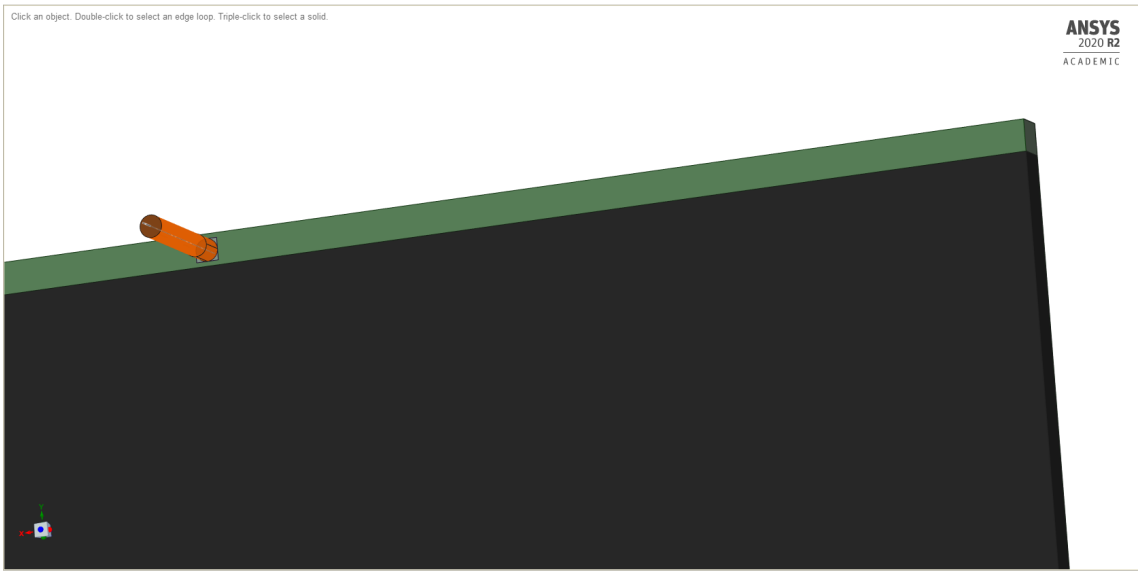

Figure 4.4: Top Header pipe(green) and outlet pipe(orange)

the geometry of the bottom header pipe and the inlet pipe are similar to what described for the top part of the system with only one difference which is the location of the inlet and outlet pipe. The outlet pipe is located in 265mm from top right side of the system frame but the inlet pipe is located in 345mm from bottom left side.

The next step is to define the last geometry part which is the main box that includes the absorber plate in the front and insulation in the back. this is the largest part of the geometry and our flat plate collector geometry will be completed after creating this main part which is located between the two headers. in Figure 4.5 the mentioned region is shown in purple color.

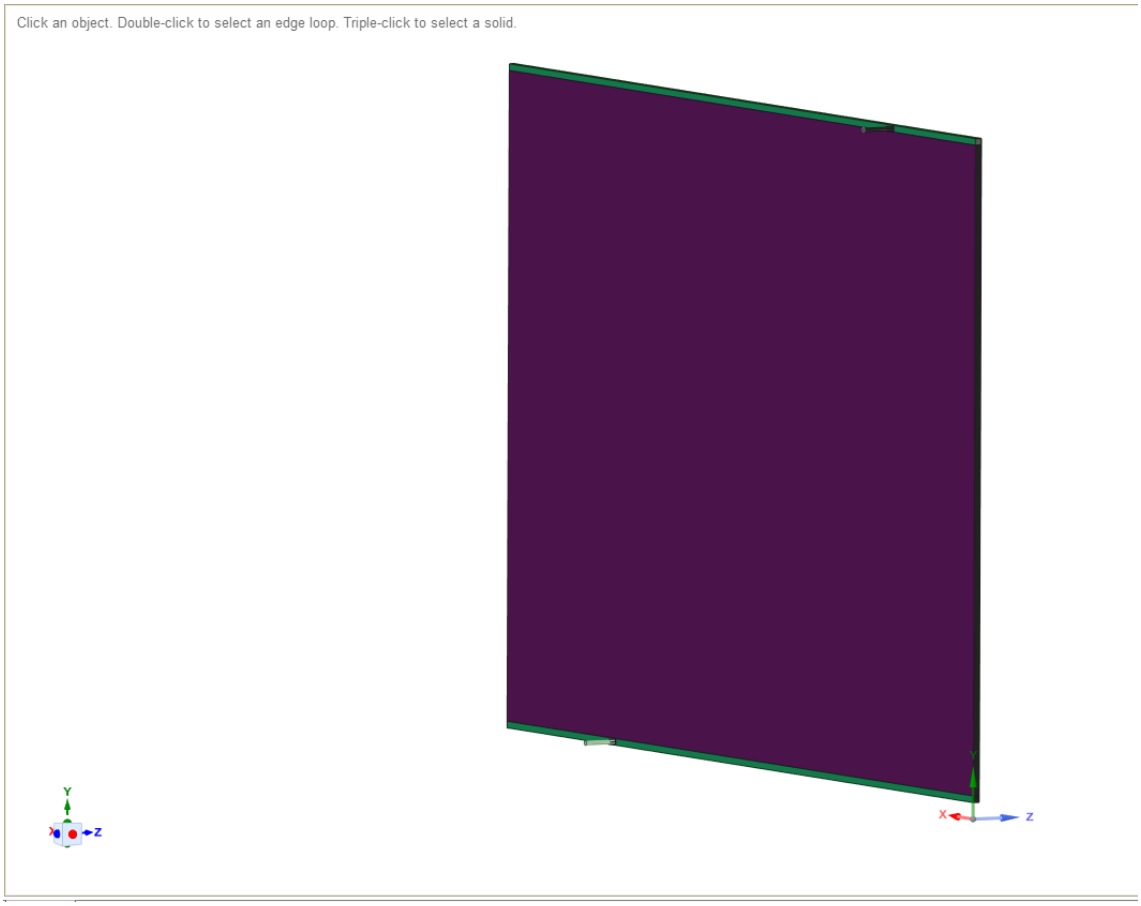

Figure 4.5: Main box region(purple)

The length of this region towards the vertical axis is 1495mm and towards the horizontal axis is 1055mm. the width of this region is similar to the rectangular headers which equals to 10mm.

The reason for creating five separate regions in our geometry is that different equations and boundary conditions govern each of these regions so it is needed to make them separately to have freedom to modify and define their own boundary conditions and different meshing grid for each of these parts individually. For instance inside the header pipes are empty but inside the main box of the geometry is formed with honeycomb structure so despite the fact that these regions are connected to each other in the overall geometry, each one of them are going to behave in their own unique manners. This issue will be discussed more in the upcoming sections where we address the meshing grid and setting up the boundary conditions of the problem and most importantly the sources or the physics equations such as energy and momentum governing the numerical simulation in each region.

4.2.3 Meshing grid

Meshing grid is a step in CFD analysis which divides the geometry of the model into different nodes, to be able to numerically analysis each of these computational nodes using Navier–Stokes equation. When the meshing grid is smooth and with high number of nodes, the result is going to be more accurate but we should keep in mind to not make it with unnecessary large number of elements because it will

consume more time and computational power. A good grid of mesh provides a decent accuracy in computation while at the same time it is efficient in computational time. Another very important issue to keep in mind is that the way meshing grid is created should not affect the result so to make sure that the result is mesh independent usually we have to solve the problem with two or more different types of mesh grid and see if the results acquired is the same in each cases. In that case, we can make sure that the results are reliable and it is mesh independent. The method we use to make an efficient mesh while we are keeping the number of nodes in a reasonable range is to pay more attention to the boundary conditions and create our mesh grid in a way that it is a more detailed and smooth mesh around these areas compared to other parts. To name some of our boundary conditions as example, we can name the initial boundary condition such as inlet water or heat flux from a wall which is in the location of our absorber. also all the walls such as the surface of the pipes and other locations are considered boundary condition so we have to make the mesh grid small and smooth in these locations.

For this work, we have created two meshing grid in two separate file. The reason for that is one was supposed to be a preliminary calculation which was supposed to be more simple and run by ANSYS student version. In the student version of ANSYS the number of nodes should be kept under 512,000 nodes. However, for further investigation another grid with total of NUMBEEEEEEEER!!!!! nodes is created.

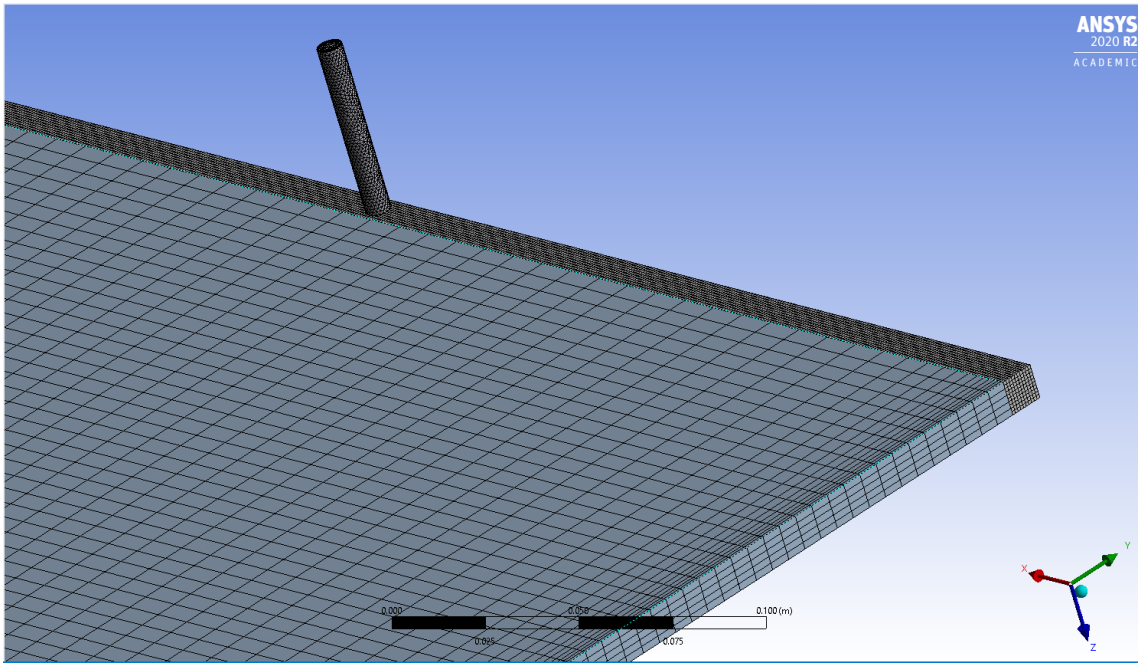

Figure 4.6: Overall view of the Mesh grid

In the Figure 4.6 It is possible to seea view of the created mesh grid. Another important issue to remember is that the size of each element should be proportional to the measurements of that specific part of the system. For instance, the size of the outlet pipe which is visible in the Figure 4.6 is much smaller than the main box which represent the absorber area. Therefore, It is natural that the meshing grid is much more detailed and smaller in the pipe compared to the main box which has bigger volume and area. The same logic applies to the top header which is

connected to the outlet pipe. There is also another factor which is the fact that the mesh grid should not change drastically from one cell to another. The inflation in element size of the mesh should be gradual and that is why the meshing in the top header has sizing bigger than the outlet pipe but smaller than the main box mesh elements. This makes sure the inflation is gradual and we do not miss any computational information because of the mesh grid.

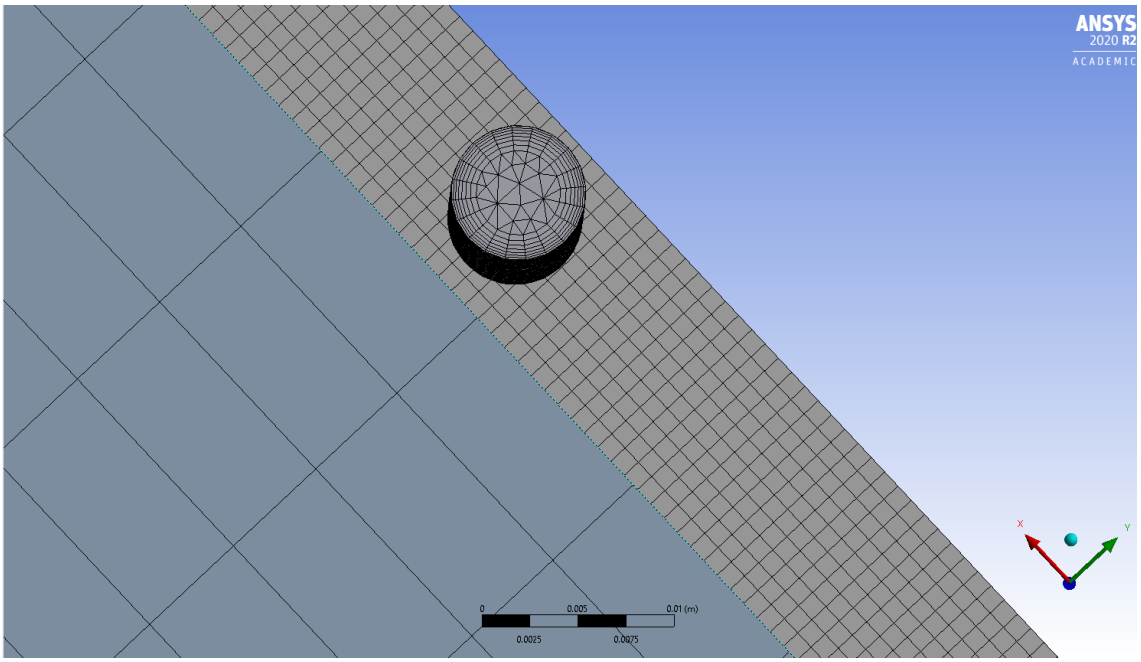

Figure 4.7: Pipe and header Mesh grid

In the Figure 4.7 It is possible to see the top header and the outlet pipe mesh grid in more detail. Notice that in the pipe region, the grid is more dense with more number of nodes near the pipe wall, to make sure the effect of boundary conditions are going to be calculated accurately. The same level of attention were applied near the front side of the collector, which represent the absorber plate and modeled as a wall with a constant heat flux of 1000 W/m^2.

Inside the main box region of the collector is not empty and it is filled with a honeycomb structure. The detail in this part is too much to build in the CAD(Computer Aided Design) software and even if we would be able to create such a detailed structure, the meshing grid of this part would be so dense and small that would not be efficient for our numerical investigation of the problem. The solution to this problem is to model this part of the system as a porous medium and avoid the ultra dense mesh grid. this method is going to be explained in more detail in the next section.

4.2.4 Setup and source terms

In this section we are going to discuss more about setting up the boundary conditions governing our model and also the details of modeling the honeycomb structure inside the collector region.

Fluid domain

The first step of defining the problem in the setup tool is to select all the domains in which our working fluid is going to pass and flow in. This means in this part we have to select all the domains of the collector as shown in Figure 4.8 since the water is going to flow in all of the collector region. To do that we select all regions and create a fluid domain in the setup.

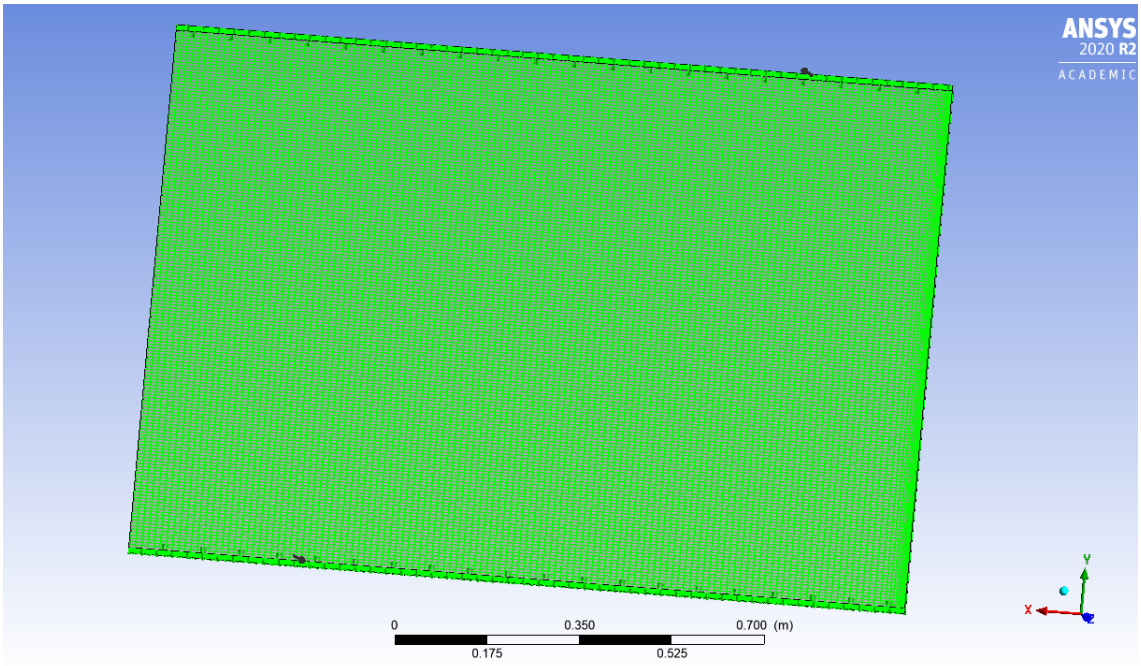

Figure 4.8: Fluid Domain

In the Basic setting we define what is going to be the working fluid in our collector which is water here. The rest of the setting are shown in Figure 4.9 and Figure 4.10.

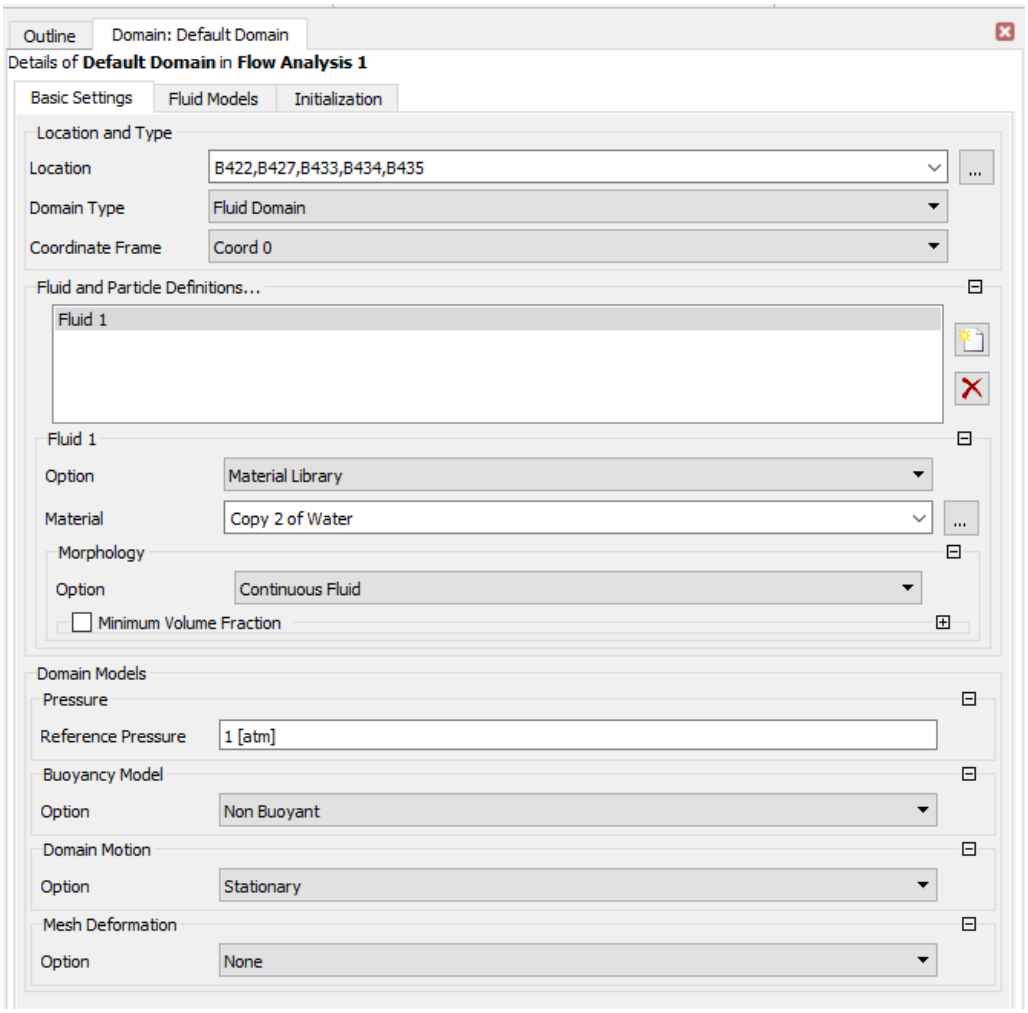

Figure 4.9: Fluid Domain basic setting

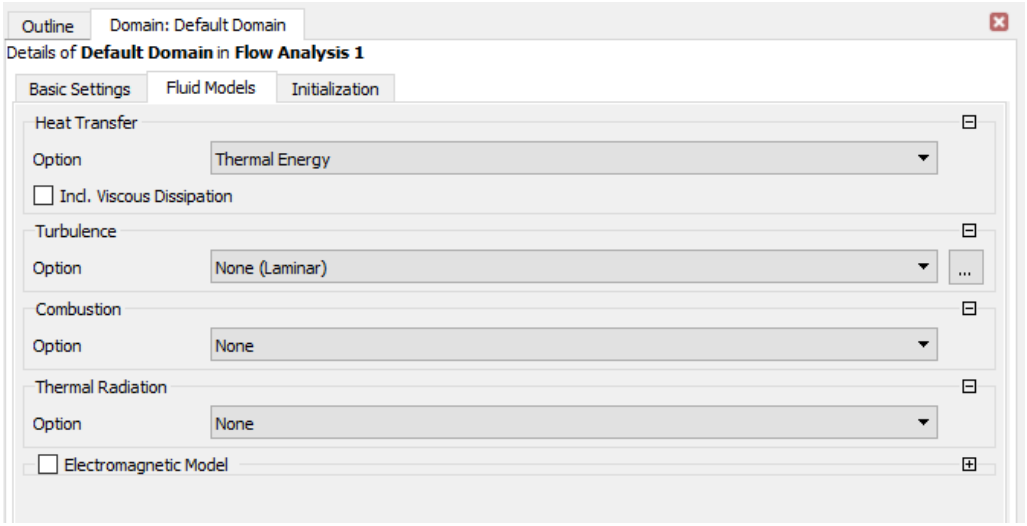

Figure 4.10: Fluid Domain - fluid model

The reference pressure is set up to the ambient air pressure which 1 atm. In the heat transfer model, we selected the Thermal energy model but there is also possible to choose the total energy model for the fluid. The thermal energy option activates

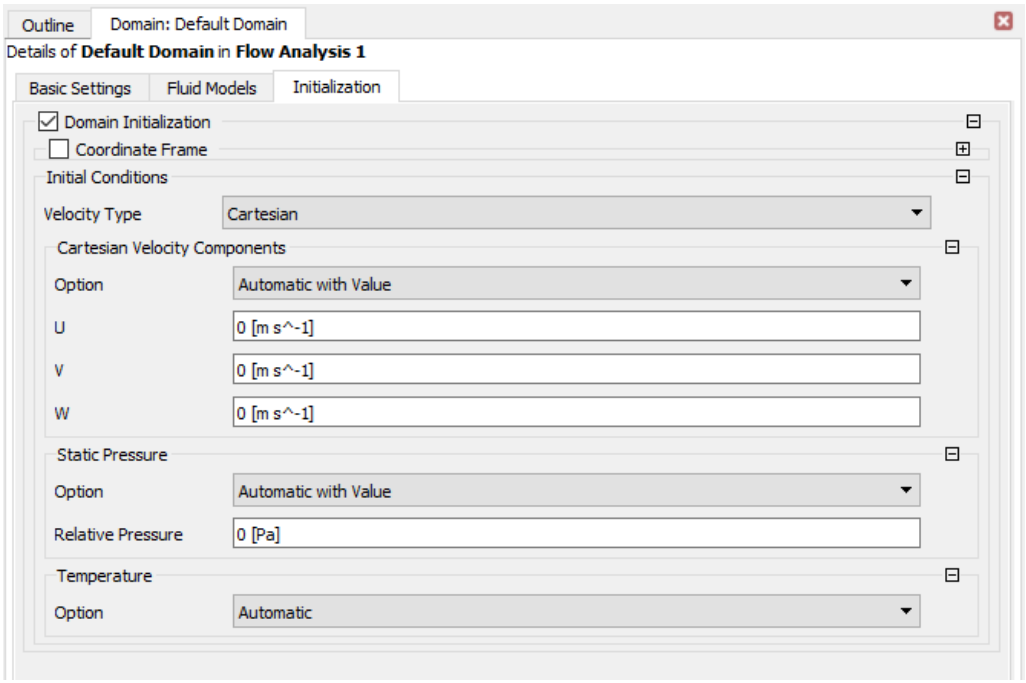

Figure 4.11: Fluid Domain - Initialization

the enthalpy-temperature equation, but does not include compressibility effects. It is used for low speed thermal models like AC flows, combustion or heat exchangers. On the other hand, The total energy option activates the full enthalpy equation, including compressibility effects. It is used for high speed flows or anywhere else where compressibility is important. In other words, when we select thermal energy model, the H(enthalpy) equation is activated and if total energy model is selected the governing equation is going to be $H + 1/2.m.V^2$. In our case, enthalpy equation is enough and there is no need to include longer equations which is more time consuming for the computation. As we can see in the next section for inlet boundary condition, he inlet flow is set to 0.77 m/s which is a low number and it gets even lower when the fluid enters the honeycomb structure region. Therefore the Reynolds number throughout the collector remains in a low range resulting in a laminar flow throughout the whole system. The ANSYS solver also verified that during the calculation. This is why the laminar flow model is selected for the turbulence model shown in Figure 4.10. The correct Initialization of the model helps the solver to reach convergence faster. Theoretically it should not affect the final result of the simulation but if set in a proper way, it can avoid the problems regarding the divergence and instability of the numerical calculation. This is why in Figure 4.11 you can see that it is set to zero velocity to bring stability to the solution. It makes sense because as mention above, the velocity of the fluid is very low especially in the channels of the honeycomb structure, which is the largest domain in our model.

Inlet

The First boundary condition we need to setup is the inlet as shown in Figure 4.13. At the inlet of the computational domain, a uniform velocity field was imposed corresponding to 0.77 m/s to match with the parameters in the experimental study done by Misirlis and Martinopoulos [20]. The temperature of the inlet fluid is static

temperature of 303 K. All the setting corresponding to the inlet boundary conditions can be seen in the figure 4.12.

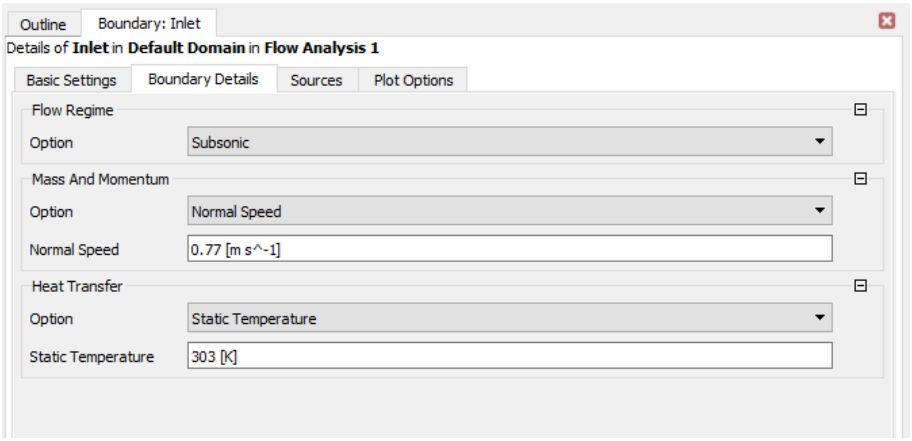

Figure 4.12: Inlet boundary settings

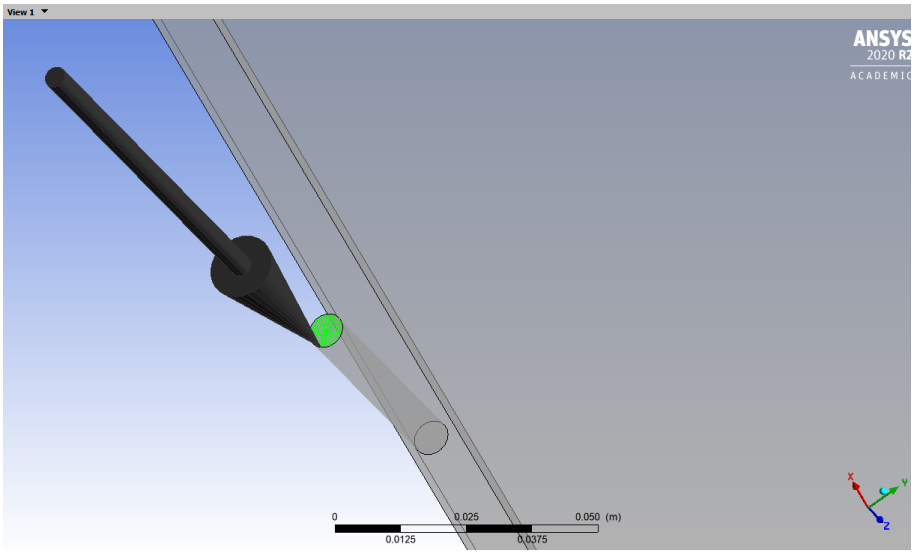

Figure 4.13: Inlet pipe region

This leaves us with the most important part which is the collector region or the main box of the collector in the middle of our collector. For this part a sub-domain was defined to give us the freedom to modify this region in a way that suits the problem the best. as briefly mentioned in the previous section, a honeycomb structure is placed inside this box where fluid can flow throw the holes and paths which exists in the structure. To develop such a shape in the geometry part in any CAD software is difficult and even if we create such structure, it will increase the number of nodes and elements in our mesh grid significantly which will result in an enormous use of CPU and memory power and takes significantly longer time to solve for the ANSYS CFX solver. Therefore it is not wise to model this part of the collector as described above. To overcome this obstacle, we suggest to model the honeycomb structure as a porous medium.

Honeycomb structure sub-domain

When a fluid passes through a porous material, it flows through long thin tortuous passages of varying cross section. The problem is how to calculate the flow rate based on nominal thickness of the layer. This was tackled by Kozeny [16] and later by Carman [5]. The result is a formula, which gives a mean velocity of flow in the direction at right angles to the layer plane in terms of its thickness and other parameters. The passage between the particles is so small that the velocity in them is small and the flow is well and truly laminar. Poiseuille's Equation for laminar flow states

$$\frac{\Delta P}{l} = \frac{-32\mu u'}{D^2} \tag{4.1}$$

Kozeny[16] modelled the layer as many small capillary tubes of diameter D making up a layer of cross sectional area A. The actual cross sectional area for the flow path is A'. The difference is the area of the solid material. The ratio is $R = A'/A$ and this is known as the porosity of the material. The volume flow rate through the layer is $\dot{V}$. Kozeny used the notion that $\dot{V} = Au$ where u is the mean velocity at right angles to the layer. The volume flow rate is also $V' = A'u'$ where u' is the mean velocity in the tube. Equating $u' = uA/A'$.

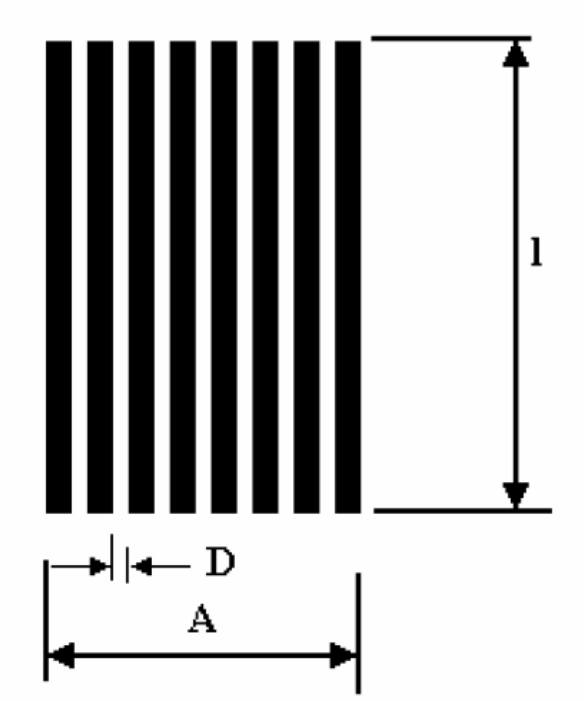

Figure 4.14: Porous medium

Carman[5] modified this formula when he realised that the actual velocity inside the tubes must be proportionally larger because the actual length is greater than the layer thickness. It follows that

$$u' = \frac{u.l'}{R.l}$$

where l is the layer thickness and l' the mean length of the passages. Substituting this in Poiseuille's Equation gives

$$\frac{\Delta P}{l} = \frac{-32\mu u l'}{l Porosity \times D^2} \tag{4.2}$$

This is the pressure loss in the porous medium in Y direction of our solar collector simulation which needs to be added in the source term for the momentum equations. The porosity of our honeycomb structure is estimated 85.5% and the channels diameter D is equal to 9.24 mm. the value for l'/l in this case is around 1. Therefore

$$S_{Y\_PM} = \frac{-32\mu v}{Porosity \times D^2} \tag{4.3}$$

To adjust the Navier-stokes equation to include the physics of our problem, we need to add a source term to each of the equations in the Navier-stokes momentum equation set4.4.

$$\begin{aligned}
\frac{\partial(\rho u)}{\partial t} + \nabla.(\rho u \overrightarrow{u}) &= -\frac{\partial p}{\partial x} + \nabla.(\mu \nabla u) + S_{total_x} \\
\frac{\partial(\rho v)}{\partial t} + \nabla.(\rho v \overrightarrow{u}) &= -\frac{\partial p}{\partial y} + \nabla.(\mu \nabla v) + S_{total_y} \\
\frac{\partial(\rho w)}{\partial t} + \nabla.(\rho w \overrightarrow{u}) &= -\frac{\partial p}{\partial z} + \nabla.(\mu \nabla w) + S_{total_z}
\end{aligned} \tag{4.4}$$

The general look of the Total source terms equations in each direction is represented in equation 4.5.

$$\begin{aligned}
S_{total_x} &= S_{x_PM} \\
S_{total_y} &= S_{y_PM} + S_{y_gravity} + S_{y_buoyancy} \\
S_{total_z} &= S_{z_PM} + S_{z_gravity} + S_{z_buoyancy}
\end{aligned} \tag{4.5}$$

S_{y_PM} is responsible for the pressure drop in the channels of the honeycomb structure in the direction of y and was calculated above by Kozney-Carman equation which resulted in equation 4.3. This value is responsible for the possibility of the working fluid, move through the y direction. The y direction is the main passage for the fluid and we do not expect the fluid to move in the x and z direction easily. Therefore we need to assign a very big value to S_{x_PM} and S_{z_PM}. in the following set of equations, the pressure drop source terms are shown.

$$\begin{aligned}
S_{x_PM} &= -10^{10}\mu u \\
S_{y_PM} &= \frac{-32\mu v}{Porosity \times D^2} \\
S_{z_PM} &= -10^{10}\mu w
\end{aligned} \tag{4.6}$$

Notice that in equation 4.5 the effect of buoyancy and gravity is only considered in the y and z direction. The reason for that is to take into consideration of the effect of gravity and buoyancy when the flat plate collector is placed inclined in a specific angle of φ which is 60° for our flat plate solar collector. In that case, The source terms for the gravity and buoyancy is calculated via

$$S_{y\_gravity} + S_{y\_buoyancy} = -\rho g \sin\varphi \,(1 - \beta(T - T_{ref}))$$

(4.7)

$$S_{z\_gravity} + S_{z\_buoyancy} = -\rho g \cos\varphi \left(1 - \beta(T - T_{ref})\right)$$

where β is the thermal expansion coefficient defined as:

$$\beta = -\frac{1}{\rho}\left(\frac{\partial \rho}{\partial T}\right)_P \tag{4.8}$$

This was the last piece of puzzle to complete all the data we need to form the equation 4.5. With this source term equation, the governing equation for mass and momentum for the honeycomb structured region is known and applied in the simulation as shown in Figure 4.15.

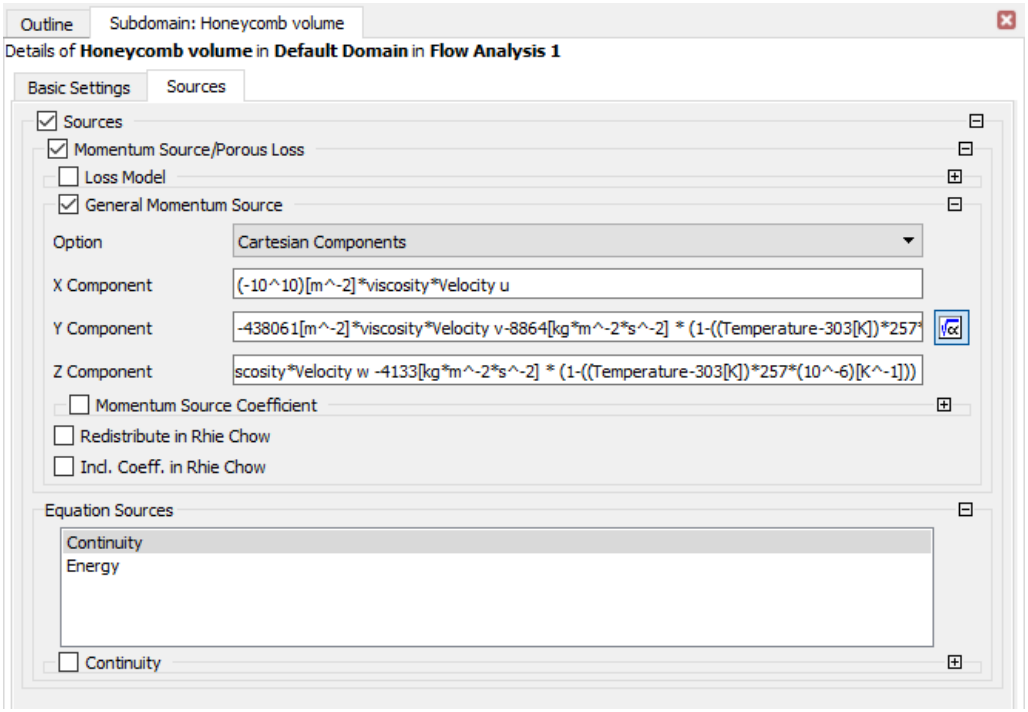

Figure 4.15: Honeycomb region momentum source term

.

Headers and pipes sub-domain

In the previous section we explained the reasons behind the source terms added for our porous medium. in that sub-domain there were two different reason which formed our final source term expression. The first one was the porous medium and the pressure drops it causes. The second one was the buoyancy and gravity correction due to the tilt angle of the collector. This second reason, does not exclusively works only for the middle region which was the honeycomb structure. In reality the whole system is tilted by a specified angle so the effect of this rotation of the flat plate collector should also be seen in other parts of the model which encompass both the header pipes in top and bottom of the collector and the inlet and outlet pipes. Therefore the source terms of buoyancy and gravity is also added to this sub-domain as you can see in Figure 4.17. In the Figure 4.16, a view of the mentioned region is provided.

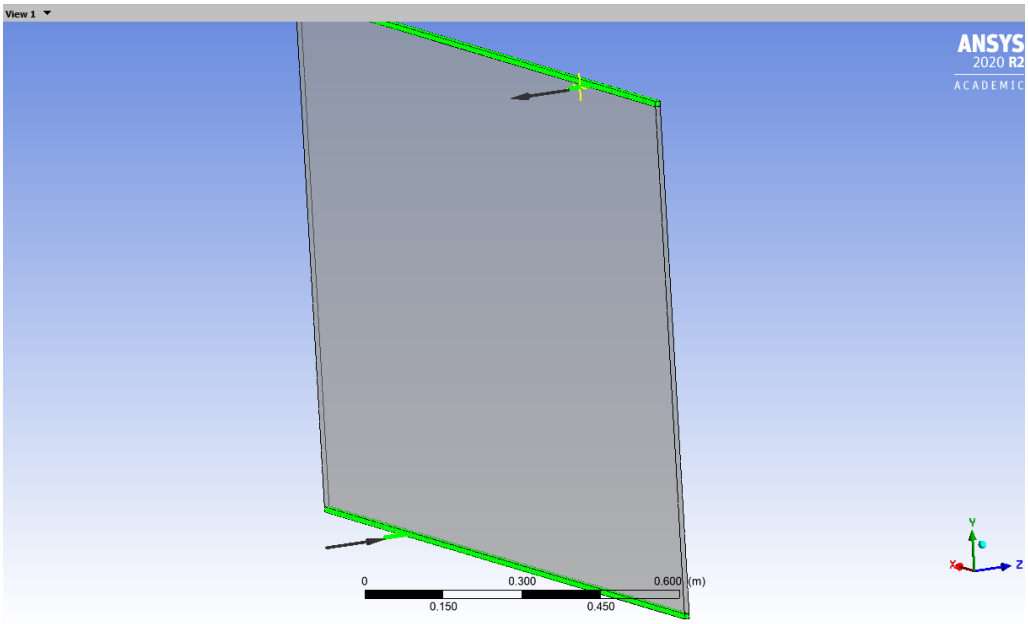

Figure 4.16: Selected regions for tilt angle correction

.

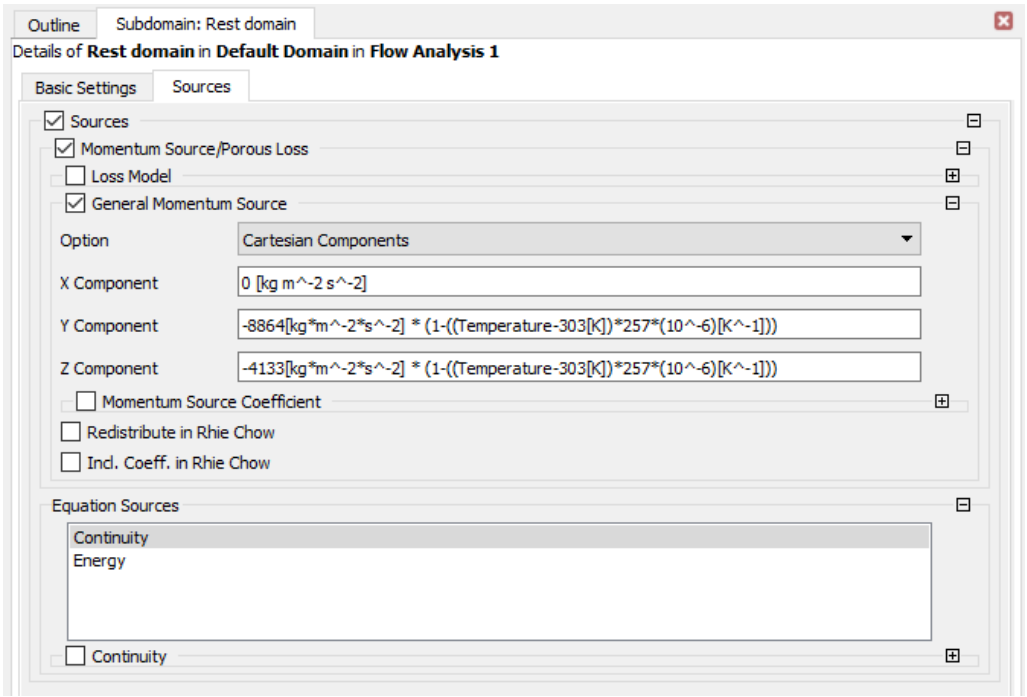

Figure 4.17: Selected region momentum source term

.

Outlet

The next boundary condition we need to apply is at the location of outlet pipe. This is the location where the heated fluid is leaving the flat plate collector system boundary. Unlike the inlet, the temperature at the outlet is unknown and it is

going to be calculated by the solver. Therefore the logical way to define the outlet boundary condition is by its pressure. Since the reference pressure in the fluid domain was set at 1 atm, for The outlet boundary layer the subsonic flow regime was selected and set to 0 pa. The setting of the outlet boundary condition can be seen in Figure 4.18. A view of the outlet pipe region is shown in Figure 4.19.

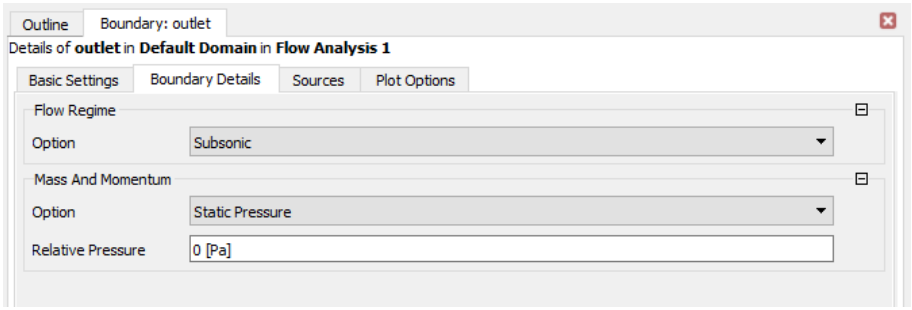

Figure 4.18: Outlet pipe boundary conditions

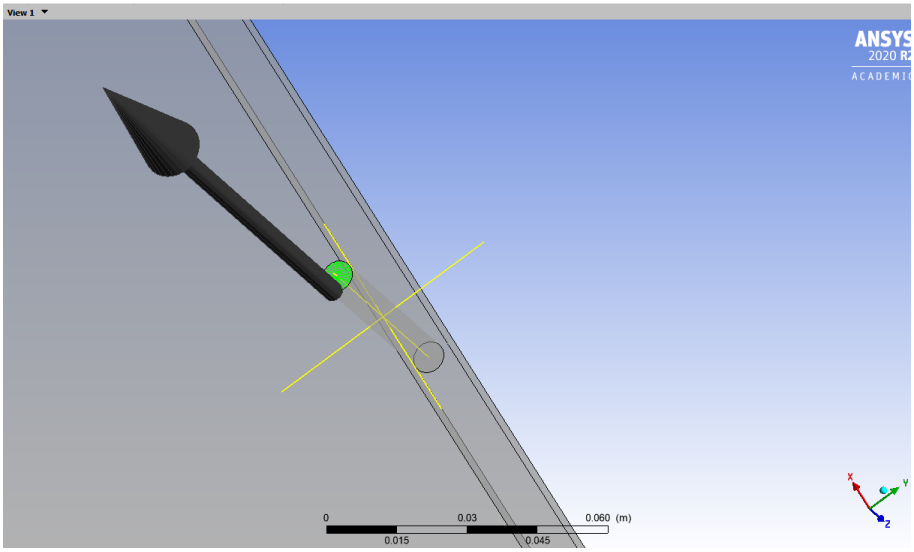

Figure 4.19: Outlet pipe region

Heat flux

The next boundary condition we are going to talk about is applying the heat flux to model the sun radiation to our collector. This boundary condition is applied to the front face of the collector which is located in the opposite side of the collector where inlet and outlet pipes are located. To put the heat flux boundary condition on this face, we introduce a heat flux function which also includes the radiation heat loss from this side of the collector as shown below:

$$TotalHeatflux[W/m^2] = Sun\,radiation[W/m^2] - \sigma(T_{wall}^4 - T_{ref}) \times \varepsilon \qquad (4.9)$$

where $\sigma = 5.67 \times 10^8 J/sm^2K^4$ is the is the Stefan-Boltzmann constant and ε is the emissivity of the wall equal to 0.85. If we insert the values into the equation above it gives us the final function we are going to use as the heat flux in boundary condition in our simulation as shown below:

$$TotalHeatflux[W/m^2] = 900[W/m^2] - 5.67 \times 10^{-8} \times (T_{wall}^4 - 303^4[K]) \times 0.85 \quad (4.10)$$

The figure 4.20 shows the tab in ANSYS software where we include this function for our boundary condition. In the Figure 4.21 the pink area is the location of the heat flux boundary condition which is on top of the honeycomb structure.

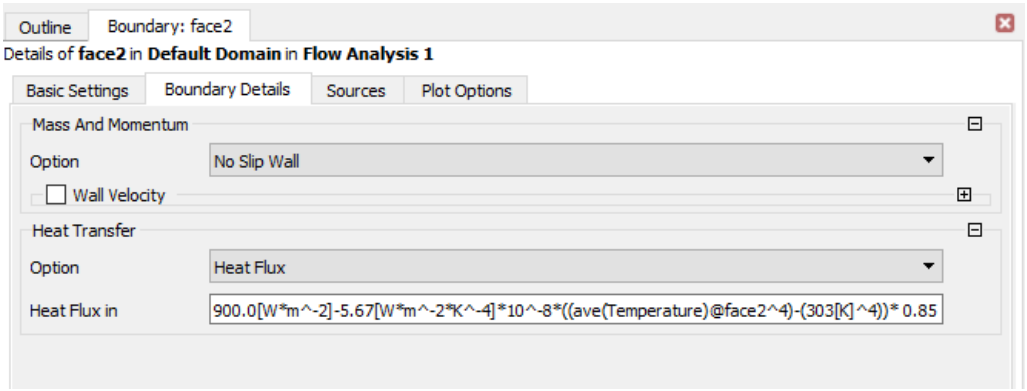

Figure 4.20: Heat flux boundary condition

.

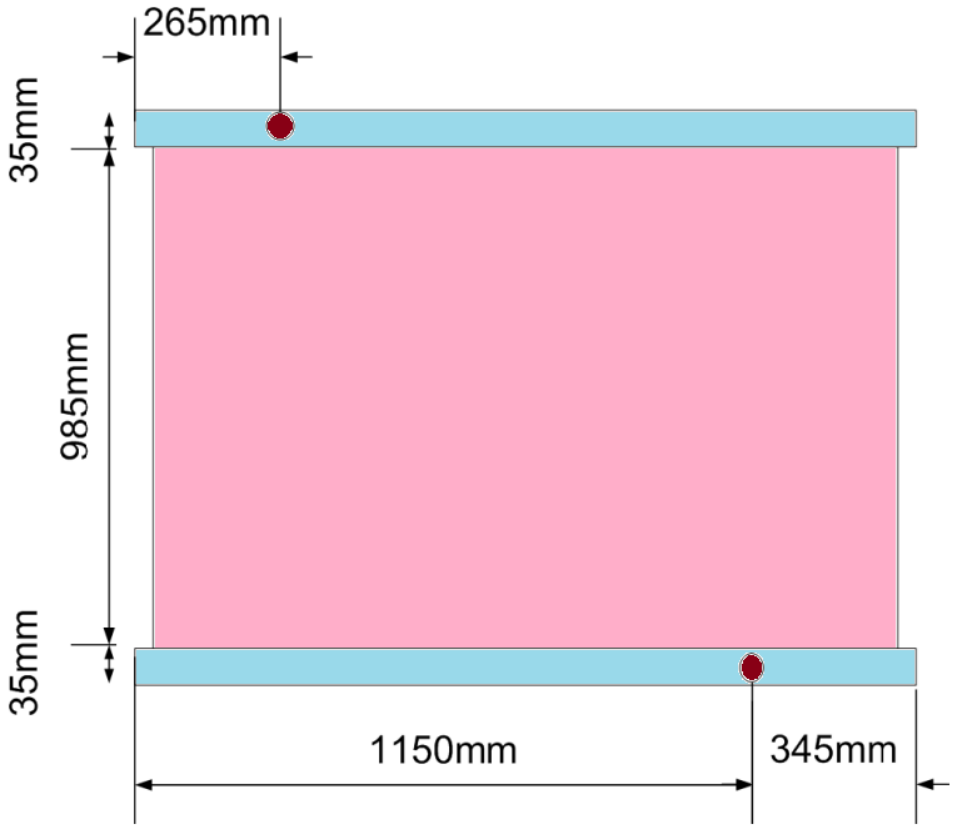

Figure 4.21: Heat flux - front face

.

Material properties

The next step of our simulation is to define our working fluid characteristic which is water in our case in ANSYS. ANSYS itself has a library including a lot of materials with predefined characteristic. But it also provides the user with the possibility to define these characteristics manually in case if they want their work to be more detailed. In our study, we did not intend to use the fluid with constant characteristics and we preferred to use the temperature dependant characteristics as shown below:

Density: $\rho(T) = 0.003284948 \times T^2 + 1.687644 \times T + 785.6677$

Dynamic viscosity: $\mu(T) = 1.406 \times 10^{-7} \times T^2 - 0.0001024062 \times T + 0.01895682$

Thermal conductivity: $\mathrm{K(T)} = 9.8135 \times 10^{-6} \times T^2 + 0.007536807 \times T - 0.7674181$

After including these relations in material properties tab, we have to generate a table in the software to turn these equations to numerical points where it can use the data for each temperature. While we generate a data table based on these functions, we need to keep in mind to include the upper and lower limits of this table based on the real physics of the problem. In our case for example, we use a water in reference temperature of 303 K at the inlet boundary condition and we do not expect the waters temperature to go over the boiling point. So the upper limit of the temperature for this table is set to the boiling point of the water. The same concept is applied for the pressure which is shown in Figure 4.22 and Figure 4.23.

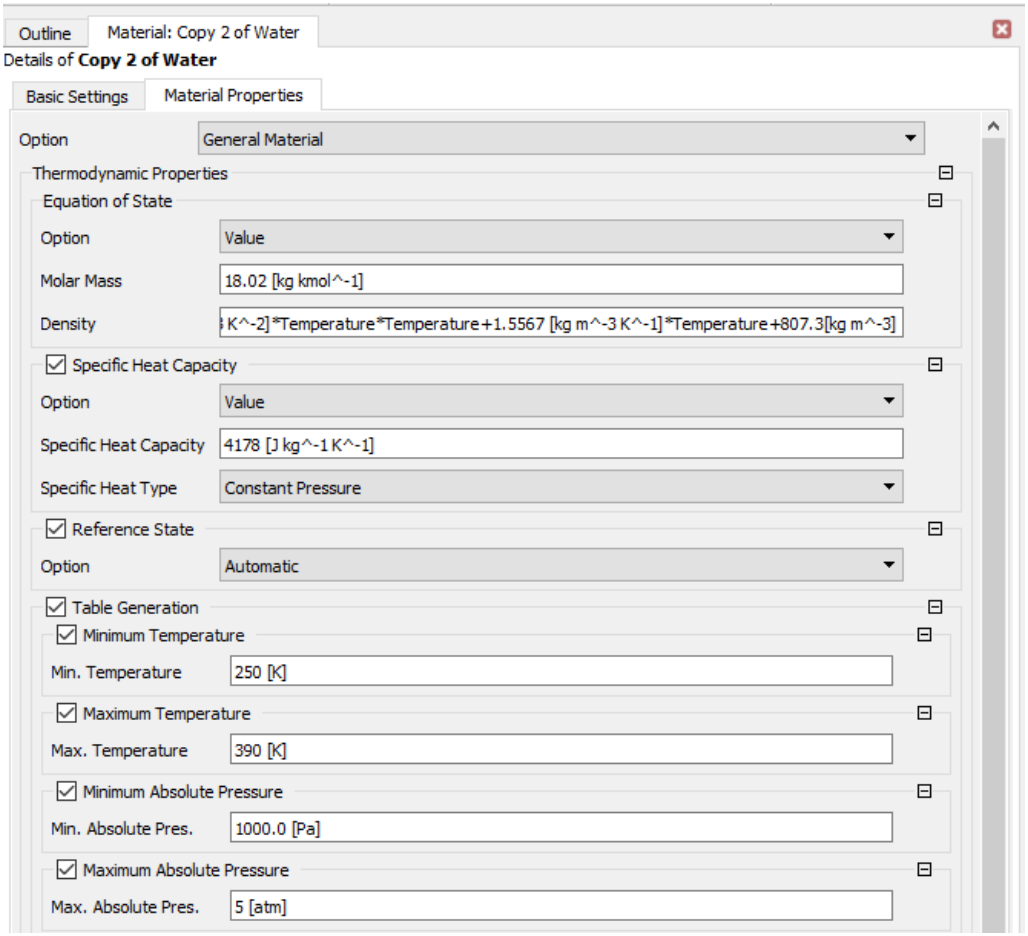

Figure 4.22: Water Temperature dependence properties part 1

.

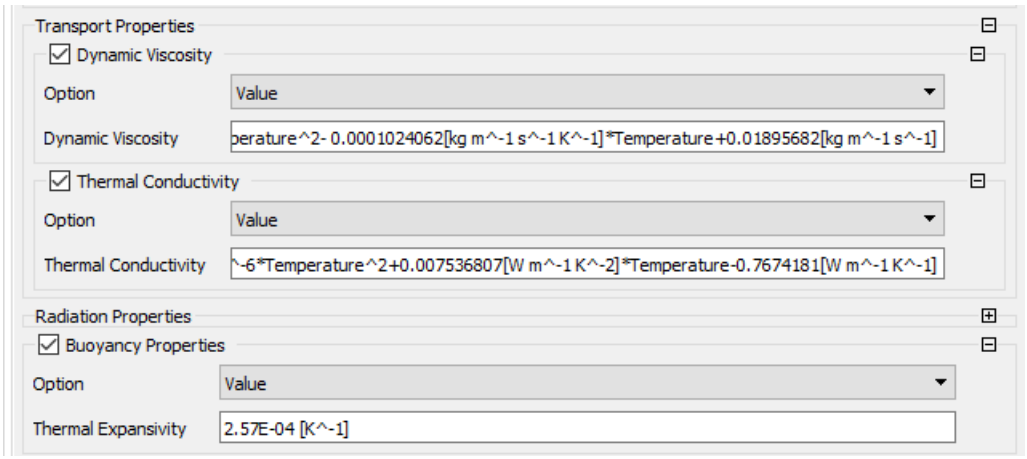

Figure 4.23: Water Temperature dependence properties part 2

.

Solver control

In the solver control section, we have to define how we are going to run our calculation. there are different options for the advection scheme and time-step controls.

The advection scheme options are:

- High resoloution
- Upwind
- Specified blend factor

For this model, since the number of nods in meshing grid is low, due to the limit of ANSYS student version, it is advised to choose a scheme which is more simple and reach conversion in an easier condition. For instance that is why the high resolution scheme is not selected. In our study we selected upwind scheme and it proved to reach convergence with not so much of difficulty. The time step of all equations were set to 0.01 at first and the momentum equations were working without a problem. However, the temperature curve were not changing and it would take a lot of time to reach its final value. Therefore the time-step for the energy equation was changed to 1 and it proved to be a better value since the fluid temperature started to change and reached convergence. In Figure 4.24 you can see the solvers control basic settings and in Figure 4.25 the energy equation time-step setting is shown.

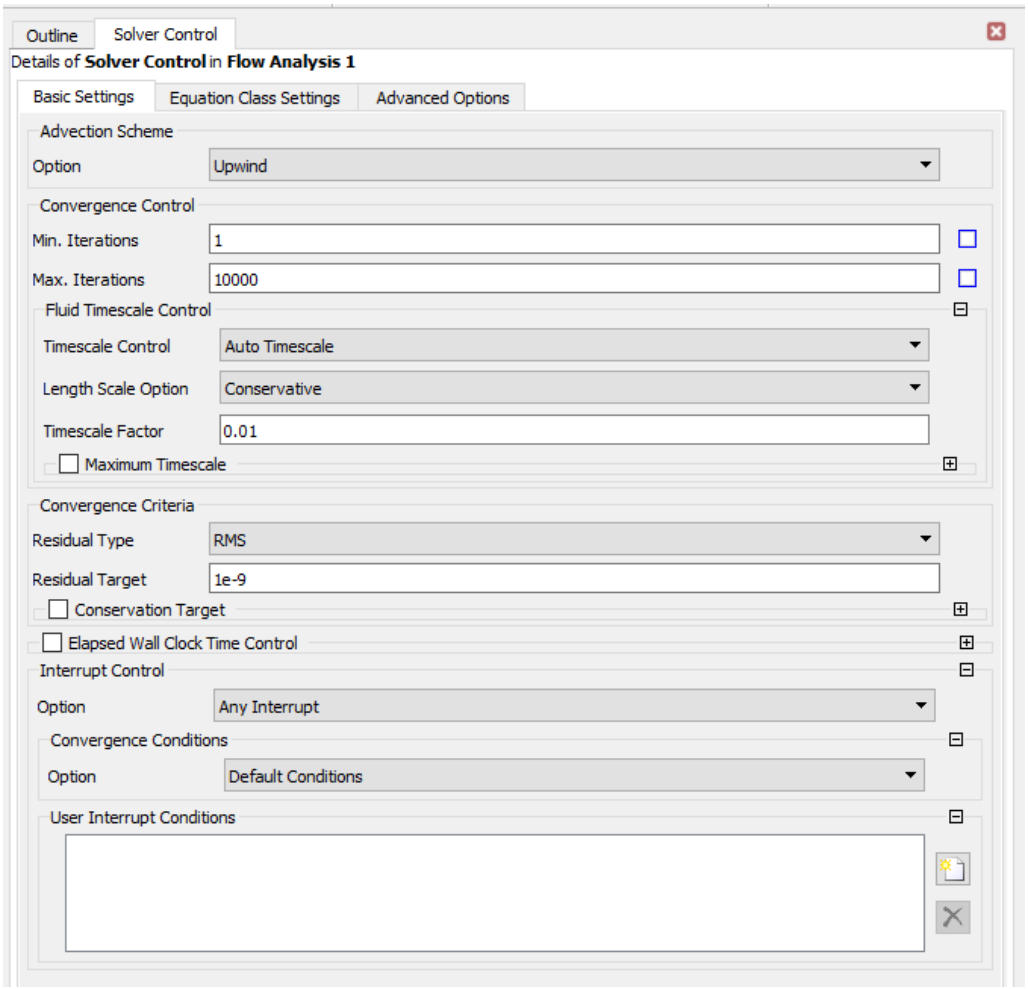

Figure 4.24: Solver control basic settings

.

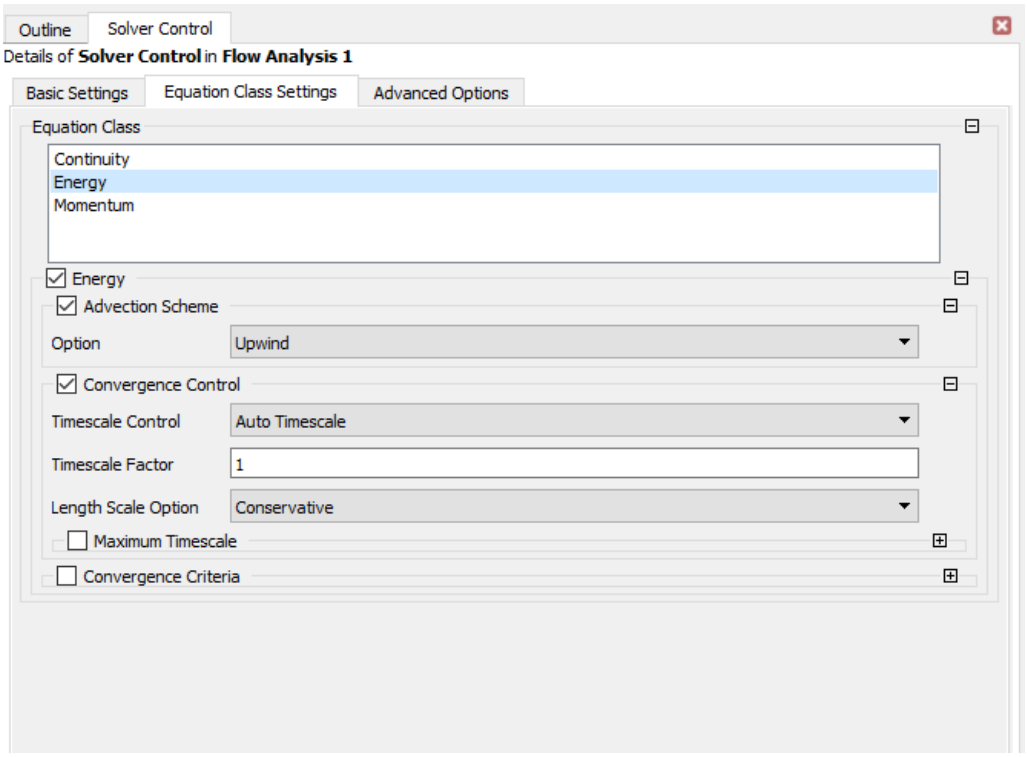

Figure 4.25: Energy equation time-step

.

Output control

To monitor some variables important to user, ANSYS provides a possibility to define an output control and monitor points so the user can also monitor the solution and the condition of convergence in a user defined location for a specific variable. In this study, to monitor the outlet temperature we defined two monitor points at the outlet. The first one is placed in the middle of the outlet pipe and the other one is located at the very end of the outlet pipe which is actually on the system boundary. Figure 4.27 and Figure 4.28 shows the way that monitor point 1 and monitor point 2 were defined. The first one is defined by the ANSYS specific programming language and the second one is by its location in the Cartesian axes. Figure 4.26 provides a view of the monitor point 2 location in the outlet pipe which is marked by the meeting point of 3 perpendicular yellow lines.

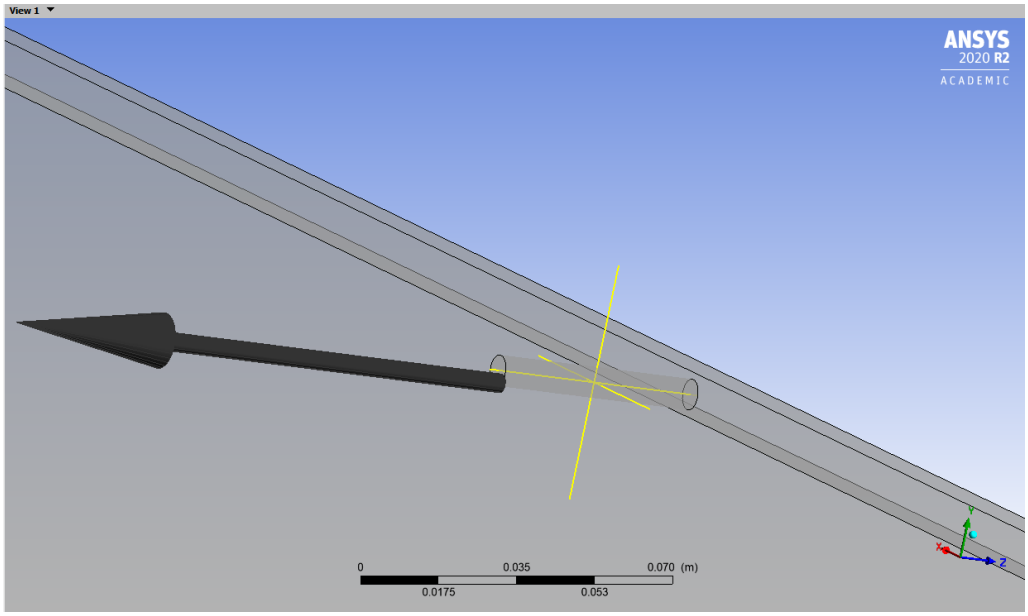

Figure 4.26: Monitor point 2 location

.

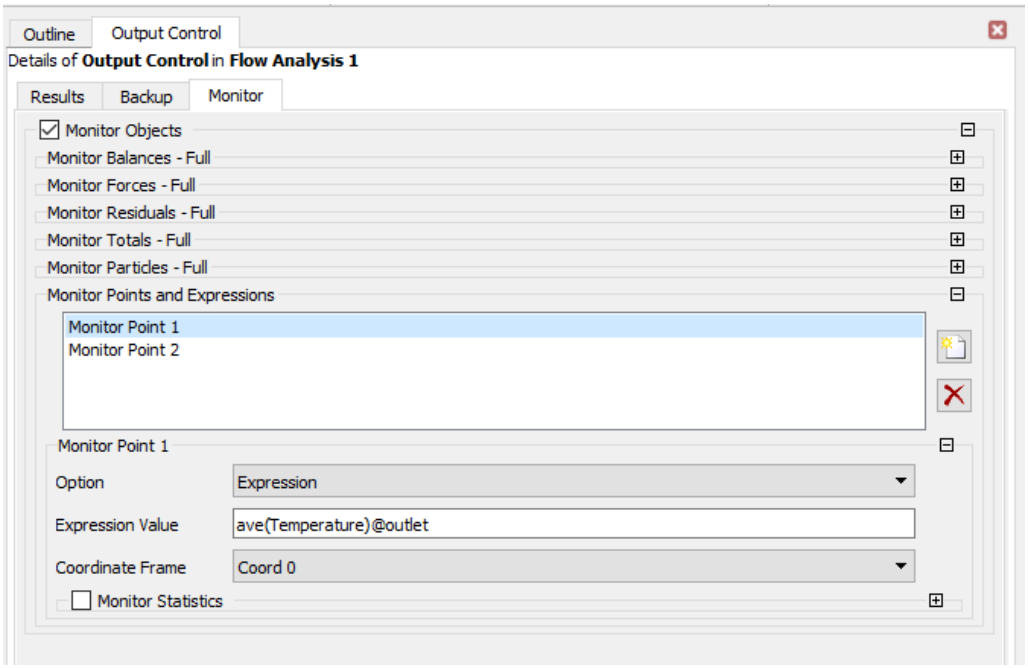

Figure 4.27: Monitor point 1 expression definition

.

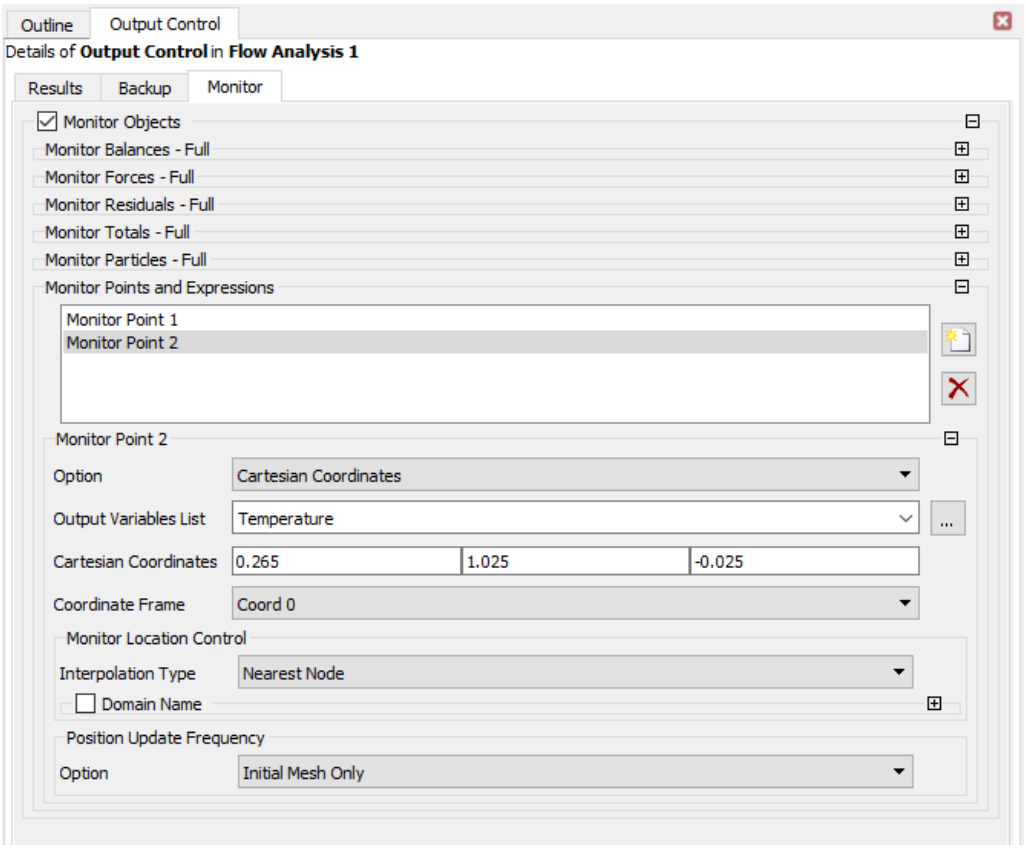

Figure 4.28: Monitor point 2 Cartesian definition

.

Chapter 5

Results

In this chapter we are going to discuss and present the result of our investigation and make comparisson between experimental datas and our simulation using ANSYS workbench R20 student version.

5.1 CFD results

The aim of this research article was to provide a CFD model of a flat plate solar collector in order to investigate the characteristics of this type of collector. The collector design was a Polymer collector with polymer honeycomb structure in the middle and no absorber plate. The working fluid which is water in our case is responsible to work as a heat absorber in our system. To further investigate this novel design, the CFD model that we discussed in this article was created to help us more understand the strong and weak points of this design and provide us with a base model that we can use in further works if there is any need to change any aspect of this proposed flat plate collector design. In the following section we are going to present the data and results created with our model and further discuss the case and evaluate the design.

Convergence The calculation ended after 20,000 iterations and all the curves for momentum, mass and energy equations reached a satisfying convergence condition. In the Figure 5.1 The convergence of momentum and mass equations are shown. The figure 5.2 shows the final state of heat transfer graph.

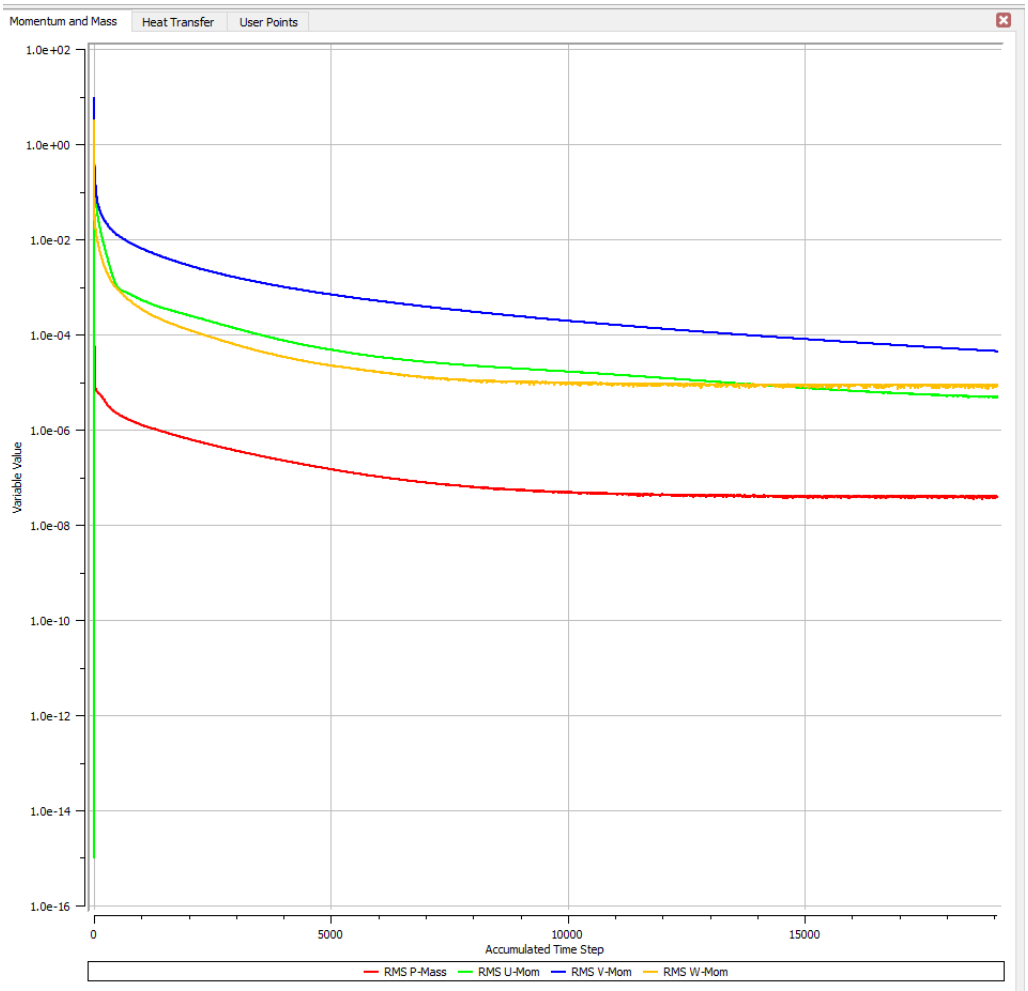

Figure 5.1: Momentum and mass convergence

.

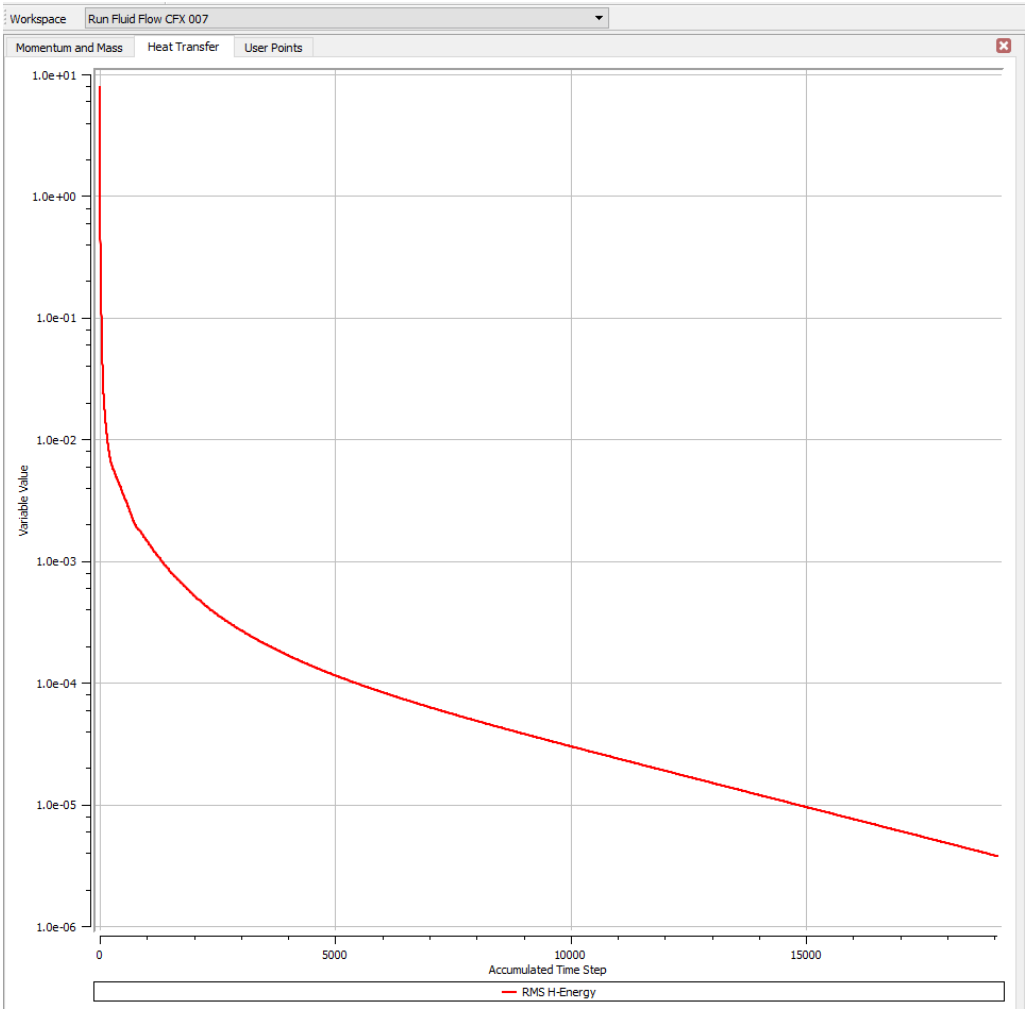

Figure 5.2: heat transfer curve

.

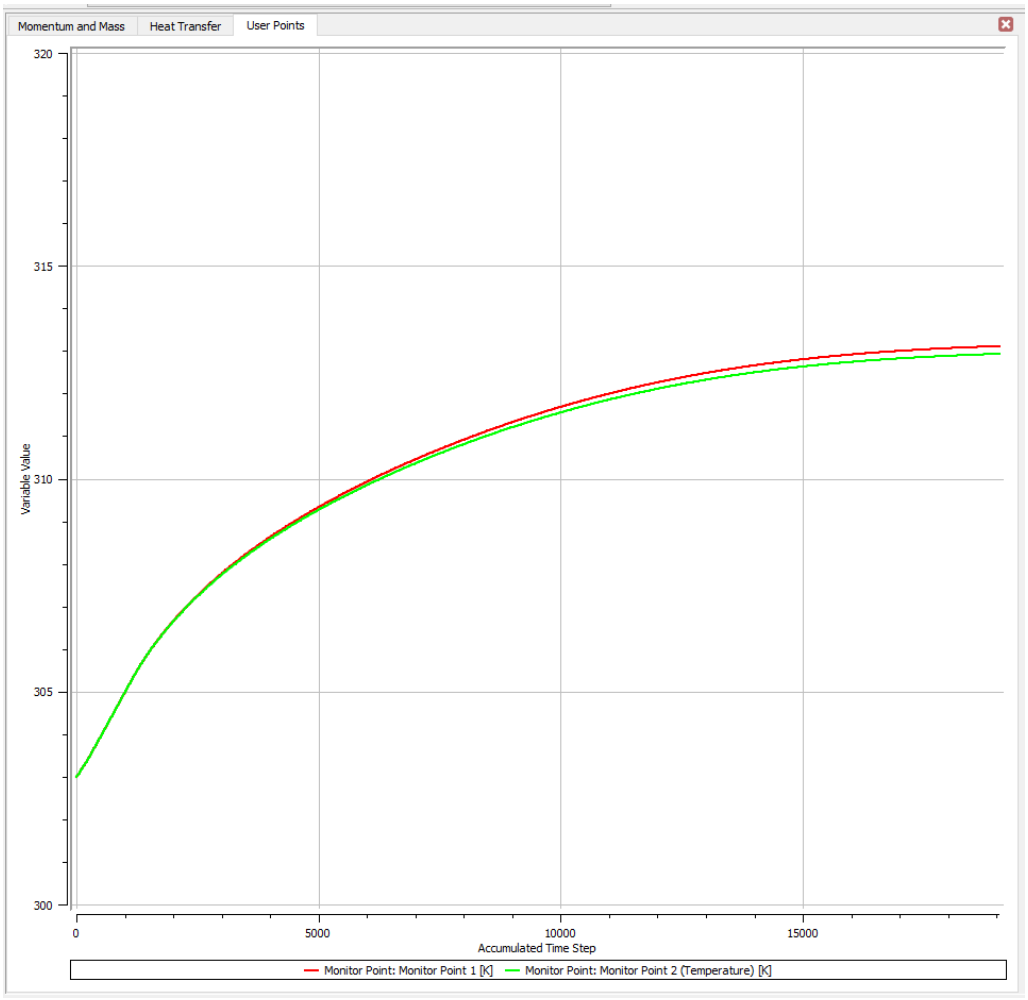

Figure 5.3: Outlet temperature

.

In the Figure 5.3 you can see the final temperature at the outlet of the flat plate collector. The green line is the monitor point 2 which was located in the middle of the outlet pipe. The red line shows the temperature at the monitor point 1 which was at the end of the outlet pipe. The final outlet temperature at this location is 313.13 Kelvin which is approximately 10 degree higher than the inlet temperature which initially set to 303 Kelvin. With the outlet temperature obtained, now we can calculate the efficiency of the collector.

5.1.1 Efficiency

To calculate the efficiency of the collector, we need to follow the formula introduced in below:

$$\eta = \frac{Energy\ exits\ the\ system}{Energy\ enters\ the\ system} \tag{5.1}$$

so it leads us to:

$$\eta = \frac{\dot{m} C_p (T_{outlet} - T_{Inlet})}{A_C I_T} \tag{5.2}$$

The variables in the Equation 5.2 are defined as:

- $\dot{m}$: Mass flow rate = 0.0289 kg/s
- C_p: Specific thermal capacity = 4187 kJ/K.kg
- A_C: Heat flux boundary layer area = 1.47257 m^2
- I_T: solar radiation in the collector plane W/m^-2
- T_{outlet} = 313.13 K
- T_{Inlet} = 303 K

Therefore the collector efficiency was calculated to be 0.9284 or 92.84 %. This number is very high compared to real flat plate collectors which usually work around 65% efficiency at the best. The reason behind this is that in this study and in our model, we only included the radiation losses from the collector and neglected the back and sides convection losses. Moreover, all the pipes including inlet and outlet, top and bottom headers were considered as adiabatic walls. If this modes of heat losses were also included in the model, we would have reached a more realistic number. However, the back and side losses are a problem of insulation and not how the collector itself works. Of course including the losses will decrease the temperature throughout the collector to a certain level and affect its performance and it is not a totally unrelated issue to the collector performance, but still it is safe to say that if the insulation of the collector is high quality, the polymer collector design can work as fine as the classic flat plate collectors in terms of thermal performance.

5.1.2 Temperature pattern

The temperature distribution throughout a middle plan in X-Y axis in the collector area is shown in Figure 5.4.

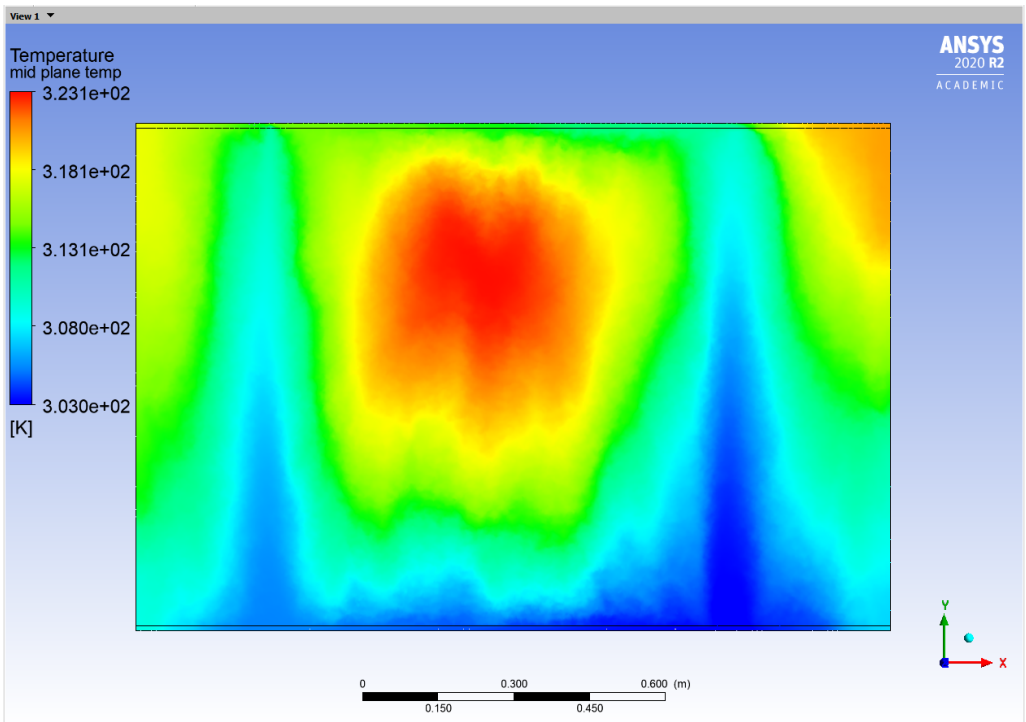

Figure 5.4: Middle plane temperature

.

The overall look of this temperature pattern in the middle plane is in agreement with the infrared photo taken from a experimental model in Misirlis and Martinopoulos work [19]. This photo is shown in Figure 5.5.

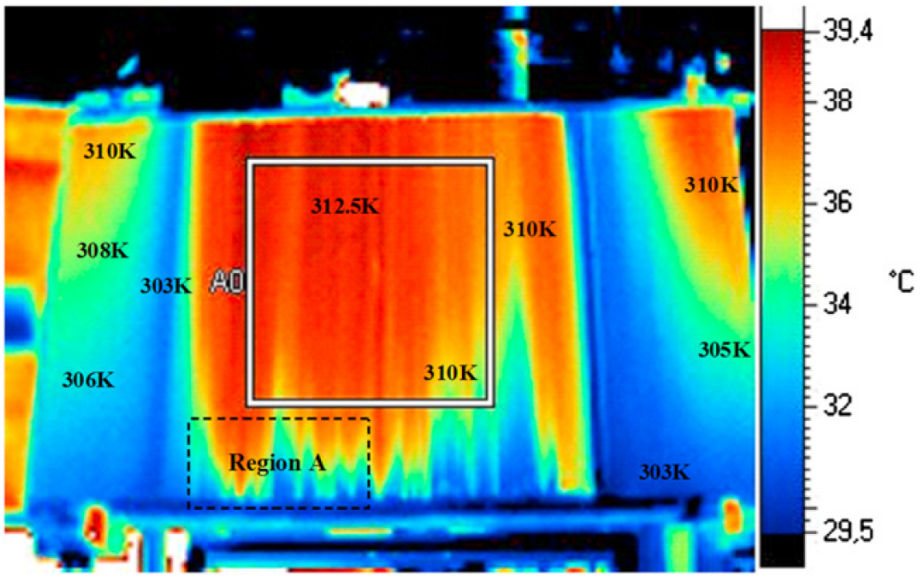

Figure 5.5: Experimental model temperature distribution [19]

. In both figures, there is a big area in middle and a little bit inclined to top of the collector, which has the highest temperature. The difference in colors between these two figures is due to different scaling. The experimental model inlet temperature in the Figure 5.5 is 295 Kelvin while the CFD model temperature distribution in Figure 5.4 was created by inlet temperature of 303 Kelvin. aside from the difference in the color, the general form of the patterns are pretty much the same and in agreement with each other. Both of the patterns also shows that in top right and top left of the collector the temperature is relatively higher than other areas. The high values for temperature shows that there is a stagnation in fluid flow so either the water there does not move at all or gets trap in circular streams. This is more obvious when comparing the temperature of top left area being a little bit lower than the top right are. The outlet location is located in the top left of the collector so it makes it more easier to the flow trapped in the top left area to find an exit. That is why the temperature in this area is slightly lower than the right left area of the collector. the blue lines resembling the lowest temperature are formed near the inlet and outlet pipes where the fluid moves more freely and easier compared to other areas where there is a possibility of fluid getting trapped in the collector.

5.1.3 Flow pattern and velocity

The Velocity distribution throughout a middle plan in X-Y axis in the collector area is shown in Figure 5.6 which was created by a vector plane in ANSYS.

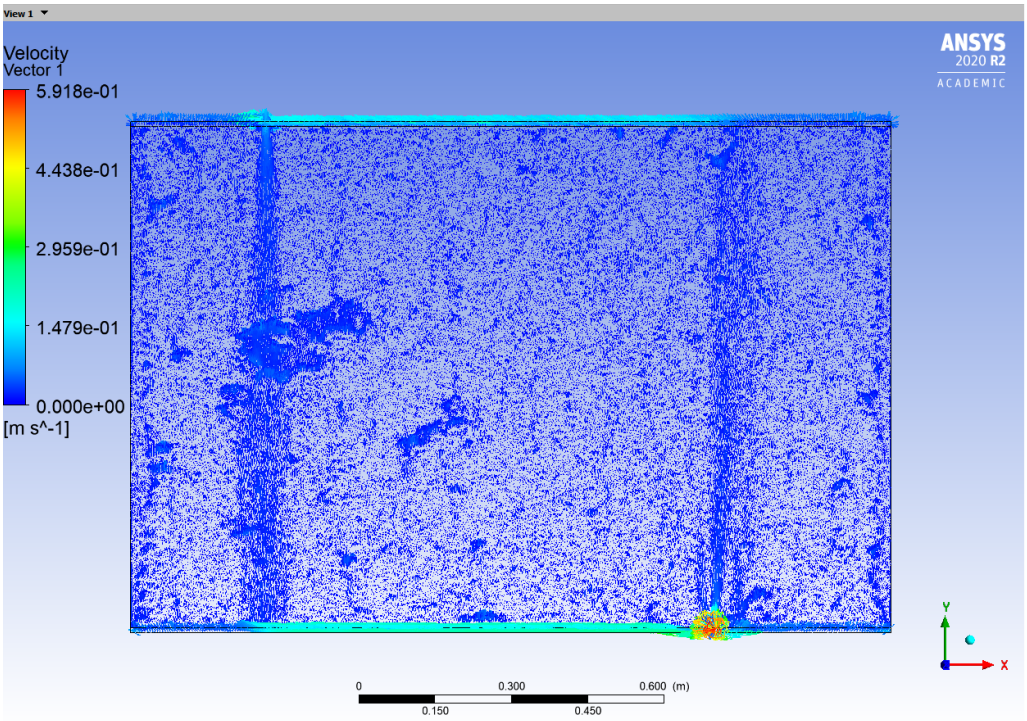

Figure 5.6: CFD flow pattern

.

The overall look of the flow pattern in the photo taken from experimental model in Misirlis and Martinopoulos work [20] is shown in Figure 5.7.

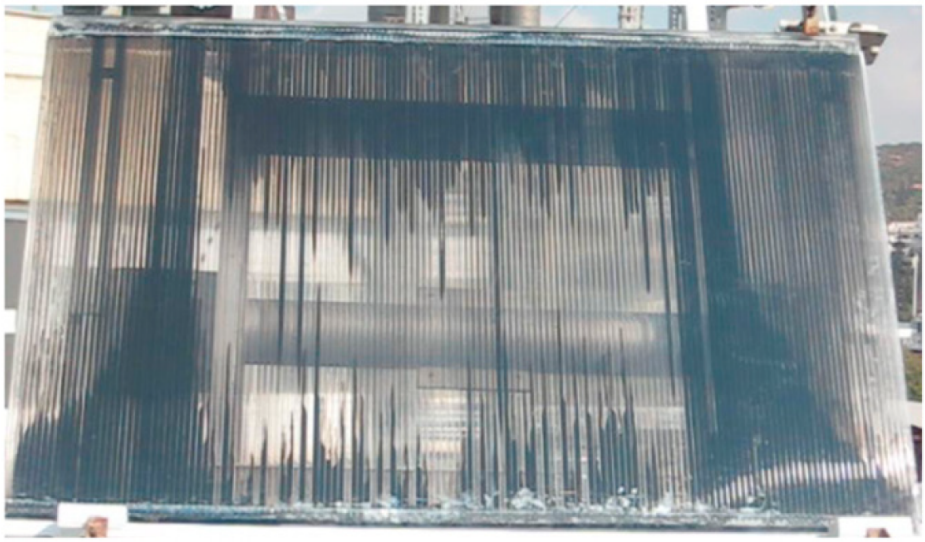

Figure 5.7: Experimental model flow pattern [20]

.

While these two patterns are not completely similar, but they have the two most important streamlines in common. The columns of fluid flow above inlet pipe and below the outlet pipe. the lower part of these two columns are more wide in the experimental model photo. This difference is mostly because the mesh grid size

in the CFD model was limited due to the student version of ANSYS therefore the results always loses a portion of detail and the final result accuracy. When the mesh grid is coarse, it cannot capture the exact pattern of the flow in each cells. However, the main two columns of streams which is a more important factor was captured also in the CFD simulation. In addition to that, the CFD generated pattern also shows the regions that flow is trapped in re-circulation such as the top right of the collector. This region also can be seen in the experimental model. In Figure 5.8 a focused view of the top right corner of the flat plate collector is shown. As it was predicted by the temperature distribution map in the previous section, the re-circulation streams are present in this area. in the honeycomb channels water can only move upward and downward. The ideal situation is that all the arrows point to the upward direction. That would mean that there is no circulation streams in the collector and the design is working fine. However, In Figure 5.8 there are many arrows pointing towards the bottom of the collector indicating that there is a circulation stream in that region which traps the fluid and send it back to the heat flux area again which makes the temperature of that region go higher than the outlet temperature. The same logic also applies to the left top corner of the collector. In this case, the circulation is a little bit weaker compared to the right top corner because this region is closer to outlet pipe and trapped water has a better chance to find its way towards the outlet compared to the top right corner.

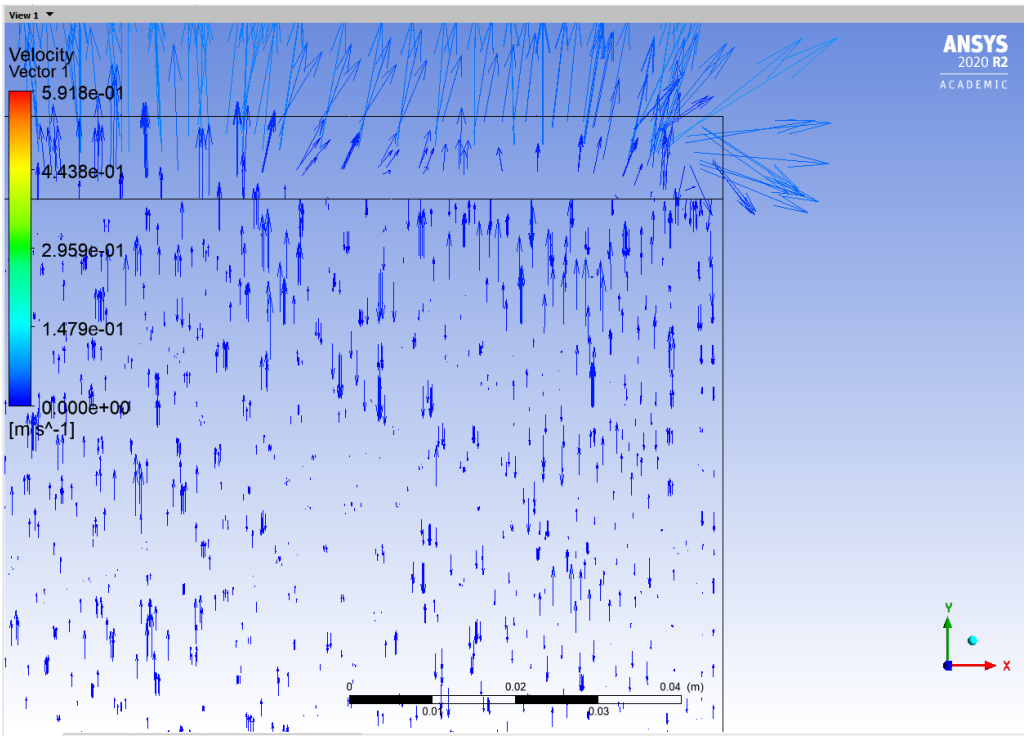

Figure 5.8: Top right region velocity vectors

.

Similar behavior of flow can be seen in the middle of the collector where we also had an increase in temperature. This is also shown in the Figure 5.9.

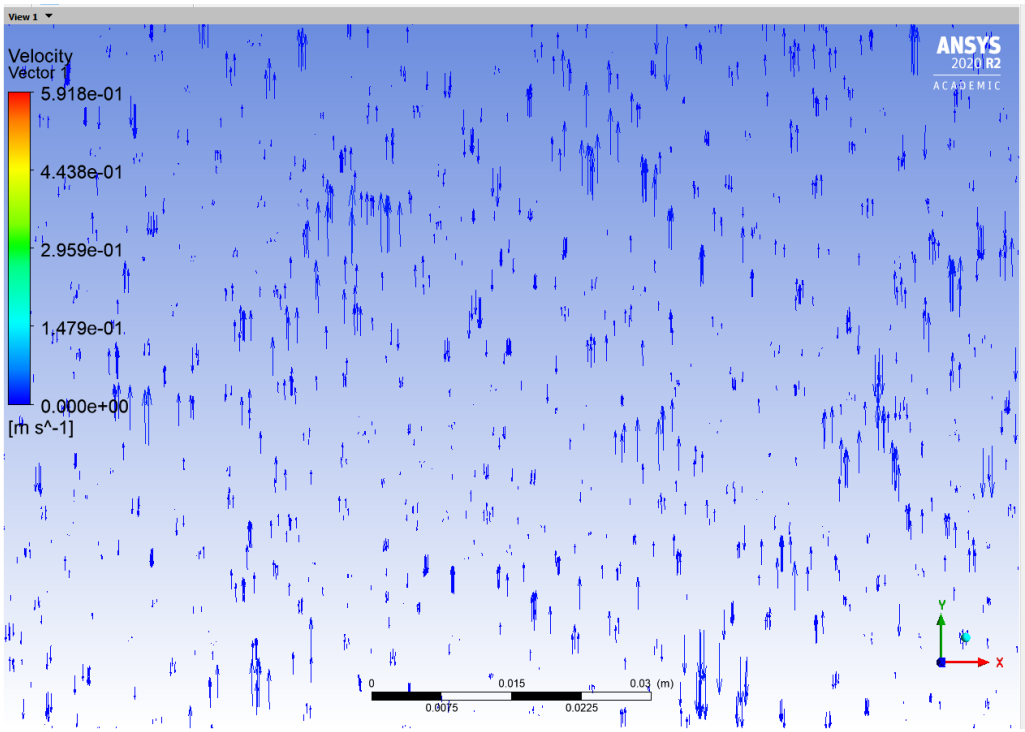

Figure 5.9: Middle region velocity vectors

.

In contrast to the above cases, The regions in the main two columns of stream above inlet pipe and below the outlet pipe are showing a good behavior of flow and it is only going upward and there is no sign of circulation in those regions. This region can be seen in Figure 5.10.

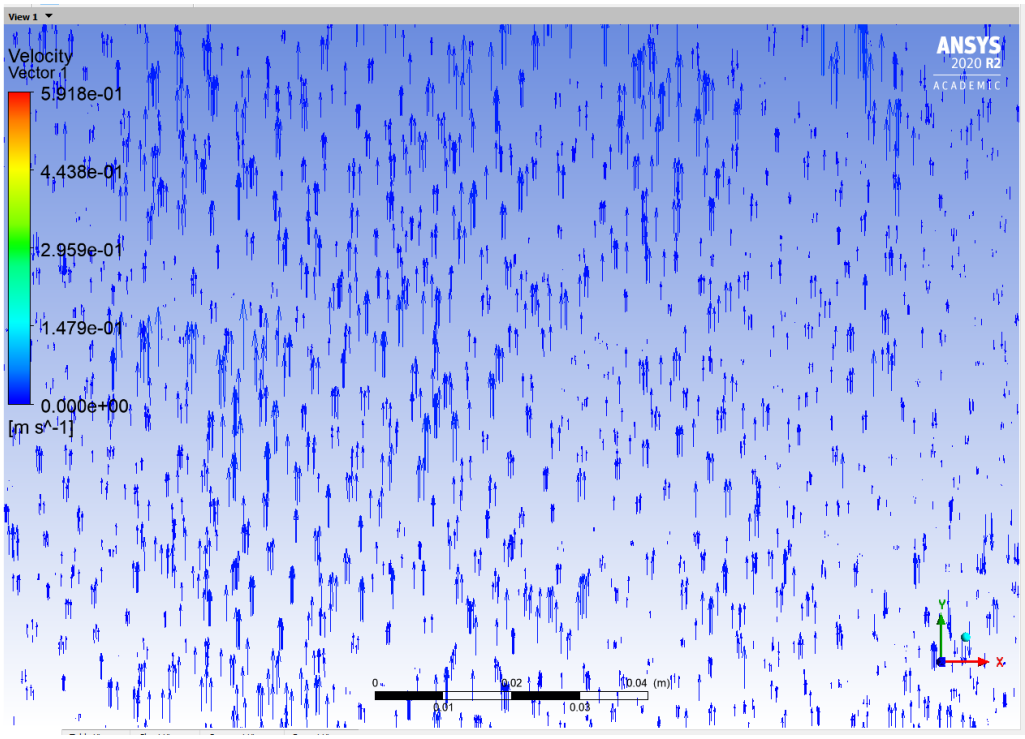

Figure 5.10: Upward stream above inlet pipe

. These columns continue to go upward until they reach top header pipe with no problem.

In the Figures 5.11 and 5.12 an enlarged view of stream lines near the inlet and outlet pipes are shown.

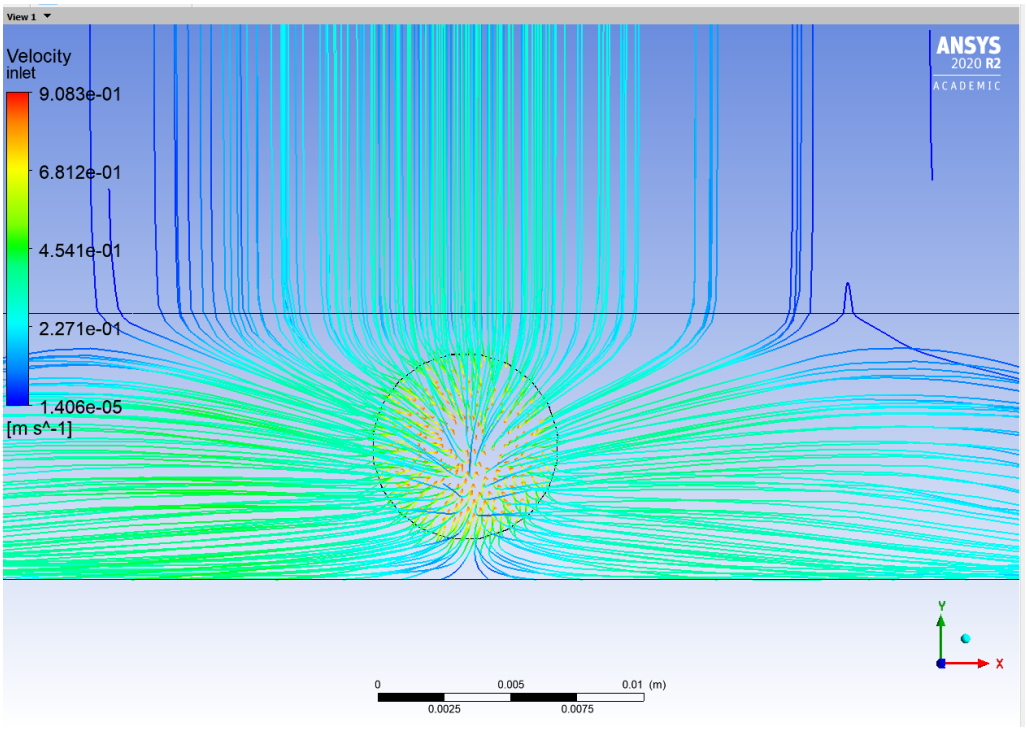

Figure 5.11: Inlet stream lines

.

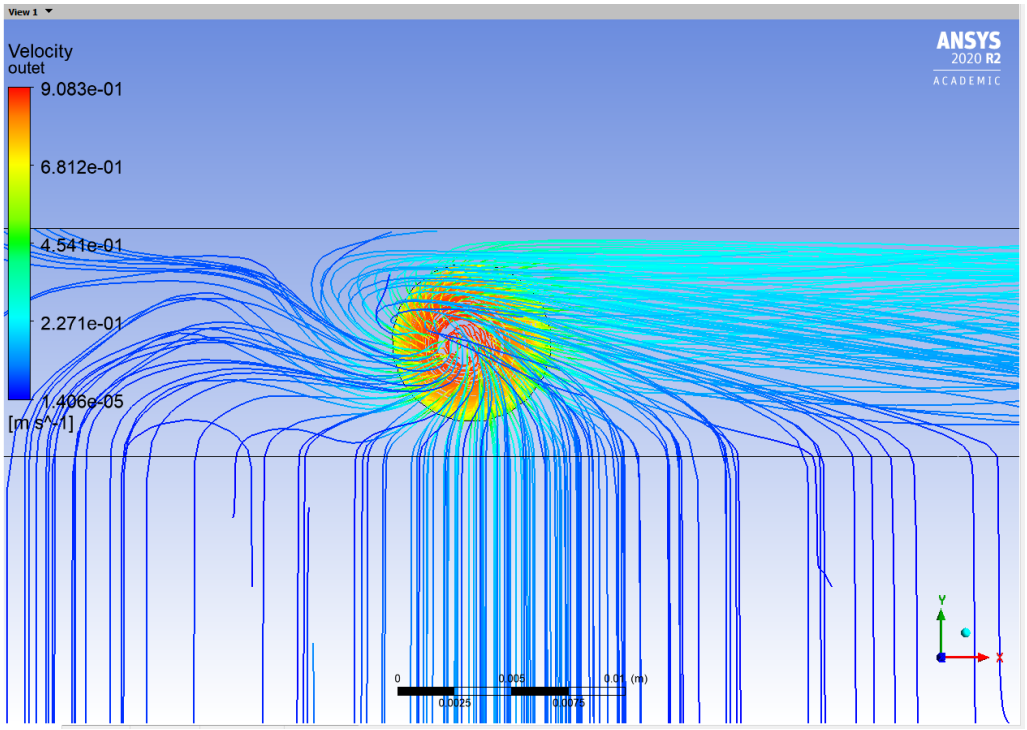

Figure 5.12: Outlet stream lines

.

If we focus on the region exactly near the inlet pipe, we also notice a large re-circulation currents forming in that region as shown in Figure 5.13. The reason for this behavior is that the current is entering the system with relatively high velocity from the inlet pipe. after its complete exits from the inlet pipe and entering the main area of the collector, it faces a sudden change in the geometry therefore it forms a large area of re-circulation near the inlet pipe.

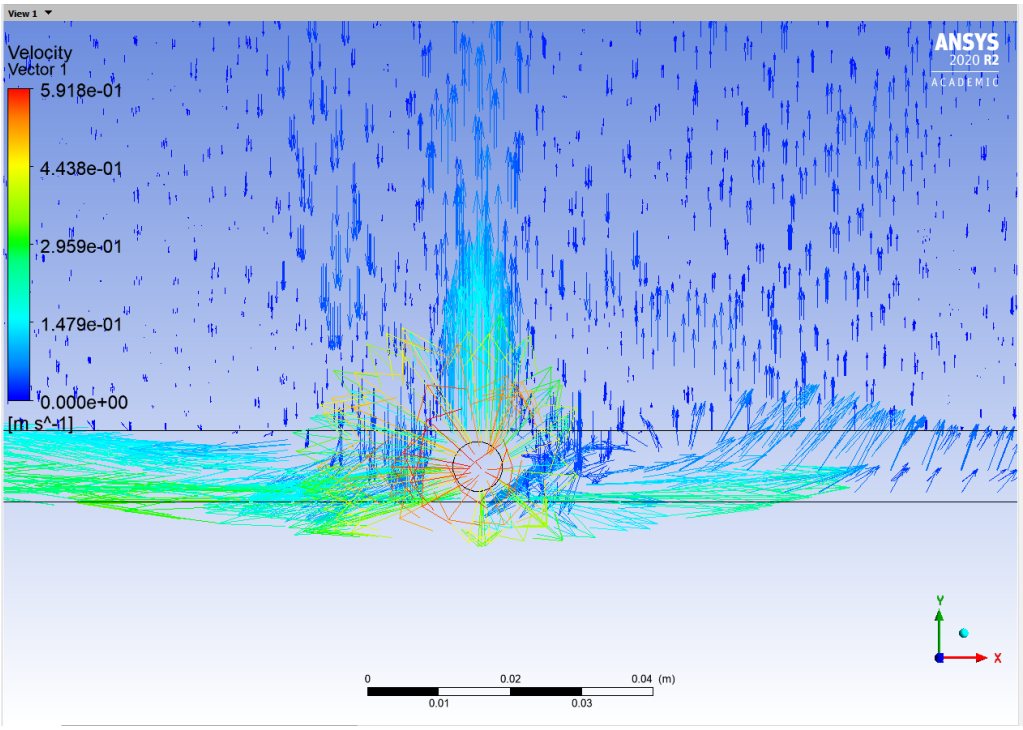

Figure 5.13: Near the inlet pipe velocity vectors

.

5.1.4 Pressure contour

The static pressure drop terms are sum of two separated expressions. The first one is the pressure drop due to the flow filed inside the porous medium which is the honeycomb structure region in our collector, where the pressure drop is following the Hagen–Poiseuille formula, and the other term refers to the share of gravity which is the main contributor in the overall pressure drop. The pressure drop in the honeycomb region is relatively small compared to the share of gravity in this term. the reason behind that is the flow velocity inside the honeycomb region is very small, something of the order of 0.1 m/s. Thus, the pressure distribution is basically decided by the share of gravity effect in the final result. Even though the static pressure distribution inside the honeycomb is limited, the absolute values of the velocity vary. However, the overall effect of the velocity variation is limited, therefore it does not have a noticeable effect in the stable distribution of the static pressure presented in Figure 5.14. Therefore, the velocity distribution is mainly important for the comprehension and investigation of the different flow regions developed inside

the collector. This velocity distribution affects the temperature distribution, but does not have a quantitatively important effect to the static pressure.

Regarding the static pressure, a typical colour contour is presented in 5.14. It can be seen that the distribution of the static pressure is strongly depending on the height increase. Thus, as the height is increasing the static pressure is decreasing, since an important part of it is converted to hydro static pressure. At the same time, the pressure losses are increasing as the flow moves inside the collector. it is also visible that the left side of the collector is affected sooner by pressure drop compared to the right side of the collector. This is because the velocity of the flow in these two region differs since the location of inlet and outlet pipes are not in the middle of the collector or symmetrical in any sort.

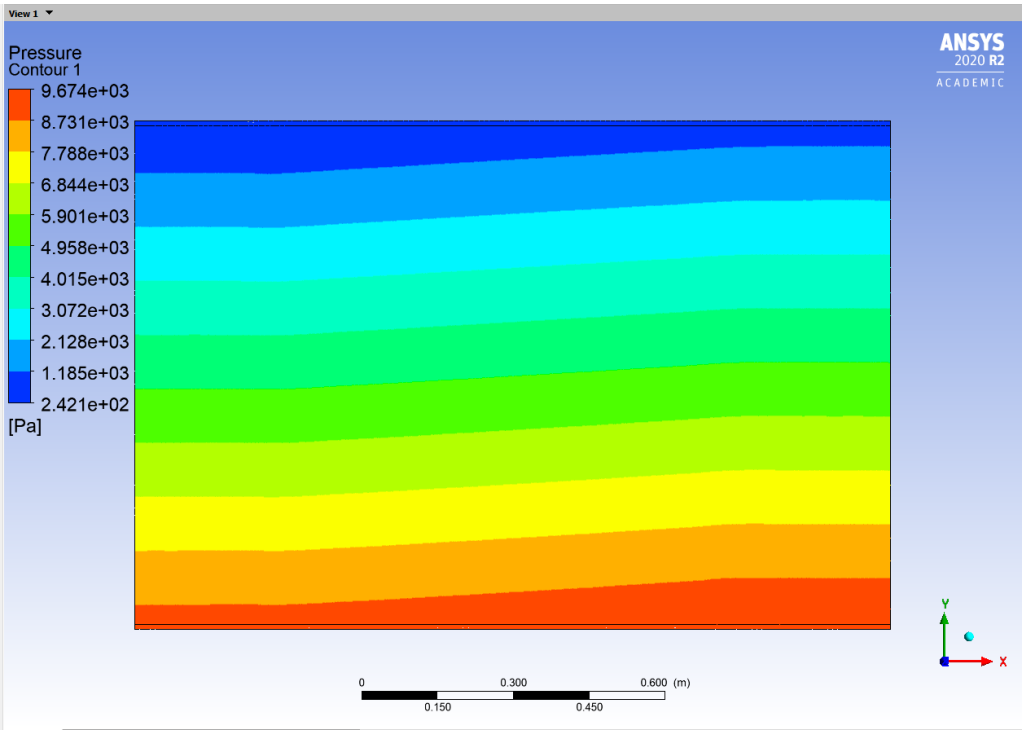

Figure 5.14: Pressure contour at the middle plane

.

5.2 Conclusion

The Master thesis presents a CFD investigation inside a novel honeycomb polycarbonate solar flat plate collector. Unlike the classic design of flat plate collectors which usually have metal riser pipes and an absorber plate bonded with the riser pipes, in this proposed novel design, a transparent honeycomb structure made of polymer is replacing the metal riser pipes. The working fluid which is black colored water to enhance the radiation absorption was used as working fluid. Another change in the flat plate collector design was to remove the usual absorber plate made of metal. The water is flowing through the channels of the honeycomb structure instead of the riser pipes, and the working fluid itself works as the absorber material in this new design. In the old classic designs, the thermal conduction of materials is important so it will lead to an increase cost of material in production phase. Moreover, the way the riser pipes and the metal absorber plate are attached to each other to create a decent conductive bonds between absorber plate and the tubes is very important in the classic design and it is a time consuming and relatively difficult task in production of flat plate collectors. In our new design all this two problems were avoided so it results in flat plate collector which is easier to produce with lower production costs. To mention other benefits of the polymer collectors compared to classic design of flat plate collectors, it is worthy to note the reduction in the total weight of the system up to 50% by replacing the metal parts of the collector with polymer structures. Another advantages of this is to enhance the durability and life time of the collector regarding the corrosion.

In this research article, we have investigated the thermal performance of the polymer solar flat plate collector using CFD simulation via ANSYS Workbench R20 student version and compared it to available experimental data. The determined average efficiency of the collector was found to be similar to that of the low-cost flat plate collectors commercially available. Furthermore, the polymer collector CFD model provides us with detailed inside look of the behavior of the flow inside the collector. The flow filed development and temperature distribution provided by our CFD simulation was showing a significant similar behaviour compared to experimental data and they were in a reasonably good agreement. The flow patterns formed inside the collector and the stream lines provided by CFD simulations were showing a similar flow pattern compared to the photos made in experimental models of the same design. The same similarity was observed in the temperature distribution pattern of the flat plate collector. The regions and their shapes with higher temperature, were the same in both CFD model and experimental data.

Therefore, It can be concluded that the CFD model developed for this research article is is capable of providing reliable results both qualitatively and quantitatively. Both the experimental data and the CFD computations revealed that there were large problematic regions inside the solar collector which decrease its efficiency, suggesting that the CFD model is a useful tool for further investigations and optimisation of the collector. In the results section we addressed the reasons behind this problematic behaviours and discussed it in detail. Thus, it can be concluded that All the weak points of this design were addressed in this article and established a base ground for future researches to further improve this poly-carbonate flat plate collector design.

Bibliography

[1] ASHRAE, E. (2007). Ashrae/iesna 90.1 standard-2007-energy standard for buildings except low-rise residential buildings. *American Society of Heating Refrigerating and Air-conditioning Engineers*.

[2] Assilzadeh, F., Kalogirou, S. A., Ali, Y., & Sopian, K. (2005). Simulation and optimization of a libr solar absorption cooling system with evacuated tube collectors. *Renewable energy*, *30*(8), 1143–1159.

[3] Barone, G., Buonomano, A., Forzano, C., & Palombo, A. (2019). Solar thermal collectors, In *Solar hydrogen production*. Elsevier.

[4] Brownson, J. R. (2013). *Solar energy conversion systems*. Academic Press.

[5] Carman, P. (1948). Some physical aspects of water flow in porous media. *Discussions of the Faraday Society*, *3*, 72–77.

[6] Cengel, Y. (2014). *Heat and mass transfer: Fundamentals and applications*. McGraw-Hill Higher Education.

[7] Cengel, Y. A. (2010). *Fluid mechanics*. Tata McGraw-Hill Education.

[8] Duffie, J. A., & Beckman, W. A. (1980). *Solar engineering of thermal processes*. Wiley New York.

[9] Hollands, K., Unny, T., Raithby, G., & Konicek, L. (1976). Free convective heat transfer across inclined air layers.

[10] Hottel, H. C. (1942). Performance of flat-plate solar heat collectors. *Trans. ASME 64*, *91*.

[11] Jafarkazemi, F., & Ahmadifard, E. (2013). Energetic and exergetic evaluation of flat plate solar collectors. *Renewable energy*, *56*, 55–63.

[12] Kalogirou, S. A. (2013). *Solar energy engineering: Processes and systems*. Academic Press.

[13] Kingslake, R. (2012). *Applied optics and optical engineering v6* (Vol. 6). Elsevier.

[14] Klein, S. (1975). Calculation of flat-plate collector loss coefficients. *SoEn*, *17*, 79.

[15] Klein, S., Duffie, J., & Beckman, W. (1974). Transient considerations of flat-plate solar collectors.

[16] Kozeny, J. (1927). Flow in porous media. *SB Akad. Wiss, 2a*, *126*.

[17] Krarti, M. (2018). *Optimal design and retrofit of energy efficient buildings, communities, and urban centers*. Butterworth-Heinemann.

[18] Liu, B. Y., & Jordan, R. C. (1960). The interrelationship and characteristic distribution of direct, diffuse and total solar radiation. *Solar energy*, *4*(3), 1–19.

[19] Martinopoulos, G., Missirlis, D., Tsilingiridis, G., Yakinthos, K., & Kyriakis, N. (n.d.). Investigation of the heat transfer behaviour of a novel polymer solar collector.

[20] Martinopoulos, G., Missirlis, D., Tsilingiridis, G., Yakinthos, K., & Kyriakis, N. (2010). Cfd modeling of a polymer solar collector. *Renewable Energy*, *35*(7), 1499–1508.

[21] McVeigh, J. C. (2013). *Sun power: An introduction to the applications of solar energy*. Elsevier.

[22] Orosz, M., & Dickes, R. (2017). Solar thermal powered organic rankine cycles, In *Organic rankine cycle (orc) power systems*. Elsevier.

[23] Reddy, J. N. (1993). An introduction to the finite element method. *New York*, *27*.

[24] Rosli, M., Misha, S., Sopian, K., Mat, S., Sulaiman, M. Y., & Salleh, E. (2014). Parametric analysis on heat removal factor for a flat plate solar collector of serpentine tube. *World Appl. Sci. J*, *29*(2), 184–187.

[25] Sabharwall, P., Aufiero, M., & Fratoni, M. (2019). Heat transfer and computational fluid dynamics for molten salt reactor technologies, In *Advances of computational fluid dynamics in nuclear reactor design and safety assessment*. Elsevier.

[26] Sarbu, I., & Sebarchievici, C. (2016). *Solar heating and cooling systems: Fundamentals, experiments and applications*. Academic Press.

[27] Sayigh, A. (2012). *Solar energy engineering*. Elsevier.

[28] Sekhar, Y. R., Sharma, K., & Rao, M. B. (2009). Evaluation of heat loss coefficients in solar flat plate collectors. *ARPN journal of engineering and Applied Sciences*, *4*(5), 15–19.

[29] Souka, A., & Safwat, H. (1966). Determination of the optimum orientations for the double-exposure, flat-plate collector and its reflectors. *Solar Energy*, *10*(4), 170–174.

[30] Tian, Y., & Zhao, C.-Y. (2013). A review of solar collectors and thermal energy storage in solar thermal applications. *Applied energy*, *104*, 538–553.

[31] Tripanagnostopoulos, Y., Souliotis, M., & Nousia, T. (2000). Solar collectors with colored absorbers. *Solar energy*, *68*(4), 343–356.

[32] Tsirakoglou, T. (2015). Numerical simulation of a flat plate collector.

[33] Wäckelgård, E., Niklasson, G., & Granqvist, C. (2001). Selectively solar-absorbing coatings. *Solar Energy: The state of the art*, 109–144.

Nomenclature

β	Tilt angle
$\dot{m}$	Mass flow rate
$\dot{q}$	heat transfer rate
η	Efficiency
κ	Heat conductivity of the material
μ	Dynamic viscosity
ρ	Density
σ	Stefan Boltzman constant
ε	emissivity
A	Surface area
E	Energy
h	Convection heat transfer coefficient
T	Temperature
T_a	Ambient temperature
T_s	Surface temperature
U	heat loss
D	pipe or channel diameter
f	Friction
g	gravity acceleration
h	heat transfer coefficient
I	Radiation intensity
L	length
N	number of covers
Nu	Nusselt number

P	Pressure
Pr	prandtl number
Q	total heat
R	Porosity
Re	Reynolds number
t	Time
u,v,w	Velocity vectors in x,y,z directions
W	Tubes distance